Investigation and Analysis of Micro Plasma Arc Welding of SS-316L Sheet

A Thesis submitted to Indian Institute of Technology Guwahati

for the award of the degree of

Doctor of Philosophy

By

Srikant Prasad

(Roll No. 10610320)

DEPARTMENT OF MECHANICAL ENGINEERING

INDIAN INSTITUTE OF TECHNOLOGY GUWAHATI

GUWAHATI 781039, ASSAM, INDIA

September 2019

Investigation and Analysis of Micro Plasma Arc Welding of ss-316l sheet

A Thesis submitted to Indian Institute of Technology Guwahati
for the award of the degree of

Doctor of Philosophy

By

Srikant Prasad

(Roll No. 10610320)

Under the supervision of

Dr. Sukhomay Pal & Prof. P.S.Robi

DEPARTMENT OF MECHANICAL ENGINEERING

INDIAN INSTITUTE OF TECHNOLOGY GUWAHATI

GUWAHATI- 781039, ASSAM, INDIA

September 2019

Department of Mechanical Engineering
Indian Institute of Technology Guwahati
Guwahati – 781039, Assam, India

CERTIFICATE

It is certified that the work contained in the thesis entitled "**Investigation and Analysis of Micro Plasma Arc Welding of SS-316L Sheet**" submitted by **Mr. Srikant Prasad (Reg. No. 10610320)** to the Indian Institute of Technology Guwahati for the award of the degree of Doctor of Philosophy has been carried out under our supervision in the Department of Mechanical Engineering, Indian Institute of Technology Guwahati. The work has not been submitted elsewhere for the award of any other degree or diploma.

The thesis in our opinion, has reached the standard fulfilling the requirements for the award of degree of Doctor of Philosophy in accordance with the regulations of the Institute.

Dr. Sukhomay Pal
Associate Professor
Department of Mechanical Engineering
Indian Institute of Technology Guwahati
Guwahati – 781039
Assam, India

Prof. P S Robi
Professor
Department of Mechanical Engineering
Indian Institute of Technology Guwahati
Guwahati – 781039
Assam, India

Certificate of Thesis Approval

This is to certify that the thesis titled

"**INVESTIGATION AND ANALYSIS OF MICRO PLASMA ARC WELDING OF SS-316L SHEET**" by **Srikant Prasad (Reg. No. 10610320)** fulfills all the requirements for the award of the degree of Doctor of Philosophy by Indian Institute of Technology Guwahati.

External Examiner

Doctoral Committee Chairman

Committee Member

Thesis Supervisor

Thesis Supervisor

DECLARATION

I declare that,

a. The work contained in this thesis is original and has been carried out by me under the supervision of my supervisors.
b. The work has not been submitted to any other institute for any degree or diploma.
c. I have followed the guidelines provided by the institute in preparing the thesis
d. I have confirmed to the norms and guidelines given in the ethical code of conduct of the institute.
e. Whenever, I have used materials (data, theoretical analysis, figures) from the other relevant sources due credit has been given to them with proper citation in the text of the thesis and details in the references. Further, I have taken permissions from the competent authorities and copyright owners of the respective sources for the reproduction in the thesis.

Place: IIT Guwahati
Date: **Signature of the student**

ACKNOWLEDGEMENT

I have been fortunate to have **Dr. Sukhomay Pal and Prof. P. S. Robi** as my Ph. D. Supervisors. Their constructive criticism and erudite suggestions have been instrumental in leading this research to its logical conclusion. I shall remain indebted to my supervisors for their unwavering faith in me and for their mentorship and the inspiration that I have drawn from them and this would remain a guiding beacon throughout my life. I shall forever grateful to them for their constant support and guidance in moulding me up as a researcher.

The words are insufficient to express my gratitude to my IITG Doctoral Committee members, namely- Prof. Senthilvelan, Dr. Swarup Bag, and Prof. Bishnupada Mandal, Tapas K Mandal and External examiner Dr. Inderdeep Singh (IIT Roorkee) and abroad examiner Prof Tugrul Ozel, Rutgers University (U.S.A) for their insightful comments, suggestion and encouragement. I am also thankful to Prof. S. K. Dwivedy, Head of the Department, Mechanical Engineering and his office members for organizing logistic support for the research.

In completion of this thesis, I owe a great deal to all my erstwhile research friends Dr. Biswajit Parida, Dr. Prakash Kr. Sahu, Dr. Deepak Kr. Yaduwanshi, Dr. Bipul Das, Mr. Saptarshi Dutta Mr. P. V. S. S Sridhar, Dr. Binita Nath, Dr. Manash Pratim Borthakur, Polash Dutta and others for their continuous support and discussion.

I express my appreciation to some internship students Mr. Pintu Thakur, Mr. Dibakor Boruah, Mr. Tanmoy Banik and Mr. Vigneshwaran K. for assisting me during my research work. I convey my thanks to the Central Workshop staff members Mr. Dilip Chetri, Mr. Mrinal Sarma, Mr. N. K. Das for, their kind help in development of experimental setup. My heartfelt gratitude to the technical staffs of Center for Instrumnets Facility and Mechanical Engineering labs technical officers Mr. Saiffuddin Ahmad, Mr. Sanjib Sharma, Mr. Jiten Basumatari, Mr. Nip Borah, Mr. Rituraj Saikia, and Mr. Pranjal Paul for their consistent support and taking keen interest in completion of my research work. It would be extremely difficult for me to name all my friends, researchers and well-wishers who formed a 'benign' pressure group which constantly loaded me to complete this work. I am thankful to all of them.

I am grateful to my father Late Bedu Prasad and mother Smt. Chandrabati Devi for their constant and firm care, sacrifice, inspiration and support. I specially acknowledge the unstinting support of my elder brother Dr. Vijay Verma and younger brother Dr. Rajanikant Verma without whose support the completion of the thesis would not have been reality. I feel privileged to acknowledge the love, understanding, continuous support of my wife Mrs. Anuradha Singh. I shall be failing in my duty if I do not express my special thanks to my loving daughter Shubhanshree Prasad for her understanding, encouragement and inspiration.

Here, in the reminiscence of some memorable persons, I might have missed a few names, but I ll carry their fond memories, which will be like lightening illuminates my memory years from now.

Thursday, 27 Sept 2019 **Srikant Prasad**

Indian Institute of Technology, Guwahati
Department of Mechanical Engineering
ASSAM-781039

ABSTRACT

In the recent years automotive industry is facing a major challenge to reduce vehicles' weight for reduction of fuel consumption and carbon dioxide emission. However, due to the customers' demand for higher safety and comfort levels, the average weight of vehicles show an increasing trend. Further, weight reduction can be achieved without compromising customers' demand by substituting thick sections with thin and stronger materials. Several manufacturers are exploring thin sheets for using in theirs passenger vehicles. Welding is one of the key technologies in the mass production of industrial products. The challenges encountered during the welding of thin sheets are generally found to be linked with heat input. Uncontrolled and excessive heat offered by the conventional tungsten inert gas and metal inert gas welding processes leads to burn through, distortion, buckling, twisting and joint gap variation during welding. Laser beam welding (LBW) and electron beam welding (EBW) processes offer many advantages including high seam quality, minimal weld distortion and high welding speed with higher energy efficiency for joining thin sheets. However, the high cost of LBW or EBW equipment limits the applications of these welding processes in many industries. In this regard, micro plasma arc welding (MPAW) process is one of the most useful welding techniques to join thin sheet materials.

The current research work starts with design and development of suitable fixture for successful joining of thin sheet using MPAW process. A series of welding experiments are carried out by applying full factorial design of experiment. The process parameters considered are welding current, welding speed and stand-off distance. A sufficient number of trial experiments were conducted to find suitable welding window for MPAW of 0.5mm thick stainless steel sheets. Seven weld bead geometry characteristics, namely area of fusion zone, top bead width, bottom bead width, bead height or penetration, reinforcement, width of left side of heat affected zone (HAZ) and width of right side HAZ, three tensile properties (ultimate tensile strength, yield strength and percentage elongation), micro-hardness and grain size of HAZ are considered as weld quality characteristic parameters. Three tensile test specimens are extracted from each welding condition. It is observed that most of the cases the measured three values, at each experimental condition, are close to each other. However, in few cases one measured value is far away from the other observations. Various outlier tests are applied

first time in welding for detection of extreme data. The effects of heat input and process parameters on the measured weld quality parameters are studied. Analysis of variance (ANOVA) is also applied to estimate the relative importance of individual parameter and their interaction on the total variability. Finally, regression models are developed for representing the input and output relationship of the MPAW process.

The high thermal gradient formed during the fusion welding process results in development of undesirable residual stress in the weldments. This stress is developed due to restraint by the parent metal during weld solidification. The high heat input results in non-uniform microstructure across the weld region and hence the mechanical properties of the joint are often not uniform. In order to avoid inhomogeneity in the mechanical properties and also to reduce / eliminate undesirable residual stress, the welded samples are given post welding heat treatment. Weld bead microstructure, micro-hardness and three tensile properties (ultimate tensile strength, yield strength and percentage elongation) are measured after the heat treatment. The effects of welding heat input and process parameters on the measured weld qualities of heat treated weldments are studied. ANOVA is also performed to estimate the influence of factors and their interaction on the weld quality. The post weld heat treatment results in almost homogeneous microstructure and improves mechanical properties. The developed regression models exhibit a poor correlation between the control parameters and weld qualities, except percentage elongation.

Keywords**:** Micro plasma arc welding; Weld bead geometry; Weld strength; Micro-hardness; Weld microstructure; Analysis of variance; Regression model; Outlier test; Stainless steel; Heat treatment; Thin sheet.

List of acronyms

ANOVA	Analysis of variance
BM	Base material
DOE	Design of experiment
DOF	Degrees-of-freedom
EBM	Electron beam welding
EDX	Energy dispersive X-ray
EN	Electrode negative
EP	Electrode positive
FESEM	Field emission scanning electron microscope
HAZ	Heat affected zone
I	Welding current
LBM	Laser beam welding
MPAW	Micro plasma arc welding
PAW	Plasma arc welding
SOD	Stand-off distance
SS	Stainless steel
UTS	Ultimate tensile strength
WS	Welding speed
YS	Yield stress

List of Nomenclature

A_{FZ}	area of fusion zone
BW	width of bottom fusion zone
$Elong$	Percentage elongation
H_{Avg}^{HAZ}	average hardness in the heat affected zone
H_{Avg}^{FZ}	average hardness in the fusion zone
LW_{HAZ}	width of left side of HAZ
PD	penetration depth
RH	reinforcement height
RW_{HAZ}	width of right side of HAZ
R^2	Coefficient of correlation
R_{adj}^2	adjusted coefficient of correlation
TW	width of top fusion zone
SOS_T	total sum of square
N	total number of experiments
T	sum of all observations
SOS_A	sum of square of a factor A
$SOS_{A\times B}$	sum of square of interaction of factors A and B
SOS_e	sum of square of error
SOS_M	sum of square of model
V	Variance
V_e	Variance of error
PC	Percentage contribution

Contents

Abstract i

List of acronyms iii

Nomenclature iv

Chapter 1: Introduction

1.1 Motivation of the research work 1

1.2 Objectives of the research work 3

1.3 Contribution of the thesis 4

1.4 Organization of the thesis 4

Chapter 2: Literature review

2.1 Introduction 7

2.2 Overview of micro plasma arc welding process 8

2.3 Process parameters 10

2.3.1 Welding current 11

2.3.2 Welding speed 11

2.3.3 Stand-off distance 11

2.3.4 Plasma gas 11

2.3.5 Shielding gas 12

2.4 Plasma arc welding of stainless steel materials 12

2.5 Plasma arc welding of non-ferrous materials 15

2.6 Modelling of plasma arc welding process 16

2.7 Laser welding of similar and dissimilar materials 19

2.7 Summary 20

Chapter 3: Experimental procedures

3.1 Introduction 21

3.2 Design of experiment 21

3.3 Experimental setup development 25

3.4 Sample preparation for welding 28

3.5 Welding experimentation 29
3.6 Post welding heat treatment procedure 31
3.7 Determination of weld quality characteristic 31
3.7.1 Metallographic sample preparation and bead geometry measurement 31
3.7.2 Micro-hardness measurement 35
3.7.2.1 Micro-hardness of without post welding heat treated samples 35
3.7.2.2 Micro-hardness of post welding heat treated samples 38
3.7.3 Weld bead microstructure 40
3.7.4 Tensile Properties 42
3.7.5 Field emission scanning electron microscope 48
3.8 Summary 48

Chapter 4: Analysis of Weld Qualities without Post Welding Heat Treatment

4.1 Introduction 51
4.2 Analysis of weld bead geometry 51
4.2.1 Effect of heat input on weld bead geometry 52
4.2.2 Effect of process parameters on weld bead geometry 53
4.2.3 Influence of process parameters on weld bead geometry 57
4.2.4 Development of mathematical models 61
4.2.5 Checking the adequacy of the developed model 62
4.3 Analysis of micro-hardness 65
4.3.1 Effect of process parameters on micro-hardness 68
4.3.2 Influence of process parameters on micro-hardness 69
4.3.3 Development of mathematical models 70
4.4 Analysis of tensile properties 71
4.4.1 Detection of outlier 72
4.4.1.1 Chauvenet's criterion 73
4.4.1.2 Grubb’s test 75
4.4.1.3 Dixon’s Q-test 77
4.4.1.4 Cochran’s C test 78

4.4.1.5 Comparison of outlier detection methods 80
4.4.2 Effect of heat input on tensile properties 81
4.4.3 Effect of process parameters on tensile properties 82
4.4.4 Influence of process parameters on tensile properties 85
4.4.5 Development of mathematical models 85
4.5 Analysis of weld bead microstructure 87
4.5.1 Effect of heat input on weld microstructure 90
4.5.2 Effect of process parameters on weld bead microstructure 90
4.5.3 Influence of process parameters on weld bead microstructure 91
4.5.4 Development of mathematical models 92
4.6 Summary 93

Chapter 5: Discussion of Weld Qualities of Heat Treated Weldments

5.1 Introduction 95
5.2 Analysis of weld bead microstructure 95
5.2.1 Effect of heat input on weld microstructure of heat treated weldments 96
5.2.2 Effect of process parameter on grain size of heat treated weldamets 98
5.2.3 Influence of process parameters on weld bead microstructure 99
5.2.4 Eevelopment of mathematical models 100
5.3 Analysis of tensile properties 101
5.3.1 Effect of welding heat input on tensile properties 101
5.3.2 Effect of process parameters on tensile properties 102
5.3.3 Influence of process parameters on tensile properties 104
5.3.4 Development of mathematical models 105
5.4 Analysis of micro-hardness 107
5.4.1 Effect of process parameters on micro-hardness 109
5.4.2 Influence of process parameters on micro-hardness 110
5.4.3 Development of mathematical models 111

5.5 Summary 112

Chapter 6: Conclusions and future scopes

6.1 Conclusions of the presents work 113

6.2 Future Scopes 116

References 117

List of publications 123

Chapter 1

Introduction

1.1 Motivation of the Research Work

In recent years the environmental pollutions caused by automobiles and other sources have become a matter of great concern. The economic and political pressure on the automotive industry to reduce fuel consumptions and carbon dioxide emissions of vehicles constantly grew. The International Council on Clean Transportation is also directing the manufacturers for new intervention to reduce the vehicle emission. Weight reduction in vehicles can be considered as one of the most effective means of improving fuel efficiency and reducing exhaust gas emissions. However, because of customer's demand for higher safety and comfort levels, the average weight of vehicles shows an increasing trend. But reduction of the vehicle weight is mandatory to reduce the exhaust gas emissions, since it provides one of the highest fuel saving potentials. A weight reduction can be achieved by (i) substitution of heavier components with lighter and stronger components (ii) introducing new design to eliminate unnecessary/extra components and (iii) adapting new manufacturing process.

Many manufacturers are looking forward for lighter and stronger materials to improve efficiency without compromising durability, competiveness and safety of the product. In addition, material should be machinable, formable, weldable, coatable and repairable. The austenitic stainless steels are mostly used in fabrication of structural components in many industrial applications due to their superior mechanical properties at cryogenic temperature as well as elevated temperature. They also exhibit better corrosion resistance and creep rupture properties. The austenitic stainless steel family includes

several kinds of stainless steel; among them AISI 3xx series is the most weldable grade. High strength and corrosion resistance with good ductility make AISI 316L steel preferable structural material over other austenitic varieties. To reduce vehicle weight further manufacturers are also exploring the use of thin sheet in their product.

The application possibilities of thin sheets in industrial components can be enhanced by improving machinability, formability and weldability of the materials. Welding is one of the key technologies in the mass production of industrial products. The challenges encountered during the welding of thin sheets are generally found to be linked with heat input. Uncontrolled and excessive heat offered by the conventional tungsten inert gas and metal inert gas welding processes leads to a large number of problems in thin-sheet welding including burn through, distortion, porosity, buckling, warping and twisting of welded sheets, grain coarsening, evaporation of useful elements present in coating of the sheets, joint gap variation during welding, fume generation from the coated sheets etc. Other welding processes like laser beam welding (LBW) and electron beam welding (EBW) offer many advantages including high seam quality, minimal weld distortion and high welding speed with higher energy efficiency for joining thin sheets. However, the cost of LBW or EBW equipment is very high which limit the applications of these welding processes in many industries. In this regard, micro plasma arc welding (MPAW) process is one of the most useful welding techniques to join thin sheet SS-316L material.

MPAW is very popular due to its high arc energy density, good arc stability, deeper penetration with large tolerance to joint gaps and misalignment and for precise welding of thin sheet material without weld distortion. In plasma arc welding process the arc is constricted to achieve intensities close to LBW process. In addition, the PAW process does not require expensive joint preparation. However, despite of its advantages, relatively few published articles are available on the MPAW of thin sheets. These include the effects of MPAW process on mechanical and metallurgical properties of thin 316L stainless steel sheet. The quality is significantly dependent on the grain structure, such as the grain size and grain orientation. The grain structures formed in welding process are not only determined by the material properties and the environmental conditions, but also the process conditions, such as the heat input, the welding speed, the nozzle to workpiece distance etc. Therefore, finding suitable welding conditions to get a

satisfied weld quality and to avoid the formation of defects are very important for its successful applications.

The high thermal gradient formed during the fusion welding process results in development of undesirable residual stress in the weldments. This stress is developed due to restraint by the parent metal during weld solidification. It may be as high as the yield stress of the material. The high heat input during the fusion welding process also causes non-uniform microstructure development across the weld region and hence the mechanical properties of the joint are often not uniform. In order to avoid inhomogeneity in the mechanical properties and also to reduce / eliminate undesirable residual stress, the welded samples are generally given post welding heat treatment. The post welding heat treatment results in almost homogeneous microstructure and facilitates removal of metallurgical defects like dislocations, vacancies and slip planes and removal of residual stress formed during the welding process. Another important aspect of heat treatment is the prevention of brittle fracture of the weldments. Hence, the study of post welding heat treatment on the microstructure and mechanical properties of the SS 316L sheets is also important for its useful application.

1.2 Objectives of the Research Work

The difficulty in fusion welding process increases with decreasing workpiece thickness. The issues such as edges mismatch and joint gap variation exaggerate with the decrease in thickness of the substrate materials to be welded. Therefore, design and development of suitable fixture for successful welding of thin sheet using MPAW process is required. The effects of welding process parameters on mechanical and microstructure properties of the weldments need to be explored for better insight of the process. The effectiveness of post welding heat treatment for obtaining uniform metallurgical and mechanical properties also needs to be explored. The objectives of the current research work are outlined as follows:

- Investigate the effect of process parameter on weld qualities of micro plasma arc welded SS 316L weldment.
- Development of regression models for evaluating the weld qualities and identification of significant process parameters.

- Investigate the effect of post welding heat treatment on the microstructure and mechanical properties of SS 316L weldments.
- Development of regression models for evaluating the weld qualities of annealed weldments.

1.3 Contribution of the Thesis

The important contributions of this research work are summarized as follows:

- ✓ A fixture has been developed dedicated to MPAW process. The developed fixture is suitable for proper holding and positioning of the workpieces. It also assists to set a desired stand-off distance and alignment of joint line with the welding electrode.
- ✓ A detailed experimental investigation is carried out to evaluate the influence of welding process parameters on weld properties of SS 316L weldments. A process window for successful MPAW of 0.5 mm thick SS 316L sheets is also identified.
- ✓ Various outlier tests are applied for detection of extreme data in ultimate tensile stress, yield stress and percentage elongation data sets.
- ✓ Regression models are developed for evaluation of weld qualities
- ✓ A detailed experimental investigation is carried out to evaluate the influence of post welding heat treatment on the microstructural and mechanical properties of the weldments.

1.4 Organization of the Thesis

The thesis comprises of six chapters and highlight of each chapter is presented in the following.

Chapter 1 starts with the motivation of the present study. The research objectives and contribution of the thesis are also highlighted in this chapter.

Chapter 2 summarizes the research works carried out by other researchers in the field of plasma arc welding process. The chapter is divided into various sections starting from overview of MPAW process, influence of process parameters on weld qualities, plasma

arc welding of ferrous and non-ferrous materials and different techniques for modeling of PAW process. The literature review reported in the chapter is summarized at the end.

Chapter 3 will showcase the experimental investigations carried for the present study. Selection of workpiece material, identification of process window, selection of process parameters with suitable levels, design of experiments, and quality assessment of welded samples and post welding heat treatment method are included in this chapter.

Chapter 4 includes the various techniques used in this study for analysis of weld qualities. The weld quality attributes are correlated to process parameters to investigate their effect on the weld qualities without post welding heat treatment. Mathematical models are also developed for representing the input and output relationship of the MPAW process. Various outlier tests are also discussed for detection of extreme data.

Chapter 5 includes the analysis of post welding heat treated weldments. The effect of individual process parameters on mechanical and microstructural properties of the SS 316L weldments are analyzed. The comparison of weld qualities before and after heat treatment is also presented in this chapter.

Chapter 6 summarizes the present study and reports the findings of the research work. This chapter also outlines possible future research scopes of the present study.

Finally the thesis ends with a list of *references* cited in this thesis.

Chapter 2

Literature Review

2.1 Introduction

During the 1890's, arc welding was developed with bare metal electrodes but the weld quality was poor due to formation of nitrides and oxides. The importance of shielding the arc and molten metal from the atmosphere was then realized. In the early 20th century, various methods of covering electrodes were tested. After World War II, welding technology advanced quickly and several arc welding processes were developed. Modern welding power sources comprise electric arc, plasma arc, resistance heating, induction heating, laser beam, electron beam, microwave radiation, friction, etc. All those welding processes have some advantages and disadvantages, and none of these processes is suitable for every application. The common welding processes use for joining thin sheets are tungsten inert gas (TIG) welding, metal inert gas welding, plasma arc welding (PAW), laser welding and electron beam welding processes. Among these, micro plasma arc welding (MPAW) is one of the most useful techniques to join thin sheet materials.

Robert M. Gage invented plasma arc welding process in 1953, patented in 1957 and commercialized in 1964. It has better control in lower welding current ranges (Prasad et al., 2006). In PAW process an electric arc is formed either between a tungsten electrode and water cooled copper nozzle, called as non-transferred arc, or between a tungsten electrode and workpiece, called as transferred arc. A pilot arc is struck between a tungsten electrode and the copper nozzle within the torch (non-transferred arc mode), usually by applying a high-frequency open-circuit voltage. The plasma gas is ionized in its passage through the arc, due to restricted shape of nozzle orifice, and ionization is increased to a very high temperature. The high velocity plasma jet and very narrow

diameter of the nozzle realizing very high temperature up to 20,000 °C. When the torch is brought in close to the workpiece, welding current is initiated and the arc is transferred from the electrode to the workpiece and temperature up to 1700 °C can be obtained on the surface of the workpiece (Davies, 2002).

The arc is forced to pass through a water cooled copper nozzle which causes the constriction of the arc. A coherent, calumniated and stiff plasma is formed due to constriction therefore it does not get deflected and diffused. These factors make PAW a low heat input and high energy density welding process. The main difference between PAW and tungsten inert gas welding is that the electrode of PAW is within the body of the torch thereby separating plasma from the shielding gas. Shielding is generally obtained from the gas coming out from the torch. Due to the low ionization potential (1.5 eV), argon gas is preferred for obtaining plasma gas (Foesta et al., 2006). Filler metal may or may not be used. Shielding gas may be single inert gas or mixture of inert gases (Brien, 1991). The molten metal flow surrounding the keyhole flow to the rear region and solidifies to form weld bead. The quality of weld pool stability depends on heat transfer rate, fluid flow behaviour, variation in welding condition and process parameters (Junahu et al., 2011). Plasma arc welding can be used to join most metals in all positions. It provides better control of the arc and smaller heat affected zones as compared to conventional arc welding process (Brien, 1991).

The survey of the available literature is carried out with the intention to ideate the research trend in line with the objectives of the present research work. This chapter is divided into various sections and sub sections to outline the salient results of the reviewed literature. The literature review is started with exploring the MPAW process. Than the influence of process parameters on weld quality is explored. In this regard section 2.3 is devoted to report results of various research works regarding the influence of welding speed, welding current, stand-off distance, plasma gas and shielding gas on MPAW process. The PAW of ferrous and non-ferrous materials are reviewed and reported in section 2.4 and 2.5, respectively. Various methods used for weld quality modeling is reviewed in section 2.6. Finally the chapter is summarized in section 2.7.

2.2 Overview of Micro Plasma Arc Welding Process

One common way of defining micro-welding is based on the dimensions of the parts to be welded. Micro-welding would deal with parts with characteristic dimension

smaller than a few hundred micrometers but larger than hundred nanometers. So far a universally accepted criterion has not been arrived regarding the size. There are other effective ways to define micro-welding such as based on industrial application areas, process characteristics and equipment characteristics. Presently researchers consider the MPAW process, in which the fusion zone size is less than 100 μm (Zhou, 2008). Through MPAW process literatures for welding of very thin stainless steel sheet up to 0.1 mm is available which is called as foil welding. The MPAW can be defined as the joining of very small (micron size) sections through fusion process. Though the phenomenon of the process remains the same, some of the factors which are less importance in the macro-scale like, surface tension, deformation, thickness, amount of fusion, etc. have high influence at the micro-scale (Gajapathi et al., 2010). The factors affecting the micro welding process are: (1) Thermal aspects; heat input, heat distribution (2) Mechanical aspect; the evaporative forces generated by high energy density heat input, constrained thermal expansion, pool dynamics, surface tension, diffusion, dissolution body forces and externally applied forces. (3) Geometrical aspects; joint design, gap and shape stability. These phenomena have significant effects on the weld quality (Zhou, 2008). During micro welding, precise control over the machine parameters is required, since little change in heat input changes the quality of micro weld.

MPAW process is a variation of the PAW process where current level use is lower than 15 A, and higher than 0.1 A. This can be efficiently used for welding thin steel sheet in the range of 0.1 mm to 1 mm, but precise control of process parameters is required. The recent trends in welding shows a very fast development in the area of MPAW, fine plasma arc welding (FPAW) and variable polarity plasma arc welding (VPPAW) based on power supply uses in the plasma arc. The MPAW process provides better control and high precision depth. In the welding of sheet thickness up to 0.1 mm various problems arises with the conventional welding processes. Due to high heat input, burn throughout, porosity, distortion, buckling, wrapping and twisting of welded sheet, grain coarsening, evaporation of useful element, joint gap, and fumes generation from coated sheet etc. occurs. The MPAW process is a suitable tool to control over all these defects (Prasad et al., 2012).

In MPAW process the allowable variation in the joint mismatch should be very low so that there is continuous contact between the joint edges. These will ensure that

both edges melt and fuse together thereby a smooth weld bead is obtained. Proper cleaning of the component surfaces is necessary to avoid formation of oxides and porosity (Tesang et al., 2003). The MPAW system and detailed diagram of the nozzle is shown in Fig. 2.1.

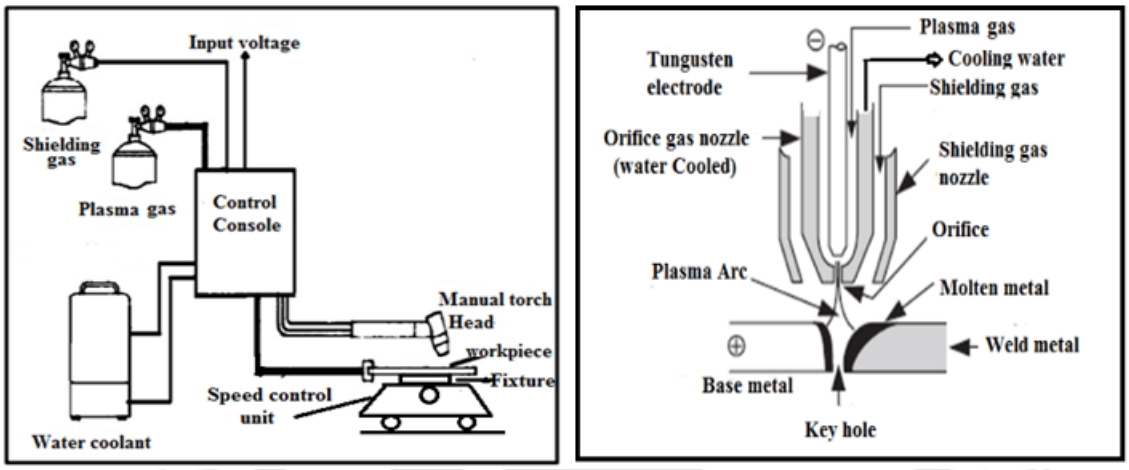

Fig. 2.1 Micro plasma arc welding system and plasma torch.

The PAW technique appears to be a better choice for many joining applications due to high weld quality than TIG welding and lower equipment cost compared to electron and laser beam welding processes. In addition, it has high tolerance to joint misalignment compared to laser or electron beam welding. The practical PAW process is widely accepted in the aerospace, chemical, shipbuilding, and nuclear industries (Prasad et al., 2012). Compared with TIG, the micro plasma arc welding has better arc stability, low current arc stiffness, and is less sensitive to arc length variation. The arc length can be varied up to 20 mm without adversely affecting the arc stability which may cause excessive arc spreading thereby have effect on bead width or heat concentration at the work (Lucas, 1990; Tesang et al, 2003).

2.3 Process Parameters

Welding parameters, namely welding current, welding speed, stand-off distance, nozzle diameter, etc. contribute significantly in governing penetration capability, energy density and temperature distribution in the weld, thereby influencing the microstructural evolution of material. In this section, the effects of various process parameters are reviewed with the objective to figure out the most influencing process parameters in MPAW process.

2.3.1 Welding current

Weldment width increases with increase in current. On the other hand, the variation in voltage with the increase of continuous current is almost constant, since arc is constrict and approximately columnar in nature. The variation of weld bead width is significant with welding current at lower welding speed. The parameters which can control the weld bead geometry are mainly the welding current and welding speed (Larson, 1965).

2.3.2 Welding speed

The welding speed has significant effect on shape and size of pore. At low welding speed, the weld metal will remain in liquid state for longer period. The longer period results in weld pool supersaturating with hydrogen present in the parent metal and thereby favors nucleation, growth, and escape of the grown bubbles from the molten metal. On the other hand, with high welding speed, since the weld metal remains in the liquid state for shorter time, there is not enough time for growth and escape of the hydrogen bubbles. Under this condition, though the pore density is high, the sizes of the pores are small. This has effect on the mechanical and metallurgical properties of the weldment (Larson, 1965).

2.3.3 Stand-off distance

Tseng *et al.,* (2012) studied the MPAW process on AM 350 (UNS S35000) precipitation hardening alloy of thickness 0.1 mm to produce an edge joint. They studied static volt-ampere characteristics, influences of; (i) shielding gas on arc characteristic, (ii) nozzle stand-off distance and (iii) process parameters on weld geometry. They found that the slopes of volt ampere characteristics are almost same and arc stand-off distance had negligible effect on weld width to penetration depth.

2.3.4 Plasma gas

Welding could not be carried out at a plasma gas flow rate less than 0.3 L/min, since sufficient arc energy for the creation of fusion zone could not be generated. On the other hand, arc-induced melting of the plasma nozzle, burning of weldment, undercut and porosities were observed at high plasma gas flow rate (Prasad et al., 2011). Argon is the preferred as plasma gas due to its low ionization potential which ensures dependable

pilot arc and reliable starting of the arc. Plasma gas also prevents the electrode from contamination (Chang, 2008). The diameter of the orifice and flow rate of plasma gas have great influence on the keyhole diameter. As the plasma gas flow is increased, the rear side width of the keyhole increases. The stability of the arc changes with the flow rate of plasma gas. However the stable state of the keyhole formation depends on the process parameters like welding current and welding speed (Zhang and Zhang, 1999).

2.3.5 Shielding gas

Shielding gas purity can have significant effect on welding quality, weld bead coalescence, weld surface appearance, weld colour and porosity level (Karimzadeh et al., 2005). The shielding gas flow rate should ensure prevention of gas entrapment in the fusion zone and subsequent protection of the weldment from oxidation (Prasad et al., 2011).

2.4 Plasma arc welding of stainless steel materials

Tseng *et al.,* (2003) investigated the effect of process parameters such as welding speed, arc current, arc length, argon shielding gas, and clamp distance of MPAW process on the weld bead geometry and quality of stainless steel 304 edge joint weldments. They also studied the effect of hydrogen in shielding gas on weld morphology and arc characteristic. The experimental results reveled that collimated arc shape was mainly responsible for the weld morphology. Yoshioka *et al.,* (1993) discussed the welding of AISI 304 stainless steel plate of 0.1 and 0.3 mm thickness with high power density (1.1×10^4 W/mm^2) using nozzle diameter of 0.1 mm and 0.2 mm. They showed that welding capability does not depend on the stand-off distance. Current was varied from 1 A to 3 A for 0.1 mm thickness and 7 A for 0.3 mm plate thickness. They found relationships between plasma gas flow rates and weld width. Bharatha et al., (2014) investigated the effect of process parameters on the weld bead of AISI 316. Zhang, **(**1999) investigated the stability of keyhole plasma arc welding on 3 mm thick SS 304 material on flat position. Understanding of the keyhole is critical for obtaining good weld quality. The weld pool and the keyhole were simultaneously observed during the welding. The results revealed that by increase in the welding current and decrease in welding speed did not affect the width of the keyhole. The keyhole width does not give adequate information about the stability of the keyhole. Tam et al., (1989) studied

mechanized plasma arc butt welding of thin gauge mild steel sheet experimentally and theoretically. Huang (2011) studied and compared the influence of activating flux on the arc profile, weld morphology, microstructure and angular distortion of tungsten inert gas welding and PAW. They found that the penetration capability of arc welding on stainless steel is highly dependent on the activating flux. He also showed that depth/width ratio of the weld affect the angular distortion.

Lee et al., (2004) used a split-Hopkinson pressure bar to study the effects of strain rate on weld qualities. They used optical microscope, SEM, and TEM techniques to study the fracture characteristics and microstructure of the plasma arc welded SS 304L Weldment. The results revealed that the strain rate and the mode of welding current had an influence on the impact behavior. It was demonstrated that the flow stress increased with increase in strain rate at a constant strain. With an increasing strain rate martensite increased. They also observed higher dislocation density in the fusion zone. Urena et al., (2007) investigated butt welding of 2205 duplex stainless steel sheet using melt-in mode and keyhole mode welding. They studied the influence of welding condition on the bead geometry and ferrite contain for each mode of operation and net minimum energy required in PAW welding to get superior metallurgical weldability.

Luo et al., (2002) analyzed the surface microstructure and polarization curves in a NH_2SO_4 solution of steel Cr19Ni9 weldment joint by submerged arc welding and MPAW. Result showed that the heat affected zone and the fusion zone had a lower corrosion resistance than the parent material, while the submerged arc welded joint had increased corrosion resistance. This increase in corrosion resistance is due to the rapid solidification of the melted layer. Rapid solidification of the melted layer refines its microstructure, decreases micro segregation and inhibits the precipitation of chromium carbides at the grain boundaries. Tovar et al., (2009) studied the corrosion behaviour of 316L stainless steel materials, welded by MPAW technique, under four flowing conditions in basic (LiBr) and acidic (H_3PO_4) solution by polarization measurements. Study revealed that the materials welded with backing gas and without filler alloy exhibited better corrosion resistance. Tovar et al., (2011a) investigated general corrosion behaviour of MPAWed AISI 316L material in phosphoric acid at temperature range of 25–60 °C and Reynolds number of 1456. They found that the microstructure of the weldment is modified due to the MPAW. The current density value obtained from polarization curve increased with temperature. ZRA tests showed the highest IG value at

60 °C temperatures and nearly zero for all other temperatures. Tovar et al., (2011b) also investigated the effect of MPAW on microstructure and pitting corrosion in different weld zone of AISI 316L material in heavy LiBr brine. The results showed that the corrosion resistance was very poor in the heat affected zone. They found that there was a relation between the effects of the MPAW process on the microstructure and their pitting corrosion resistance. The fusion zone possessed vermicular morphology characterized by columnar grains containing delta-ferrite. Both the heat affected zone and base metal exhibited an austenitic microstructure. They found weaker micro hardness value in the HAZ and fusion zone compare to the base metal. Multi corrosion attack occurred in the fusion zone due to micro-segregation of Cr at the ferrite-austenite inter-phase boundaries.

Prasad et al., (2011b) studied the effects of MPAW process parameters namely, back current, peak current and pulse width on the weld quality characteristics such as microstructure, weld pool geometry, grain size, tensile properties and hardness of SS 304L thin sheet. The grain size in the fusion zone and heat affected zone were found to be around 45 µm. The tensile properties were found better than the parent metal. Prasad et al., (2011c) also investigated the effects of process parameters like back current, peak current and pulse width on the tensile strength of thin Inconel 625 sheets weldment joint by MPAW process. They used central design matrix to carry out the experiments by selecting four factors in five levels. They also developed mathematical model using surface response method and the developed model was further checked by analysis of variance technique. They found that UTS was more sensitive to the peak current and pulse current. Prasad et al., (2011d) developed mathematical model for prediction of weld pool geometry of SS 304L sheets welded by MPAW process. They also developed mathematical model to predict the grain size and hardness of SS 304L welded sheet (Prasad et al., 2011e) and Inconel 625 welded sheet (Prasad et al., 2011f). Tsuchiya et al. (1973) welded 16 mm thick mild steel plate using PAW. They designed a large plasma torch to control the equipment to carrying 1000 A current with straight polarity and used copper backing plates.

Kim et al., (2011) investigated the effect of hybrid laser and PAW welding process for welding zinc-coated steel. The zinc vapour generates from the lapped surface which expeled the molten pool and the expulsion causes numerous weld defects, such as spatters, porosity inside the weldments and blow holes on the surface of the weldments.

They suggested laser-arc hybrid welding process as an alternative method for the lap welding of zinc-coated steel because the arc can preheat or post-heat the weldment according to the arrangement of the laser beam. They investigated the effect of laser-arc arrangement, laser-arc inter-spacing distance and arc current using a full-factorial experimental design. It was found that the heat input from plasma arc is reduced by 40% compared to laser-TIG hybrid welding process.

2.5 Plasma arc welding of non-ferrous materials

Voropai et al., (1971) developed a technique for investigation of butt welding of asbestos metal gasket which is made of aluminium of thickness 0.2-0.3 mm. They used pulsed MPAW at low current with steady stable arc which destructed the oxide film on the joined metal. Pure argon gas was used as plasma gas with purity of 99.98 % and helium as protective gas with purity more than 99.5%. Su et al., (1997) studied plasma transferred arc welding for repairing of IN-738LC super alloy components. Tensile tests and micro-hardness test were conducted on the welded specimens. Tensile test was conducted at room temperature, 760 °C, and 980 °C. Microstructures and shape of the weldment were studied using SEM, EDS, EDS and optical microscope. They found 96% weld strength compared to the IN738LC base materials. IN-738LC is considered susceptible to weld cracking during fusion welding, but using a low-heat input they could minimize cracking. Vander et al., (2003) investigated the weld quality of similar (NiTi to NiTi) and dissimilar (NiTi and haste alloy) materials using PAW. Mechanical property deteriorated after welding of NiTi material. In the investigation of dissimilar welding, they found that the fusion zone contains a number of brittle phases which decrease the weld quality. They concluded that welding of two shape memory alloys with different transformation temperature is challenging. Plasma welding of NiTi to NiTi does not influence the Ni/Ti ratio in the weld. Fusion welding of NiTi to Haste alloy C276 and stainless steel is extremely difficult. The NiTi has a lower melting point than the other materials. Brittle phases are formed close to the fusion line and there is a tendency of the NiTi to absorb elements from the Haste alloy C276 and steel.

Karimzadeh et al., (2005) investigated the influence of MPAW process parameters such as welding speed, welding current and flow rates of shielding and plasma gases on grain size and porosity in 0.8 mm thickness Ti6Al4V alloy welded joint. Direct current straight polarity with 1 mm diameter electrode was used during the

experiment. Metallographic study reviled presence of primary β grain in the fusion zone. The measured grin size of the weld indicated that at certain threshold energy the phase transformation take place. The SEM and optical microscopy studies showed some porosity in the fusion zone which was due to the release of hydrogen gas from the molten weld zone. This study also demonstrated that the welding could not be carried out at a plasma gas flow rate less than 0.3 L/min, since sufficient arc energy for the creation of fusion zone could not be generated. With high plasma gas flow rate excessive heat was produced which lead to burn through of the base metal. They concluded that the selection of shielding gas flow rate is a complex process and needs detail investigation. Prasad et al., (2011a) welded aluminum alloy using variable-polarity PAW process. They studied the influence of process parameters such as welding current, welding speed, torch height and plasma gas flow rate on the back melting width, front melting width and weld reinforcement using factorial design approach. Chen and Xu, (2011) studied the influence of heat input on the weld quality of Ti-6Al-4V alloy sheets joint using PAW. The microstructures, facture surfaces and micro-hardness of the welded joints were examined by optical microscope, SEM and Vickers micro hardness tester. They compared the result with gas tungsten arc process. In PAW, they found reduced prior-beta (β) grain size, less hard martensite phases, better toughness and higher hardness in the fusion zone due to less heat input.

2.6 Modelling of plasma arc welding process

Keanini, (1993) developed 3-dimensional finite element model for PAW process. The model used to calculate temperature and material flow distribution of the weld pool. The results revealed that flow in vertical cross sections is dominated by a large jet driven vortex. The competing effect of jet shear and surface tension results in the formation of a stagnant region at the top of the weld pool. Startsev, (1997) investigated the interaction between the plasma welding arc and laser radiation. He used equations of continuity, momentum and energy of viscous flow, electric current flow and laser radiation transfer to develop numerical model. Sun et al., (2011) developed a 3-dimensional transient model to analyse the periodic changes of the temperature field, keyhole shape & dimensions and weld pool geometry during PAW process. For numerical analysis of the temperature fields an adaptive, combined and volumetric heat source was proposed. The predicted information of the temperature profiles, weld pool and key-hole geometry was

useful for optimizing the multi process parameters in the controlled pulse key holing PAW process. John and Mckelliget, (1992) developed a mathematical model to predict the velocity, temperature and electromagnetic fields inside the plasma torch, as well as the motion and thermal histories of particle injected into the torch. It was demonstrated that high particle feed rates which are important for industrial scale materials processing applications.

Rajamani et al., (2006) did experimental and computational analysis of heat transfer in atmospheric pressure, medium temperature range (1200 to 1600 K) and plasma flow over an aluminum cylinder to determine the degree of ionization in the plasma flow. Kotalik, (2004) developed a model to analyze the flow of argon plasma inside and outside the discharge chamber of a cascaded plasma torch. Foest et al., (2005) studied the effect of plasma appearance on temperature field, arc force, and welding residual stress using numerical analysis and experiment. They simulated welding arc and weld pool behaviour. Trelles et al., (2009) developed mathematical model of DC arc plasma torch to understand the physical processes involved in the operation. The mathematical models covered thermodynamic, chemical non-equilibrium, turbulent and radiative transport phenomena. Xu et al., (2009) developed a model to simulate the electro-magnetic phenomena and fluid field in MPAW process. They showed the effects of the nozzle necking and welding current of micro plasma arc on the arc electro-magnetic field distribution and concluded that the process parameters have significant influence on distribution of current density and electromagnet force. Experiments were conducted on fine sheet of 0.1 mm thickness stainless steel. Shinichi et al., (2009) studied the numerical simulation of the PAW heat source. They showed that the maximum electrode temperature gradually increases during EP peak current due to heat developed by the electron condensation to the electrode surface and decreases during EN peak current due to cooling caused mainly by thermionic electron emission. When EN ratio is less, the electrode get maximum temperature and get during EP current of electrode.

Karimzadeh et al., (2006) investigated the effect of epitaxial grain growth on the microstructure in the weldments of Ti6Al4V thin sheet through neural network modelling. The MPAW was performed by varying different parameters such as welding speed, welding current, plasma gas flow rate and shielding gas flow rate. The neural network model was developed to predict grain size of the fusion zone at various current

and speed parameters. They observed that for a lower energy input, grain growth of β-phase in the HAZ could be restricted by α-phase. The presence of small fraction of α-phase was enough to prevent the growth of β-phase in the fusion zone and HAZ. Chai and Hsu (2001) developed a fuzzy radial basis function neural network for an intelligence decision support system in PAW process. The system solved problem related to time consuming in back propagation neural network, fluctuation in the value of optimized parameters during welding using linguistic term for prediction of weld quality. Zhang and Niu, (2000) used artificial neural network with back propagation training algorithm for the optimization of PAW process.

Wang et al., (2002) developed an online quality monitoring system for the PAW process. Detection and analysis of arc signal is a promising approach for obtaining quality weld which improves the productivity and costs. It was shown that the power spectra of the arc signal especially in the low frequency part (0-100) Hz greatly varieties with the variation of the weld pool. Two algorithms were developed to detect the behavior of key hole. Wang et al., (2010) developed a multi-control system for controlling the various parameters in MPAW to get good quality weld on ultra-thin sheet. They optimized the parameters such as peak current, base current, arc ending current, arc striking current, pulse duty cycle, pulse frequency, welding current upslope and down slope time, pre gas supply time and post gas supply time for joining ultra-thin sheet using MPAW.

Hsiao et al., (2008) optimized the process parameters such as welding speed, welding current, torch stand-off distance and plasma gas flow rate in PAW process using grey Taguchi method. They considered root penetration, width of weld groove, and weld pool undercut as quality parameters. There was 31.8% improvement in the Grey relational grade. Bharatha et al., (2014) investigated the effect of process parameters on the weld bead geometry of AISI 316 weldment. ANOVA technique was used to identify the effect of welding speed, current, electrode diameter and root gap on the strength of the weldment. It was found that the welding speed and current are the most influencing parameter for the wending strength.

2.7 Laser welding of similar and dissimilar materials

In the recent time, parts and components of industrial products are being made more small-scale for sustainable manufacturing. This creates an increasing need for micro-joining processes. Laser beam welding process is considered as most suitable welding process in this regards because it permits accurate heat control compared with other arc welding processes. It is capable of welding any type of material and in any joint configuration. Saha and Waghmare (2020) welded 0.2 mm, 0.56 mm and 0.85 mm thick SS-316 sheets using Ytterbium fiber laser in butt joint configuration. They considered UTS, weld bead width and micro-hardness as weld quality parameters. They found that the composition of base material and heat input significant control the weld quality and laser power, welding speed and focal distance are the significant process parameters. The energy required for full penetration increased with workpiece thickness. Due to grain refinement and δ-ferrite formation, the micro-hardness values were higher in the fusion zone. Kumar et al. (2017) welded 1.5 mm thick AISI 304 and AISI 316 similar materials using Nd:YAG laser in butt joint configuration. They considered laser power, pulse width and welding speed as input parameters and UTS weld bead width and hardness as weld quality parameters. They observed that the pulse width, material composition and heat input significantly control the grain size and phase fraction. They also observed finer grain structure with higher mechanical properties at low energy input compared with the higher energy input.

Cui et al. (2013) studied laser welding of 3 mm and 6 mm thick SS304 plates. They found narrow ‘Y’ shape weld bead without macro defects with welding speed of 20 mm/s and 2kW laser power. Zhang et al. (2020) studied the influence of laser power on the weld bead geometry, mechanical properties and microstructure of 6 mm thick high strength low alloy steel in laser welding. Ventrella et al. (2010) studied laser welding of 0.1 mm thick SS-316L foils by varying pulse energy. They observed increasing weld strength upto certain pulse energy and then decreased. Tan and Shin (2015) studied the laser keyhole welding experimentally and numerically for joining 0.2 mm thick AISI 304 sheet. They found highest welding productivity with medium welding speed and higher power. The austenite columnar dendrite was observed in the fusion zone and decreasing grain size with cooling rate. Liao and Yu (2007) investigated laser spot welding of 0.8 mm thick SS-304 sheet by varying laser energy and incident angle. Chatterjee et al.

(2019) did laser welding on 0.45 mm thick AISI 316 sheet. They used laser pulse duration, current and welding speed as input parameters and welding strength, hardness, residual stress and surface roughness as weld quality parameters. Baghjari and Mousavi (2013) welded SS-420 rod of 20 mm diameter using laser welding process. To reduce the hardness of the fusion and HAZ, post welding heat treatment was carried out.

2.8 Summary

The survey of available literature is carried out with the intention to develop prior knowledge about the process and to track the trend in the current research in PAW and MPAW. The survey leads to the impression that efforts made in welding thin stainless steel sheets using MPAW process is less compared to other processes. The survey also leads to the impression that welding of SS 316L sheet using MPAW process is very limited. The available literature seems to concentrate less on estimation of quantitative contributions of each process parameters and their interaction on the weld qualities. There is no attempt to identify outliers prior to analysis in welding. Hence, it is regarded as the possible thrust area for conducting the further research and attempted in the present study. The survey also discloses various heat treatment methods adopted for elimination/minimization of residual stress and homogenization of microstructure in the welded samples. However, no remarkable attempts are found that deals with heat treatment of thin welded sheet. Therefore, this study also motivates to investigate the post welding heat treatment of thin SS 316L sheets joint by MPAW process.

Chapter 3

Experimental Procedures

3.1 Introduction

This chapter outlines materials selected for MPAW experiments, methods used for testing of welded samples for measuring different weld quality characteristic and post weld heat treatment technique adapted to improve the welding quality. In the present study, welding current, welding speed and stand-off distance are selected as the process parameters. After the selection of suitable levels for each parameter, a full factorial design of experiment is implemented for conducting the experimental runs. Once the experiment is completed, test samples are prepared from the welded specimens for the measurement of mechanical properties namely, micro-hardness, ultimate tensile strength (UTS), yield strength and percentage of elongation. Elaborate explanations are also given for macro-microstructural analysis. Details of different experimental procedures followed during the present research work are highlighted in the following sections.

3.2 Design of Experiment

Design of experiment (DOE) is a statistical technique used to investigate the effects of multiple factors (also called variables or parameters) on the responses, simultaneously and economically. DOE is a highly effective technique wherever it is suspected that the performance of a process or product may be controlled by more than one variable. Among the available DOE techniques full factorial design, which considers all possible combinations of the levels of the variables, is the best. This would work fine, apart from the number of required experimental runs is very large. It is usually impractical to carry out that

large amount of experiments, particularly in welding. In these conditions, Taguchi orthogonal arrays or fractional factorials are used. The choice of a DOE technique depends on the objectives of the study and the number of parameters to be examined. The number of factor considered is only three. The objectives of this work are to explore the effects of input parameters on the welding quality and develop relationship between weld quality and process parameters. Therefore, the experimental runs are designed using full factorial method. Because this method allows studying the effects of main factors and interactions between the factors on the responses. The following steps are used to conduct the experiment in this research.

Step 1: *Identification of quality characteristics* – The quality of welded joint is evaluated by many characteristics, such as weld bead geometric parameters, tensile properties, hardness, distortion, deposition efficiency, microstructure etc. Among these bead geometry parameters (bead area, bead width, bead height and reinforcement) plays significantly role in deciding the mechanical properties of the weld (Kumar and Parmar, 1986; Zhang et al. 1996; Correia et al. 2004). Welded joints are highly inhomogeneous and it is considered to be the weakest link in many engineering structure. So, tensile property (UTS, yield strength and percentage elongation) of welded structure is very important mechanical property. Hardness is another important response parameter. It usually takes into account the resistance to localized plastic deformation induced by mechanical indentation. And obviously, weld bead microstructure is essential to analysis and define the variation of mechanical properties. Therefore, in this research, seven weld bead geometry characteristics, namely area of fusion zone, top bead width, bottom bead width, bead height or penetration, reinforcement, width of left side of heat affected zone (HAZ) and width of right side HAZ, three tensile properties (UTS, yield strength and percentage elongation), micro-hardness and microstructure are considered as weld quality characteristics parameters.

Step 2: *Identification of control factors* – The control factors refer to those which can be easily varied and controlled by the operator or designer in regular working environments. The MPAW process is influenced by many process parameters where

selection of suitable combination of different parameters is important for successful welding. The effect of process parameters is often investigated by measurement of various mechanical properties of the joints that include UTS, yield strength, percentage elongation, hardness of the joints, etc. Apart from these mechanical properties, weld dimensions are also sometimes used as the index for studying the effect of control parameters on the welded joints. Various process parameters involved in MPAW process is mentioned in Chapter 2. Form the preliminary investigation and information from published literature, it is observed that welding speed, welding current and nozzle to workpiece distance or stand-off distance (SOD) are the major influencing factors in the PMAW process. Hence, these three welding parameters are considered as the controllable factors in this research.

Step 3: *Selection of factor levels* – A sufficient number of trial experiments (mentioned in the Section 3.5) have been carried out to find suitable welding window for MPAW of 0.5 mm thick stainless steel sheets. The primary purpose for the trial experiments was to find the range of the welding parameters so that it would be safe for setting parameters at levels where the welding would not end in a failure (such as melt-through, unstable welding, heating without melting and discontinuous arching) half way through an experiment. The process parameters or control factors and their notations with their various levels are shown in **Table 3.1**.

Table 3.1 Welding parameters and theirs various levels used in developing design matrix

Sl. No.	Parameter Name	Notation	Unit	Level 1	Level 2	Level 3	Level 4
1	Welding current	WC	A	8	9	10	11
2	Welding speed	WS	mm/s	2.7	3.7	4.7	–
3	Stand-off distance	SOD	mm	1.0	1.5	2.0	–

Step 4: *Development of an appropriate design matrix* – A three factors, three/four mixed levels full factorial design matrix is considered in this work. This design requires thirty-six experimental runs. Four levels are considered for welding current and three levels for each welding speed and stand-off distance. The design matrix is shown in **Table 3.2**.

Table 3.2 Design matrix of full factorial design

	Process parameters		
Exp. No.	**Welding current (A)**	**Welding speed (mm/s)**	**Stand-off distance (mm)**
1	8	2.7	1
2	8	3.7	1
3	8	4.7	1
4	9	2.7	1
5	9	3.7	1
6	9	4.7	1
7	10	2.7	1
8	10	3.7	1
9	10	4.7	1
10	11	2.7	1
11	11	3.7	1
12	11	4.7	1
13	8	2.7	1.5
14	8	3.7	1.5
15	8	4.7	1.5
16	9	2.7	1.5
17	9	3.7	1.5
18	9	4.7	1.5
19	10	2.7	1.5
20	10	3.7	1.5
21	10	4.7	1.5
22	11	2.7	1.5
23	11	3.7	1.5
24	11	4.7	1.5
25	8	2.7	2
26	8	3.7	2
27	8	4.7	2
28	9	2.7	2
29	9	3.7	2
30	9	4.7	2
31	10	2.7	2
32	10	3.7	2
33	10	4.7	2
34	11	2.7	2
35	11	3.7	2
36	11	4.7	2

Step 5: *Experimentation using the design matrix and measurement of responses* – The MPAW experiments are carried out as per the design matrix (**Table 3.2**) at random order, to avoid the possibility of systematic and personal errors infiltrating

into the system. The detailed description of the experimental procedure and determination of the responses are given in section 3.3 and section 3.7, respectively.

Step 6: *Development of response models* – The details of the developed mathematical models and their validations are described later in Chapter 4. The effect of the considered individual factor and interaction between factors are also discussed.

3.3 Experimental Setup Development

The welding experiments and weld quality measurements reported in this thesis were conducted at the Department of Mechanical Engineering, Central Workshop and Central Instrumentation Facility, belonging to IIT Guwahati, India.

It is evident that difficulty in fusion welding process increases with decreasing workpiece thickness. The issues such as edges mismatch and joint gap variation exaggerate with the decrease in thickness of the substrate materials to be welded. Therefore, the successful welding of thin sheet using MPAW process depends on the availability of required equipment such as, power source, cooling unit, welding torch; accurate position of the welding torch with respect to the weld line, precise motion control, adequate fixturing and careful cleaning procedures. The welding machine used for the study is ARCRAFT Plasma Equipment's Pvt. Ltd. make semi-automatic digital micro plasma welding machine (Model: MP-50). The power source is a constant current source with 1 A – 50 A power supply. A tungsten electrode with a diameter of 1.2 mm and tip angle of 20° is used along with 1.2 mm diameter copper nozzle. Argon gas was used as both plasma and shielding gas at a flow rate of 2 liter per minute. The details of other factors which were kept constant for all the experiments are shown in **Table 3.3**. A photograph of the experimental setup is shown in Fig. 3.1(a). Adequate fixturing is also necessary for proper holding and positioning of the workpiece. A dedicated fixture (shown in Fig 3.1b) is designed and fabricated to conduct the welding experiments for this research. Two clamp plates are tighten over the workpiece sheets with the help of screws and copper backing plate at the bottom.

It is difficult to set a desired stand-off distance around 1-5 mm during the welding. Therefore, a setup is designed and fabricated to control the stand-off distance, shown in

Fig. 3.1(c). The welding torch is mounted on a plate which is clamped on a fixed arm. There is an apparatus to set the desired gap (*i.e.*, stand-off distance) between the welding torch and workpiece. The welding experiments are performed on a motor driven flat platform, shown in Fig. 3.1(d). The welding platform runs smoothly over an aluminium rail track. The speed of the working platform can be varied in the range of 1 mm/s to 10 mm/s. The work pieces are tightly hold using specially designed two mild steel clamps and thus reduced weld distortion.

The alignment of joint line with the welding electrode is an important factor to get consistent weld quality. In thin sheet welding, a small sideways displacement of the electrode results in improper welding since the size of the plasma arc is very small. A setup is fabricated (shown in Fig. 3.1e) to align the welding torch with the joint line before actual welding. The welding is performed perpendicular to the rolling direction of the sheet. The light scattering technique is used to identify the rolling direction, shown in Fig. 3.1(f). Light always scatter normal to the rolling direction of the sheet. The details of the machines and equipments, which were used in this work, are given in **Table 3.4**.

Table 3.3 Parameters considered with fixed level

Sl. No.	Fixed parameters	Value
1	Plasma gas type	99.9% Argon
2	Shielding gas type	99.9% Argon
3	Plasma gas flow rate during welding	2 Liter per minute
4	Shielding gas flow rate during welding	5 Liter per minute
5	Nozzle diameter	1.2 mm
6	Workpiece material	Stainless steel 316L
7	Material thickness	0.5 mm
8	Tungsten Electrode diameter	1.2 mm
9	Electrode tip angle	20 degree
10	Setback distance of electrode	1 mm
11	Water temperature of cooling tank	25 ^{0}C
12	Gas pre flow	2.5 second
13	Gas post flow	2.5 second
14	Secondary up slope and down slope current	2 second

Table 3.4 Detailed specifications of all the machines and equipment used in this work

Machine/Equipment	**Specifications**
Welding machine	Type: Micro Plasma Arc Welding machine Make: ARCRAFT Plasma Equipment's Pvt. Ltd. Model: MP-50
Optical microscope	Make: Carl Zeiss Model: Axiotech-100HD, 3D • Magnification: 500X-5kX • Table movement: 3-axis measuring system, reflected light measuring stage 75 mmx55 mmx50 mm • Tubes: Binocular phototube (Sliedentopf principle), 20°/23, 100 vis /100 doc • Camera: Axio-Cam and Axiovision 4.8.2 software in built
Dynamic UTM	Make: BISS Model: MEDIAN- 250 UT-04-0250 • Capacity: 250 kN, Actuator displacement:50 to 150 mm • 0–100 Hz cycling frequency • Hydraulic grips of 0-12 mm flat specimen and 3.5-19 mm round specimen. • Test: Tensile, compression, cyclic fatigue, fracture toughness, flexural, shear and three point bend test • Control mode: Load rate, elongation rate, strain rate, load hold • Testing method: Load control and position control (strain and displacement)
Hardness tester	Make: Buehler Model: Micromet-2101 • Indentation force: 1, 10, 50, 100, 300, 500, 2000 g force • Dwell time: 5 to 60 s at interval of 5 s
FESEM	Make: Zeiss, Model: Sigma • Specimen chamber:330mm inner dia, 270 mm height • Specimen weight: Up to 0.5 kg tilted; up to 2 kg not-tilted • Movement: X/Y = 125 mm, Z = 50 mm, T = –10° to +90°, R = 360° continuous • Specimen stage: 5-axis motorised Cartesian • Chamber detectors: Inlense, SE-2, NEBSD • Magnification range 300 X to 1000 kX
Heat treatment Furnace	Make: Metatherm furnce pvt. Ltd. Model: mtf-887 Power – 18kw, Max temp – 1400 ^{0}C
Grinding machine	Make: BUEHLER; Model: Automet- 250
Ultrasonic cleaner	Make-Buehler; Model: siplimet-2
Laser cutting machine	2.5 kW CO_2 laser cutting machine Make: LVD Company; Model: Orion 3015

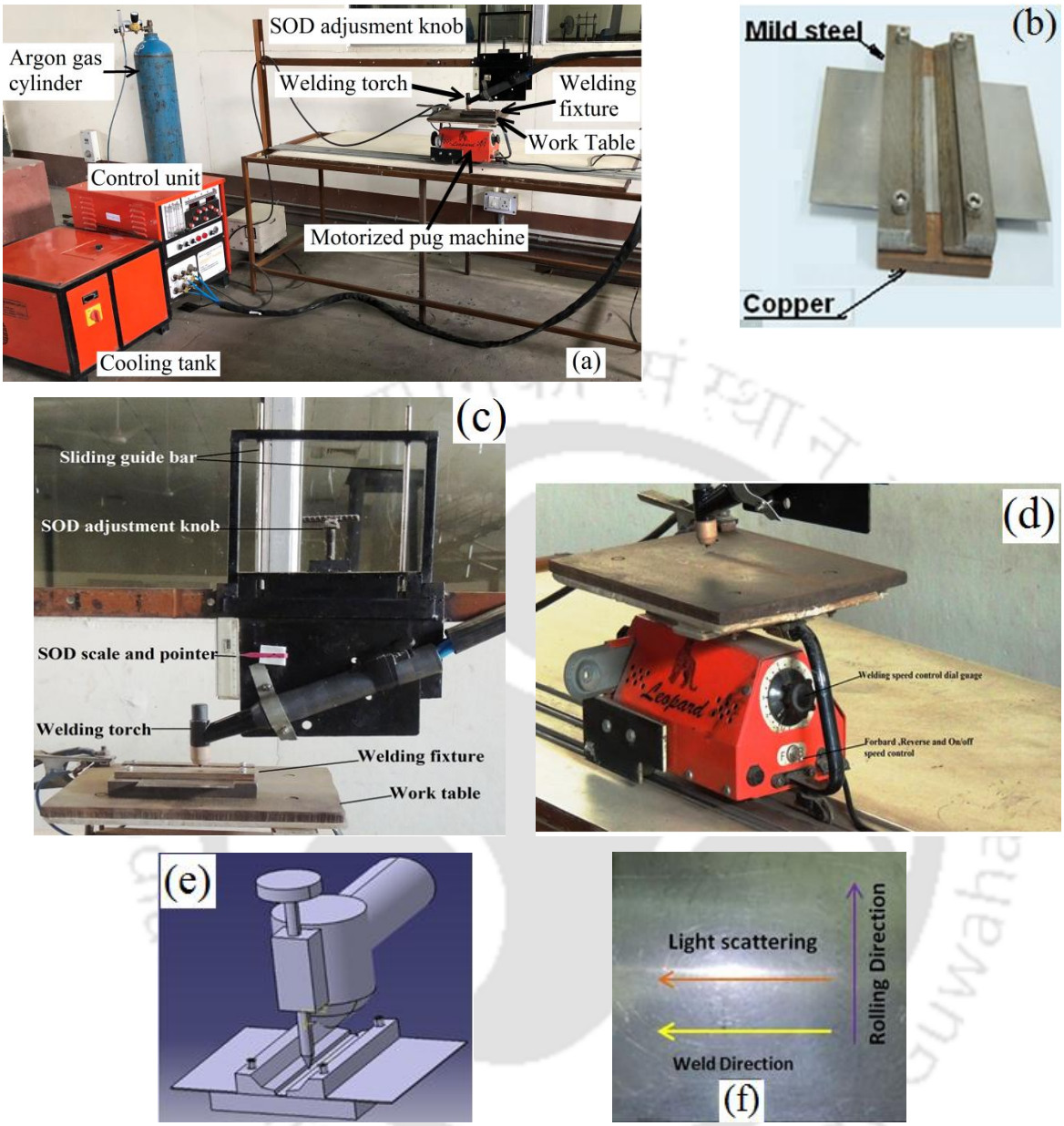

Fig. 3.1 (a) Complete MPAW setup (b) workpiece holding fixture (c) welding torch holder to set desire stand-off distance (d) motor driven welding platform (e) setup for weld line adjustment and (f) detection of rolling direction.

3.4 Sample Preparation for Welding

Austenitic stainless steel 316L sheet of 0.5 mm thickness was used as workpiece material. Two rolled sheets with length and width of 150 mm and 100 mm, respectively, of each were used to make single side square butt weld along the length. Energy dispersive X-

ray (EDX) analysis was performed to estimate the chemical composition of the base metal, which is shown in **Table 3.5**. The measured mechanical properties of the workpiece material are shown in **Table 3.6**. The welding specimens were thoroughly cleaned by emery papers and then acetone to remove surface oxides before welding. The edges were also properly matched to ensure zero gaps between the sheets to be welded. All the welding was carried out perpendicular to the rolling direction of the sheet.

Table 3.5 Chemical composition of workpiece material (in weight percentage)

C	Mn	Si	P	S	Cr	Mo	Ni	Fe
~0.03	1.10	0.50	0.10	0.10	17.40	1.90	10.40	Balance

Table 3.6 Mechanical properties of workpiece material

UTS (MPa)	Yield stress (MPa)	Percentage elongation (%)	Young's modulus (GPa)	Micro-hardness (HV)
720.1	338.7	74.05	203.9	168.0

3.5 Welding Experimentation

The fusion welding of thin sheets is quite challenging than welding thick plates. High heat is generated during the conventional arc welding processes, which in turn causes various issues such as burn-through, porosity, grain coarsening, distortion, buckling, and twisting of welded sheets, joint gap variation during welding, etc. Use of the proper welding process, joint gap and process parameters is one tool to address this issue. A feasibility study was conducted with varying welding current and speed to identify welding window for successful joining. The stand-off distance was considered as 1 mm and other parameters were considered as per **Table 3.3**. While identifying parametric envelops, four modes of welding namely: heating, partial welding, full welding and burn through (shown in Fig. 3.2) are observed visually. The feasibility window of welding current and speed for successful joints is shown in Fig. 3.3. A full depth penetration (good welding) was observed within 8 – 11 A welding current, below of that material did not melt whereas above 11 A current workpiece materials melted and holes were made. Also partial penetration was observed at high welding speed. The good welding was found in the range of 8 – 11 A welding current and 2.7 – 4.7 mm/s welding speed. Therefore with these feasibility ranges and information

from the published literature the design matrix is developed and main experimental runs are carried out as per **Table 3.2**. After the welding experiments, testing samples are extracted for various weld quality measurement (discussed in section 3.7) and post weld heat treatment operation (discussed in section 3.6).

Welding category	Photograph of welded surface	Schematic of welded section
Heating		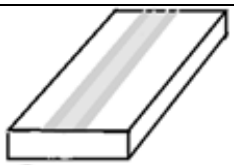
Partial welding		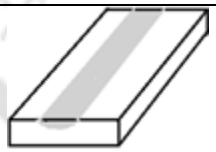
Full welding	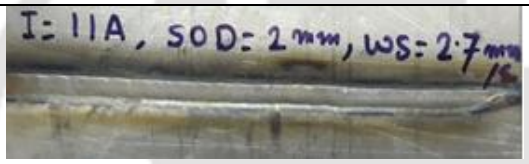	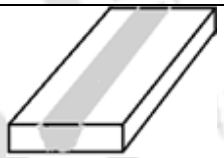
Burn through		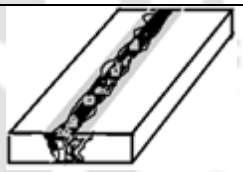

Fig. 3.2 Model of welded joints.

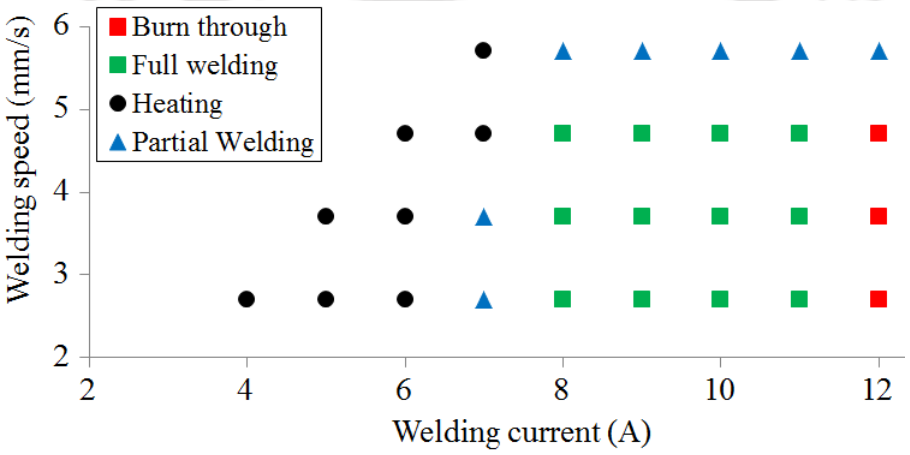

Fig. 3.3 Process window for MPAW of 0.5 mm thick SS-316L sheet.

3.6 Post Welding Heat Treatment Procedure

The high thermal gradient formed during the plasma welding process results in non-uniform microstructure across the weld region. This may lead to variation in the mechanical properties across the weld zone. In order to avoid this inhomogeneity in the mechanical properties, the welded samples were given post welding heat treatment. The welded samples were kept in a resistance heated muffle furnace and heated to 1000 ºC. The samples were then soaked at this temperature for 120 minutes and subsequently water quenched to room temperature. The heat treatment cycle was decided based on the standard heat treatment cycle followed for the SS 316L (ASM Handbook, 1991). Water quenching was followed to avoid the re-precipitation of chromium carbide which may occur during slow cooling in the temperature range 816 – 427 °C (ASM Handbook, 1991).

3.7 Determination of Weld Quality Characteristic

The experimental runs are conducted as per the design matrix shown in **Table 3.2**. After completion of the experiments, test samples are extracted to measure weld bead geometries, tensile properties, micro-hardness and microstructure. The details of sample preparations, measurement procedures and results obtained from these investigations are reported in the following paragraphs.

3.7.1 Metallographic Sample Preparation and Bead Geometry Measurement

To make a good sample that permits once to identify and study the weld bead geometry with an optical microscope, the following steps were followed. Single specimen was cut normal to the welding direction from each welded sheet; 3.5 cm way from the start and the end points, the location of the extracted sample is shown in Fig. 3.4. The cut surfaces were polished with coarse to finer grade emery papers (in order of 200, 400, 600, 800, 1000, 1200, 1500, and 2000 grade), followed by two-stage cloth polishing in wet condition by using alumina particles. The samples were washed between each polishing step using mild soap solution. After polishing, the samples were rinsed with alcohol and then etched with Glyceregia (15 cc HCl + 10 cc Glycerol + 5 cc HNO_3) to examine the bead geometry. Finally, the samples were again rinsed with water and alcohol to stop further

etching and to avoid stains and then they were dried with an air dryer. The polished and etched surface of the weld region was observed under an optical microscope and the weld bead geometry was measured using AXIOVISION software attached with the microscope.

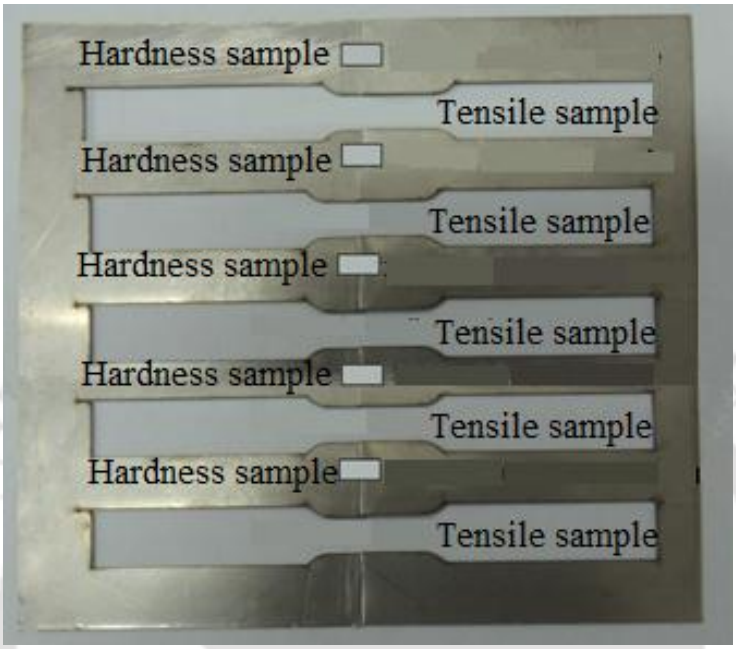

Fig. 3.4 Photograph of samples extraction for testing

A schematic diagram of the weld bead geometry without post welding heat treatment is shown in Fig. 3.5. A total of seven bead geometry parameters namely, area of fusion zone (A_{FZ}), width of top fusion zone (TW), width of bottom fusion zone (BW), penetration depth (PD), reinforcement height (RH), width of left side of HAZ (LW_{HAZ}) and width of right side of HAZ (RW_{HAZ}) were measured for each welding condition. The weld bead geometry parameters were not replicated. Typical photographs of selected weld bead geometries, without post welding heat treatment, are shown in Figs. 3.6(a) – 3.6(d). Different penetration and reinforcement scenarios can be seen in the macrostructure of the photographs. The measured weld bead geometry parameters for each welding condition, without heat treatment, are given in **Table 3.**7. Full depth of penetration was not observed in few welded samples. The widths of the bottom fusion zone of those samples could not be included for further analysis.

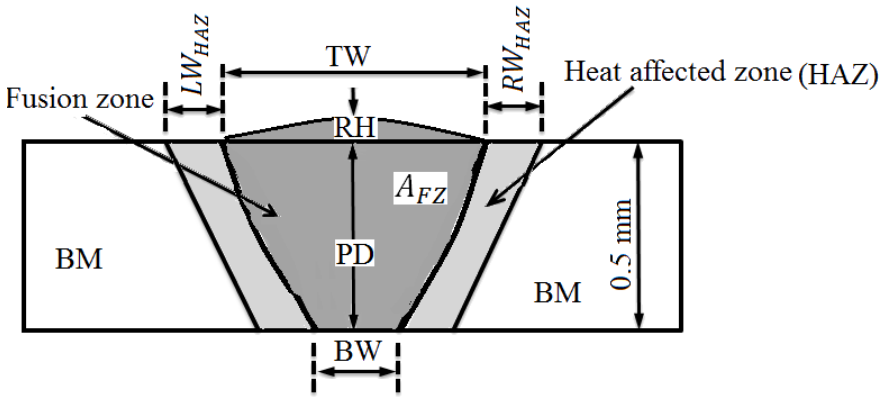

TW: Width of top fusion zone
BW: Width of bottom fusion zone
PD: Penetration depth
RH: Reinforcement height
A_{FZ} : Area of fusion zone
LW_{HAZ} : Width of left side of HAZ
RW_{HAZ} : Width of right side of HAZ
BM : Base metal

Fig. 3.5 Schematic diagram of weld bead geometry

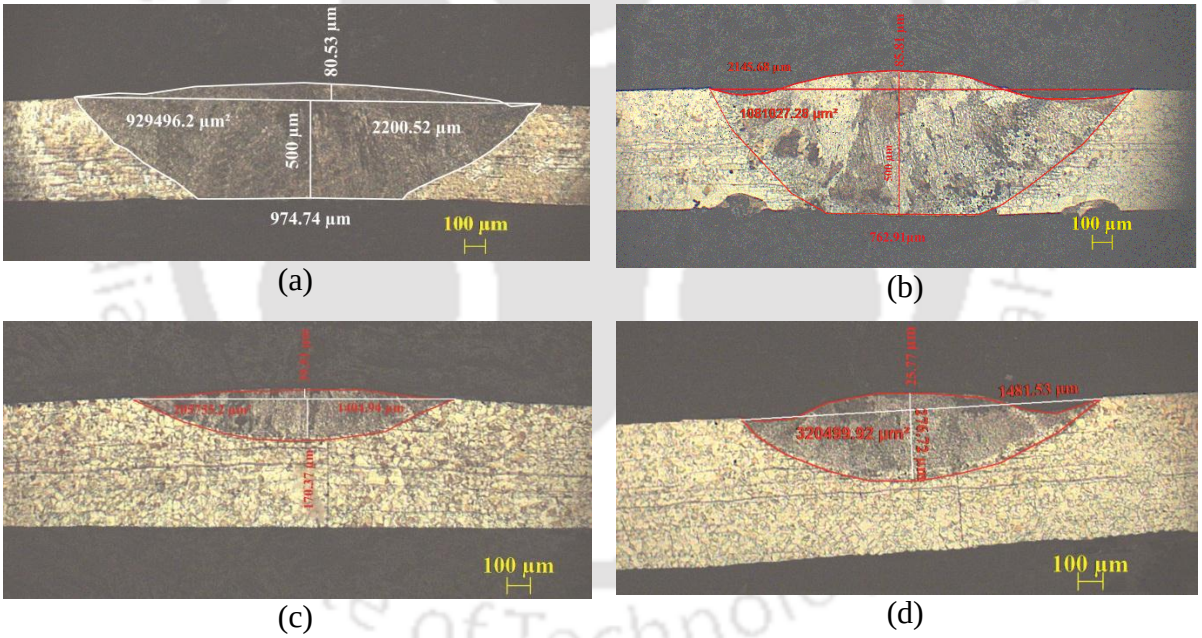

(a) (b) (c) (d)

Fig. 3.6 Sections of weld bead geometry under different welding conditions and without heat treatment: (a) Exp. No. 19 – Full penetration with reinforcement

(b) Exp. No. 7 – Full penetration with undercut

(c) Exp. No. 15 – Lack of full penetration with reinforcement

(d) Exp. No. 27 – Lack of full penetration with undercut

Table 3.7 Weld bead geometry parameters, without heat treatment, corresponding to Table 3.2

Exp. No.	A_{FZ} (μm^2)	TW (µm)	PD (µm)	BW (µm)	RH (µm)	LW_{HAZ} (µm)	RW_{HAZ} (µm)	Avg. HAZ width (µm)
1	556031.1	1650.40	409.88	–	65.12	101.45	98.45	99.95
2	351631.3	1332.81	360.66	–	48.13	116.12	114.34	115.23
3	132869.9	1279.03	138.29	–	29.63	140.79	141.79	141.29
4	684410.9	1721.03	513.71	–	75.13	92.50	89.40	90.95
5	402665.1	1295.19	387.99	–	70.07	119.50	120.50	120.00
6	230592.9	1300.23	247.11	–	36.91	85.76	79.56	82.66
7	1081027.0	2145.68	500.00	762.92	85.81	120.34	119.78	120.06
8	498951.0	1232.45	500.00	208.70	81.32	115.67	113.56	114.62
9	341326.9	1238.57	368.40	–	62.04	79.34	80.45	79.89
10	739472.8	1784.13	495.238	578.09	60.32	162.78	163.34	163.06
11	574240.7	1480.69	539.02	493.56	83.07	136.13	137.54	136.84
12	359548.9	1380.39	367.93	–	70.90	144.28	142.20	143.24
13	597896.1	1737.70	449.18	–	56.10	129.16	128.54	128.85
14	511847.6	1371.67	375.97	–	45.64	113.61	115.74	114.68
15	205755.2	1404.94	170.37	–	39.51	91.60	90.12	90.86
16	726727.1	1853.92	512.03	630.85	63.83	133.23	130.47	131.85
17	494019.3	1453.86	479.02	500.00	63.15	128.87	130.15	129.51
18	314558.8	1425.67	266.67	–	30.31	112.00	114.60	113.30
19	929496.2	2200.52	500.00	974.75	80.53	101.34	101.00	101.17
20	550409.9	1409.44	527.00	385.28	76.11	118.12	121.23	119.68
21	353970.4	1461.14	301.40	–	66.71	124.25	122.16	123.21
22	726722.6	1656.10	500.00	605.47	66.35	135.49	134.32	134.91
23	692466.8	1658.57	500.00	692.67	104.90	115.89	115.56	115.73
24	387008.1	1509.80	350.62	–	91.36	88.45	87.67	88.06
25	705009.2	1933.60	500.00	441.46	48.78	99.47	102.10	100.79
26	442752.6	1617.96	353.12	–	27.16	113.56	112.70	113.13
27	320499.9	1481.53	276.72	–	25.77	99.56	102.00	100.78
28	1066316.0	2222.39	500.00	732.35	53.66	123.11	125.45	124.28
29	376473.1	2049.72	488.89	–	41.98	122.96	119.75	121.36
30	342605.9	1540.58	359.35	–	31.26	99.56	96.40	97.98
31	1175547.0	2373.75	500.00	1053.68	68.46	180.31	184.45	182.38
32	723971.6	1810.16	500.00	770.80	60.98	142.03	140.71	141.37
33	430199.1	1620.45	408.78	–	46.34	26.00	84.49	55.25
34	1179010.0	2529.55	500.00	991.62	78.54	136.45	134.42	135.44
35	891934.6	2087.74	500.00	970.05	84.90	176.34	175.35	175.85
36	532550.2	1650.04	501.22	404.85	0.00	118.67	117.34	118.01

3.7.2 Micro-hardness measurement

The Vickers hardness test is mostly used for small parts and thin sections. This method uses a diamond indenter to make an indentation which is then measured and converted to a hardness value. A Vickers's micro hardness testing equipment (Make: Buehler, Model: Micromet-2101) with a square base pyramid shaped diamond indenter having 136° included angle is used for testing in the Vickers scale. The test is carried at 500 g load for 10 s dwell time. Test samples for measurement of micro-hardness of the welded specimens (both for post welding heat treated and non-heat treated welded samples) were cut normal to the welding direction. Then the extracted specimens were polished by using 100, 1200, 1500, 2000 grade emery papers. In this research, micro-hardness values were measured at three different layers namely, top, middle and bottom layers, which are along the cross section of the specimens. The scheme of micro-hardness measurement for both non-heat treated and heat treated samples is shown in Fig. 3.7. In each specimen, seven micro-hardness values were measured in the fusion zone, among them five points (P1, P2, P3, P4 and P5) in the middle layer one each in the top (P6) and bottom (P7) layers. Six values were measured in the heat affected zone, three in each side of the fusion zone.

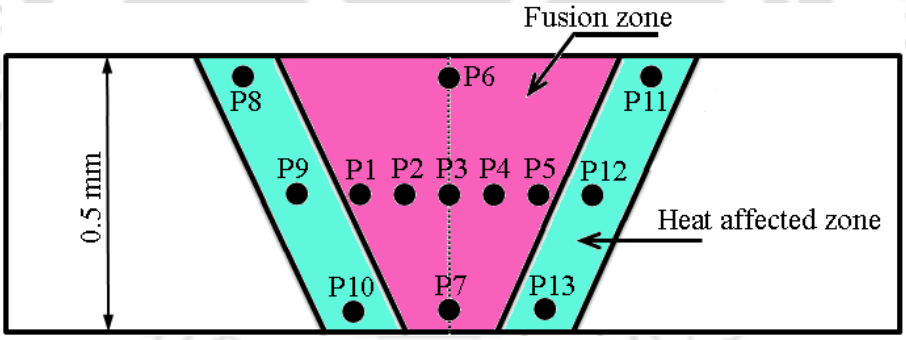

Fig. 3.7 Scheme for micro-hardness measurement of welded samples.

3.7.2.1 Micro-hardness of Without Post Welding Heat Treated Samples

A total of thirteen micro-hardness values were measured in each sample. For representation purpose photograph of a micro-hardness tested specimen is shown in Fig. 3.8. The measured hardness values in the fusion zone and HAZ are given in **Table 3.8** and **Table 3.9**, respectively, for the non-heat treated samples.

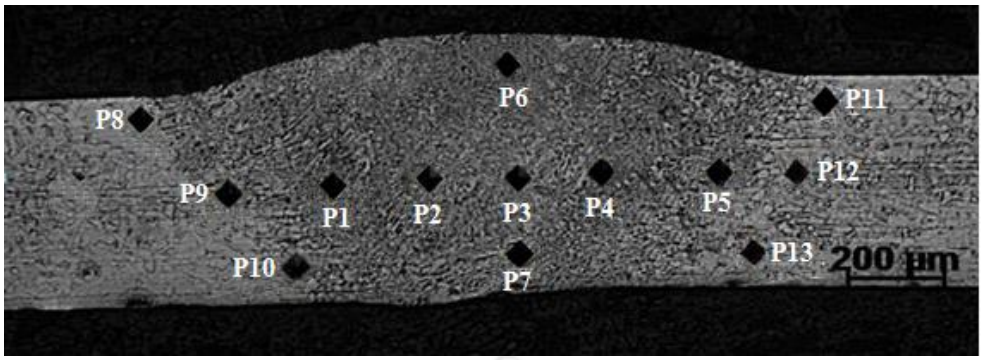

Fig. 3.8 Photograph of a hardness specimen with indentation marks (without post welding heat treated sample).

Table 3.8 Measured micro-hardness values of fusion zone, without post welding heat treated samples, corresponding to the parameters setting mentioned in Table 3.2

Exp. No.	P1	P2	P3	P4	P5	P6	P7
1	172.0	183.0	198.1	178.3	185.3	206.1	192.1
2	150.0	162.7	174.5	161.8	152.0	176.0	165.0
3	150.0	162.0	164.6	163.0	156.8	167.5	158.0
4	188.0	193.0	193.2	194.2	190.0	214.9	188.0
5	150.8	173.7	181.6	174.6	165.6	184.3	180.4
6	151.5	158.0	170.7	161.5	152.6	171.8	159.0
7	193.5	190.1	198.0	193.5	192.5	207.0	197.3
8	169.0	179.1	189.3	177.1	168.5	195.2	185.2
9	151.7	160.5	173.9	161.0	155.0	176.5	167.0
10	183.0	185.3	188.3	180.5	184.1	189.3	178.3
11	174.0	183.2	199.7	179.5	175.0	205.8	191.5
12	160.2	171.7	182.4	168.6	160.4	180.5	169.9
13	186.0	190.0	191.3	189.2	187.0	211.8	184.9
14	162.5	163.1	175.7	162.8	161.4	178.5	164.5
15	152.0	159.1	168.4	160.0	154.0	172.0	157.0
16	193.5	192.2	197.0	193.2	196.0	218.2	190.2
17	162.9	172.0	184.3	174.8	164.0	188.7	179.8
18	153.0	160.2	173.2	162.0	154.0	174.0	165.0
19	186.5	188.1	192.0	185.1	186.5	194.5	191.2
20	174.7	186.2	200.1	185.4	175.1	210.1	190.1
21	158.2	164.0	181.1	163.6	151.0	180.4	169.5
22	186.9	187.0	186.8	186.0	185.9	186.5	172.5
23	185.0	191.8	188.2	190.0	186.7	213.4	185.2
24	160.5	171.6	182.7	173.0	167.5	186.5	181.4
25	192.2	191.1	194.0	193.0	190.6	196.0	195.0
26	166.2	177.0	191.6	179.2	168.0	194.0	183.8
27	152.0	161.5	174.5	163.3	154.0	175.5	166.0
28	182.9	183.6	182.6	180.1	178.7	183.5	170.9
29	175.0	184.6	195.0	181.4	177.0	210.1	192.3
30	145.7	169.6	183.9	178.4	162.6	185.4	179.7

Exp. No.	P1	P2	P3	P4	P5	P6	P7
31	184.7	187.4	184.8	183.0	182.7	189.0	178.5
32	190.4	190.2	195.0	191.0	189.6	215.6	189.0
33	164.0	175.0	186.1	174.5	165.0	190.0	181.0
34	164.0	167.6	156.4	178.6	178.3	180.5	164.7
35	193.0	192.0	196.1	194.0	195.8	206.0	198.0
36	171.2	183.2	195.2	181.0	172.5	199.2	188.2

Table 3.9 Measured micro-hardness values of HAZ, without post welding heat treated samples, corresponding to the parameters setting mentioned in Table 3.2

Exp.	Left side of HAZ			Average left	Right side of HAZ			Average right
No.	P8	P9	P10	side hardness	P11	P12	P13	side hardness
1	180.2	171.7	190.4	180.8	176.1	174.2	192.0	180.8
2	153.0	152.0	149.7	151.6	154.6	151.5	148.6	151.6
3	145.0	155.5	156.0	152.2	150.2	156.0	154.0	153.4
4	173.0	170.6	164.5	169.4	170.9	173.2	168.4	170.8
5	162.7	155.1	172.0	163.3	157.5	156.5	162.6	158.9
6	149.0	152.0	146.0	149.0	151.2	153.0	147.0	150.4
7	170.2	173.0	170.0	171.1	171.9	171.6	169.2	170.9
8	171.7	163.9	180.1	171.9	172.3	162.5	181.4	172.1
9	151.2	154.5	148.4	151.4	150.0	153.6	149.5	151.0
10	160.1	166.0	160.9	162.3	159.0	164.5	159.8	161.1
11	181.6	173.9	189.0	181.5	183.2	174.0	191.0	182.7
12	158.0	158.2	163.6	159.9	150.7	164.5	160.2	158.5
13	170.0	167.0	160.0	165.7	167.5	173.0	163.0	167.8
14	159.2	160.0	160.2	159.8	146.6	154.1	149.7	150.1
15	148.6	150.0	147.6	148.7	147.0	151.3	149.0	149.1
16	174.5	173.0	166.2	171.2	175.5	174.1	167.3	172.3
17	165.4	158.0	176.2	166.5	166.0	156.5	174.0	165.5
18	150.0	152.5	147.0	149.8	148.5	151.0	146.5	148.7
19	166.3	172.5	165.3	168.0	164.8	170.1	166.4	167.1
20	177.0	168.2	188.0	177.7	179.0	170.2	190.1	179.8
21	160.3	154.7	153.8	156.3	158.0	155.4	152.5	155.3
22	160.8	162.0	156.9	159.9	163.9	160.5	158.0	160.8
23	171.1	168.0	162.0	167.0	168.0	169.0	167.6	168.2
24	163.8	156.5	174.0	164.8	164.3	157.0	164.5	161.9
25	166.0	167.2	165.0	166.1	169.5	166.3	162.0	165.9
26	169.2	161.0	179.5	169.9	170.0	160.5	178.0	169.5
27	150.2	153.5	148.4	150.7	147.0	150.6	148.5	148.7
28	159.0	161.2	155.9	158.7	156.5	160.0	157.5	158.0
29	183.8	174.0	190.0	182.6	182.0	173.5	188.4	181.3
30	160.3	154.0	164.1	159.5	158.7	153.8	160.0	157.5
31	158.7	160.4	154.3	157.8	160.0	158.4	153.1	157.2
32	173.2	171.2	165.0	169.8	174.0	171.6	166.2	170.6
33	166.0	159.2	177.0	167.4	165.5	160.0	178.4	168.0
34	150.1	154.0	151.3	151.8	154.9	153.1	150.2	152.7
35	170.0	172.0	169.2	170.4	171.0	173.0	170.0	171.3
36	175.2	166.0	185.0	175.4	178.2	164.0	184.2	175.5

3.7.2.2 Micro-hardness of Post Welding Heat Treated Samples

A total of thirteen micro-hardness values were also measured as per Fig. 3.7 of the post welding heat treatment samples. For representation purpose photograph of a micro-hardness tested specimen is shown in Fig. 3.9. The measured hardness values in the fusion zone and HAZ are given in **Table 3.10** and **Table 3.11**, respectively.

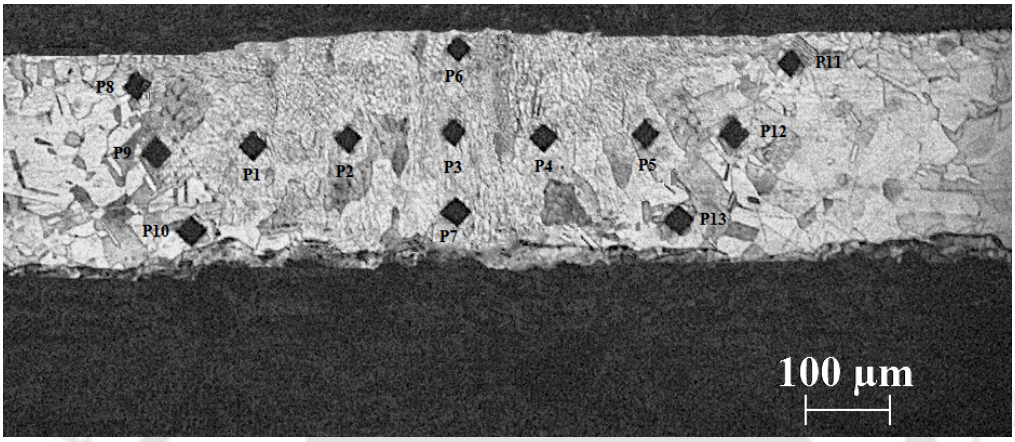

Fig. 3.9 Hardness specimen with indentation marks (post welding heat treated sample).

Table 3.10 Measured micro-hardness values of fusion zone, post weld heat treated samples, corresponding to the parameters setting mentioned in Table 3.2

Exp. No.	P1	P2	P3	P4	P5	P6	P7
1	207.6	210.9	212.0	211.9	200.6	219.8	199.0
2	179.4	178.0	178.6	180.5	170.9	186.5	175.0
3	170.0	177.8	195.8	177.6	180.8	179.5	175.6
4	209.3	211.1	217.3	211.0	210.4	222.7	215.6
5	201.5	203.0	203.8	201.8	200.0	204.3	189.0
6	179.6	178.0	180.5	176.2	182.5	185.0	172.6
7	206.6	209.0	213.0	207.6	199.1	220.1	208.7
8	209.1	211.6	213.8	212.6	209.5	217.7	199.3
9	170.0	175.6	180.6	169.5	170.5	190.0	174.2
10	205.0	208.5	210.3	202.8	199.6	219.4	206.6
11	186.8	194.0	196.0	193.6	186.6	216.0	179.2
12	190.4	195.0	192.4	194.0	195.4	198.2	188.2
13	210.0	212.0	214.1	214.0	210.3	220.7	205.3
14	186.0	196.7	200.6	195.4	185.0	199.0	183.2
15	168.6	172.7	185.4	187.5	180.5	189.7	179.0
16	206.2	209.1	216.0	212.3	205.1	224.0	216.0
17	218.3	210.6	228.6	212.7	200.4	232.5	200.3
18	176.5	182.0	181.6	184.3	178.5	190.2	175.0
19	203.0	210.6	214.3	208.5	200.6	211.0	210.7
20	202.5	210.0	211.0	206.0	206.3	217.7	198.0

Exp. No.	P1	P2	P3	P4	P5	P6	P7
21	186.4	183.0	189.7	186.5	190.3	195.5	180.0
22	198.3	194.6	212.0	195.8	199.1	216.8	210.7
23	210.0	210.9	212.3	216.8	209.4	219.6	210.4
24	200.4	203.5	209.4	202.5	202.7	215.0	190.2
25	207.1	210.6	215.9	213.5	211.9	226.3	216.6
26	212.0	199.5	201.6	219.7	210.2	217.0	184.3
27	181.4	186.6	199.5	184.0	180.5	190.2	183.0
28	200.1	201.6	211.8	212.5	209.2	217.2	212.6
29	199.6	207.3	209.0	206.9	194.3	218.8	199.3
30	182.6	188.7	189.1	200.5	182.0	199.2	180.0
31	190.4	192.0	213.0	189.5	183.3	215.9	209.6
32	204.3	208.7	211.9	206.5	200.9	219.5	214.5
33	207.4	210.9	212.3	209.5	208.3	218.6	204.9
34	182.5	182.0	189.5	182.6	181.2	212.5	205.0
35	210.6	213.0	218.0	214.4	211.5	223.5	215.0
36	209.5	212.7	214.9	205.4	210.0	220.0	202.1

Table 3.11 Measured micro-hardness values of HAZ, post welding heat treated samples, corresponding to the parameters setting mentioned in Table 3.2

Exp.	Left side of HAZ			Average left	Right side of HAZ			Average right
No.	P8	P9	P10	side hardness	P11	P12	P13	side hardness
1	207.4	199.1	187.7	198.1	206.3	205.3	189.6	200.4
2	178.3	174.5	171.7	174.8	177.6	169.3	175.3	174.1
3	169.0	165.0	150.0	161.3	168.3	152.0	147.0	155.8
4	199.8	204.1	200.6	201.5	189.4	206.6	201.4	199.1
5	184.0	186.1	194.5	188.2	185.3	188.2	189.0	187.5
6	179.0	175.0	174.6	176.2	178.3	172.0	169.3	173.2
7	202.1	200.0	189.5	197.2	197.3	204.4	190.0	197.2
8	204.3	201.1	199.6	201.7	200.0	203.6	200.0	201.2
9	172.3	168.0	178.6	173.0	170.3	164.3	176.6	170.4
10	200.1	199.5	199.8	199.8	199.3	205.3	204.6	203.1
11	186.1	189.0	180.0	185.0	188.0	208.3	194.3	196.9
12	186.1	184.6	180.6	183.8	182.6	182.4	184.4	183.1
13	198.1	193.4	191.1	194.2	199.0	204.6	201.3	201.6
14	182.1	180.0	176.0	179.4	179.2	180.3	180.0	179.8
15	171.9	167.3	159.4	166.2	170.2	165.3	160.3	165.3
16	205.0	201.7	199.6	202.1	206.0	199.0	201.3	202.1
17	219.0	214.2	210.6	214.6	218.4	205.3	212.3	212.0
18	180.1	174.0	167.4	173.8	178.3	172.3	170.0	173.5
19	197.0	197.2	194.6	196.3	201.3	202.0	205.9	203.1
20	199.0	194.1	190.2	194.4	198.0	206.3	201.3	201.9
21	183.2	181.4	180.2	181.6	180.0	180.0	179.6	179.9
22	203.0	192.1	190.2	195.1	203.4	190.3	204.4	199.4
23	197.0	193.0	189.0	193.0	192.5	190.5	187.3	190.1
24	194.4	193.1	188.0	191.8	195.2	191.5	187.3	191.3
25	195.9	192.3	189.0	192.4	192.5	190.4	187.6	190.2

Exp. No.	Left side of HAZ			Average left side hardness	Right side of HAZ			Average right side hardness
	P8	P9	P10		P11	P12	P13	
26	201.3	195.2	185.6	194.0	200.3	192.3	187.3	193.3
27	174.0	176.0	172.6	174.2	172.0	174.0	169.3	171.8
28	205.2	193.2	191.0	196.5	204.4	198.4	199.5	200.8
29	193.4	195.1	192.2	193.6	198.4	196.6	196.7	197.2
30	183.0	177.1	170.4	176.8	180.3	179.3	176.3	178.6
31	201.5	184.1	184.0	189.9	200.1	184.5	183.0	189.2
32	203.1	199.1	189.6	197.3	199.4	204.0	190.7	198.0
33	207.1	201.3	189.8	199.4	207.0	204.2	190.4	200.5
34	189.5	180.0	179.4	183.0	190.6	180.3	172.6	181.2
35	207.3	199.5	205.0	203.9	210.4	207.4	217.5	211.8
36	205.1	201.0	198.9	201.7	189.9	202.0	199.0	197.0

3.7.3 Weld Bead Microstructure

For relevant microstructural investigation, test specimens are taken from the welded samples, both from post welding heat treated and non-heat treated conditions, in such a manner that it includes the fusion zone, HAZ and parent metal. The sliced specimens are mounted in thermosetting resin followed by metallographic polishing using different grades of polishing papers (grit sizes 600, 800, 1200, 1500 and 2000) and cloth polished using abrasive; alumina suspension in water. Glyceregi1a, (HNO_3+ HCl+ $C_3H_5(OH)_3)_3$, is used for etching purpose. The sample is dipped into the reagent solution for 15 seconds and then removed from the solution and cleaned with water. After drying, the samples are observed under optical microscope (Make: Carl Zeiss) at various magnification.

Few optical micrographs taken at various weld zones are shown in Fig. 3.10 and Fig. 3.11 for non-heat treated and heat treated samples, respectively. It can be seen that the grains size at the fusion zone cannot be measured. The high rate of heat extraction resulted in extremely very fine grains which could not be measured using optical microscope. However, the grains at the HAZ and parent metal are well measurable. The average grain size was measured by the line intercept method. The values of measured grain size are given in **Table 3.12**.

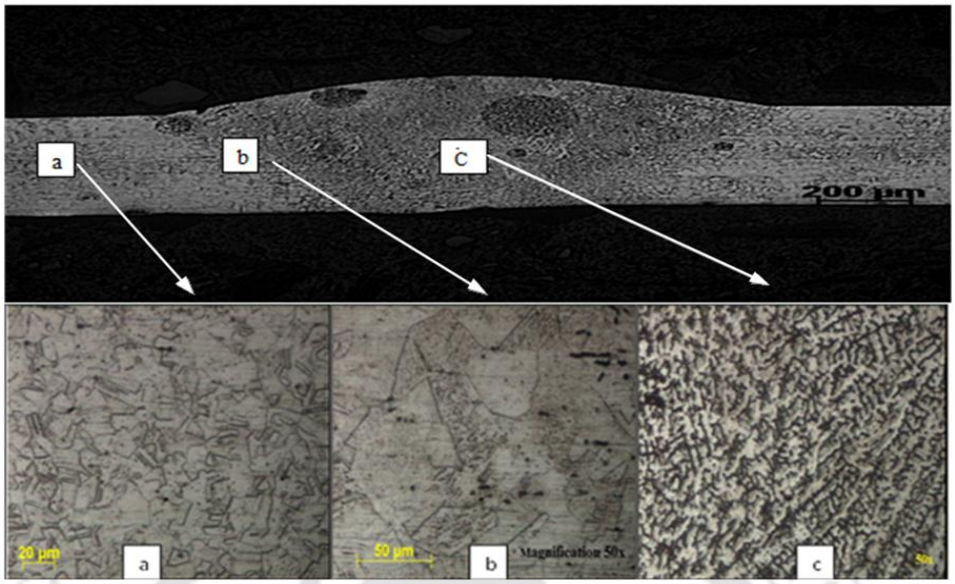

Fig. 3.10 Microstructure of Exp. No.1, without post welding heat treatment, at the (a) base metal, (b) HAZ and (c) fusion zone.

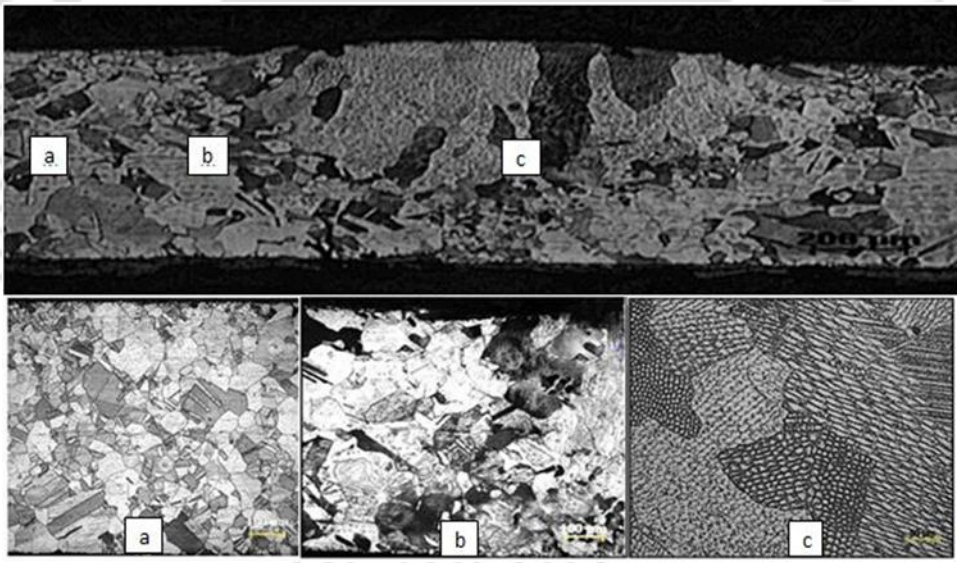

Fig. 3.11 Microstructure of Exp. No.1, after post welding heat treatment, at the (a) base metal, (b) HAZ and (c) fusion zone.

Table 3.12 Measured average grain size values of HAZ corresponding to Table 3.2

Exp. No.	Without post welding heat treated samples (µm)	Post welding heat treated samples (µm)
1	41.95	77.78
2	34.06	68.18
3	29.88	89.92
4	39.82	72.40
5	35.95	73.27
6	33.20	76.20
7	42.05	71.06
8	36.86	72.92
9	34.28	89.23
10	49.45	98.39
11	39.93	78.54
12	34.74	77.55
13	39.00	97.49
14	33.84	74.10
15	32.10	78.47
16	40.31	81.59
17	35.41	91.47
18	32.88	68.97
19	47.83	80.52
20	36.47	84.01
21	33.04	76.56
22	44.33	84.79
23	36.71	95.65
24	35.24	86.54
25	40.80	76.80
26	36.71	76.75
27	30.36	93.56
28	47.56	82.53
29	38.21	77.20
30	35.33	89.51
31	50.40	76.84
32	42.01	77.72
33	36.46	87.69
34	45.63	77.43
35	44.86	78.17
36	38.77	92.26

3.7.4 Tensile Properties

The tensile test, which is one of the fundamental material testing methods, is used in this work to determine the ultimate tensile stress (UTS), 0.2% yield stress (YS) and percentage elongation (% EL) of the joints produced against each welding experiments

during static loading. The results obtained from tensile test bring notion for acceptance of the welded product for real world applications. Moreover, the percentage of elongation, also called as ductility, can be used as an indicator for forming ability of the welded material. For without post welding heat treatment condition, three tensile test specimens are extracted for each welding condition. Similarly, for post welding heat treatment condition, two specimens are extracted for each welding condition. A schematic representation of extraction for tensile test specimens is shown in Fig. 3.12. ASTM E8M standard is adopted for the preparation of the tensile test samples. An extensometer with gauge length of 25 mm is used to measure the percentage of elongation. A hydraulically operated servo controlled universal testing machine (Make: Instron; Model: 8801) is used for the tensile testing with a constant speed of 1 mm/min and at room temperature. Stress strain curves of welded samples with minimum and maximum UTS is shown in Fig. 3.13. The broken specimens after the tensile testing are shown in Fig. 3.14(a-b). The measured UTS, yield stress and percentage elongation for both non-heat treated and heat treated samples are given in **Table 3.13** to **Table 3.15**.

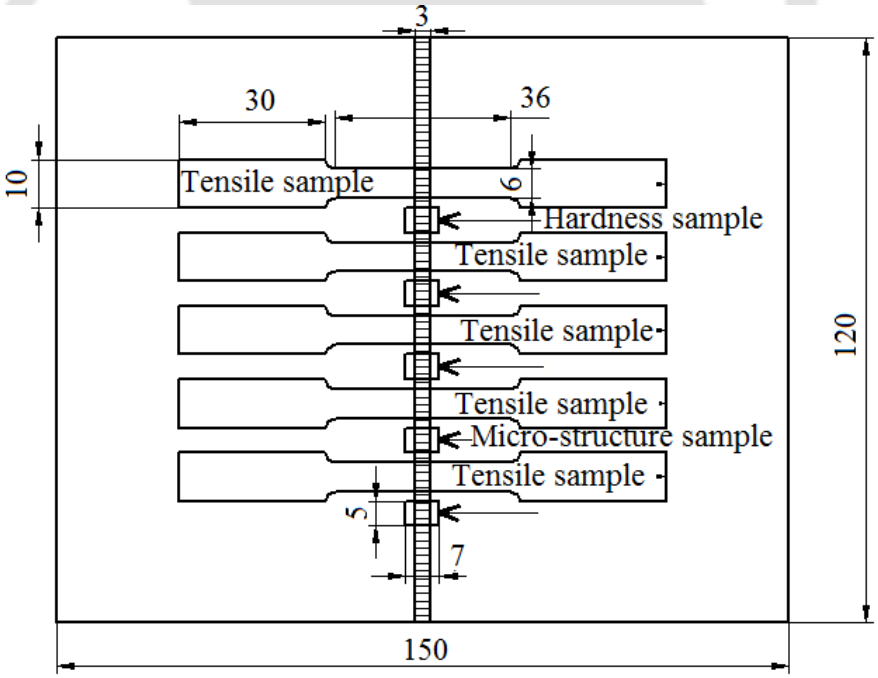

Fig. 3.12 Schematic of tensile test specimens' extraction.

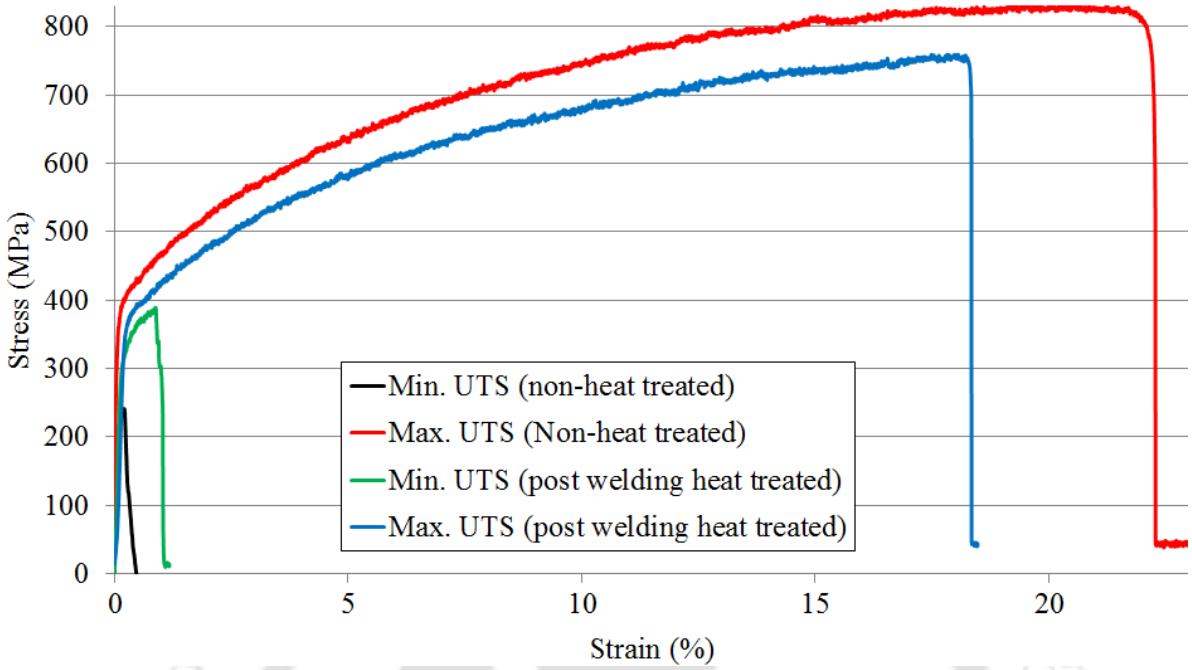

Fig. 3.13 Stress strain curve of welded joints at various conditions.

(a)

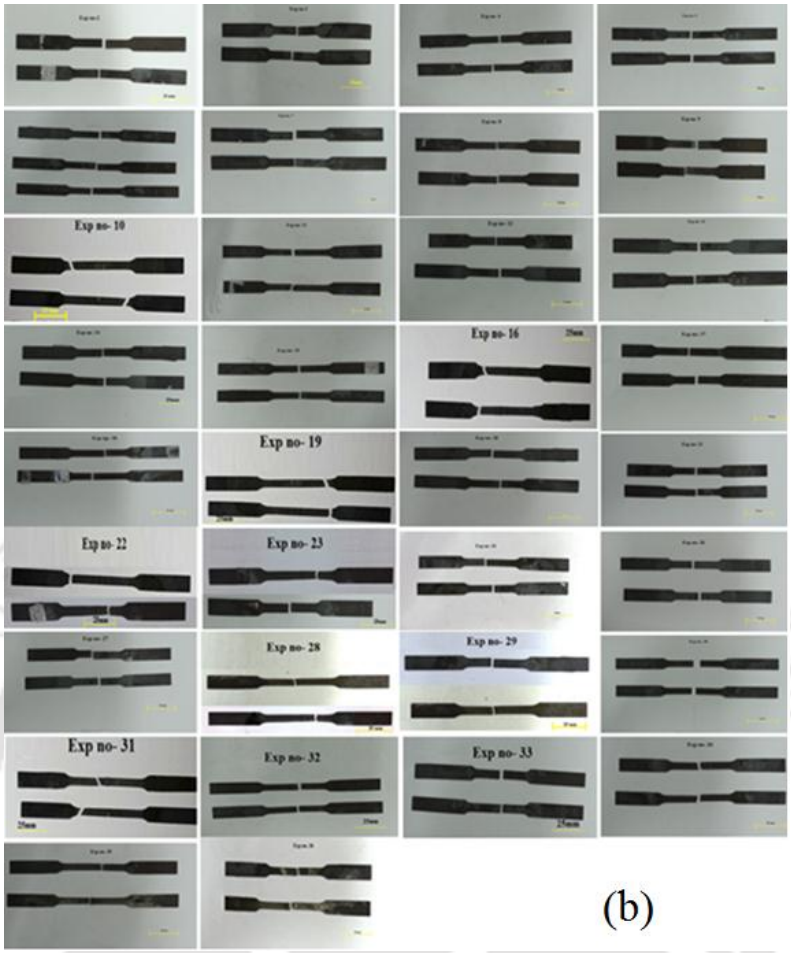

Fig. 3.14 Broken tensile tested specimens (a) without heat treatment and (b) post welding heat treatment.

Table 3.13 Ultimate tensile stress of the welded joints

Exp. No.	UTS of non-heat treated samples (MPa)			UTS of heat treated samples (MPa)	
	Specimen 1	Specimen 2	Specimen 3	Specimen 1	Specimen 2
1	572.67	573.00	517.33	587.87	605.00
2	473.00	364.67	348.00	487.01	483.98
3	241.02	244.33	266.33	388.00	350.56
4	689.33	690.66	536.67	750.56	681.33
5	447.67	460.33	675.67	550.00	535.45
6	328.67	337.00	360.67	399.00	399.33
7	738.67	700.67	692.67	706.33	713.67
8	507.67	536.67	546.67	540.12	560.67
9	391.67	373.67	363.67	540.45	535.45
10	732.00	808.67	797.67	742.67	759.00
11	621.67	581.33	622.67	605.00	635.33

Exp. No.	UTS of non-heat treated samples (MPa)			UTS of heat treated samples (MPa)	
	Specimen 1	Specimen 2	Specimen 3	Specimen 1	Specimen 2
12	430.33	438.00	442.67	733.67	375.00
13	602.33	784.64	563.00	665.00	670.33
14	445.33	415.67	427.33	568.00	552.33
15	365.67	369.33	372.00	425.00	434.33
16	676.64	673.00	679.00	679.62	723.67
17	492.00	496.00	476.67	536.67	556.33
18	382.00	396.33	387.33	389.00	494.67
19	791.67	747.33	794.67	700.80	719.33
20	580.33	561.05	591.00	606.00	610.33
21	407.00	415.00	419.00	515.67	525.67
22	771.33	775.67	785.33	738.67	741.67
23	644.33	832.33	647.00	678.00	657.67
24	478.67	481.67	492.00	532.64	549.33
25	621.16	671.00	675.67	713.67	694.34
26	507.67	518.00	517.33	564.00	568.33
27	524.00	391.00	372.67	494.33	503.00
28	741.33	737.21	731.33	749.00	754.67
29	579.67	560.33	615.33	644.00	646.00
30	448.00	457.33	455.67	525.67	594.34
31	789.00	792.33	747.33	736.00	733.00
32	650.59	689.33	682.67	636.85	679.33
33	460.67	467.67	471.33	549.67	553.33
34	702.00	688.72	680.67	728.33	739.67
35	697.67	698.00	691.33	703.67	705.67
36	670.76	660.88	680.89	588.33	583.67

Table 3.14 Yield stress of the welded joints

Exp. No.	YS of non-heat treated samples (MPa)			YS of heat treated samples (MPa)	
	Specimen 1	Specimen 2	Specimen 3	Specimen 1	Specimen 2
1	312.33	355.66	311.66	317.33	326.66
2	323.33	340.66	277.00		320.00
3	300.00	330.00	302.00	295.00	301.00
4	343.45	306.33	368.00	326.94	332.66
5	309.66	302.33	368.00	322.00	315.56
6	320.00	318.00	335.67	305.00	297.00
7	300.00	370.33	367.66	344.33	336.80
8	349.00	325.33	341.00	288.66	345.00
9	302.33	360.00	293.66	312.45	319.33
10	335.00	340.00	350.00	355.00	367.33
11	336.00	342.00	338.00	312.00	299.00
12	330.67	327.00	325.00	315.00	308.00

Exp. No.	YS of non-heat treated samples (MPa)			YS of heat treated samples (MPa)	
	Specimen 1	Specimen 2	Specimen 3	Specimen 1	Specimen 2
13	346.33	340.66	348.33	344.03	336.13
14	295.33	300.66	381.00	296.66	340.33
15	306.66	318.66	327.67	344.00	281.00
16	351.00	348.00	340.00	318.33	320.33
17	296.33	370.33	368.00	331.33	336.66
18	342.33	310.66	333.66	319.33	305.00
19	351.00	353.00	342.00	350.33	340.00
20	355.66	335.33	322.33	316.50	325.66
21	307.33	326.33	337.33	308.45	311.66
22	348.66	350.00	348.00	361.00	350.00
23	290.33	360.33	370.30	314.10	326.00
24	372.66	300.33	311.00	312.00	309.66
25	343.00	341.00	325.33	333.67	344.45
26	309.00	351.33	311.66	320.33	299.66
27	311.00	388.66	301.00	272.33	342.66
28	362.00	355.00	358.66	352.78	361.66
29	328.00	327.33	334.00	380.00	289.66
30	310.66	335.00	323.00	310.00	314.00
31	354.66	360.33	352.00	355.16	365.06
32	335.33	339.00	343.00	334.33	335.00
33	307.33	297.33	352.33	325.33	315.33
34	352.00	368.00	364.66	355.66	381.00
35	294.66	337.66	398.00	333.66	344.22
36	361.00	325.00	305.33	331.33	287.33

Table 3.15 Percentage elongation of the welded joints

Exp. No.	Elong of non-heat treated samples (%)			Elong of heat treated samples (%)	
	Specimen 1	Specimen 2	Specimen 3	Specimen 1	Specimen 2
1	6.05	7.30	6.36	16.08	17.05
2	1.43	1.56	1.51	5.40	5.51
3	0.35	0.47	0.50	0.80	0.96
4	10.50	10.50	10.50	16.25	17.30
5	2.87	1.79	2.94	7.45	6.90
6	0.54	0.76	0.58	1.04	2.00
7	19.56	18.97	19.99	20.75	18.95
8	5.20	4.38	4.83	12.45	13.25
9	1.60	1.56	1.77	3.45	4.74
10	20.87	23.20	23.62	20.45	20.65
11	7.87	8.00	8.10	17.12	17.40
12	2.25	2.08	2.30	7.34	6.32
13	6.66	6.66	7.24	16.40	16.47
14	2.15	2.16	2.18	6.23	6.25

Exp. No.	Elong of non-heat treated samples (%)			Elong of heat treated samples (%)	
	Specimen 1	Specimen 2	Specimen 3	Specimen 1	Specimen 2
15	0.69	0.55	0.79	3.04	3.55
16	11.89	12.75	13.00	19.56	21.50
17	5.79	4.80	3.90	9.23	9.06
18	0.92	0.85	0.97	2.08	2.16
19	19.50	22.34	21.98	18.96	21.50
20	6.36	7.46	6.54	11.50	11.78
21	1.80	1.66	2.07	5.75	5.90
22	20.50	21.50	21.65	19.24	20.45
23	8.12	8.20	9.25	17.50	18.18
24	3.30	3.57	3.73	8.52	8.96
25	17.45	16.30	17.60	20.04	20.20
26	4.90	4.93	4.13	12.34	9.50
27	1.52	1.03	1.05	4.76	4.95
28	21.40	21.00	21.40	19.67	18.66
29	7.25	7.30	7.50	17.51	16.80
30	2.40	2.47	2.74	6.40	7.34
31	20.00	20.16	21.30	19.05	20.56
32	14.56	14.13	13.67	20.50	19.94
33	4.23	5.17	5.23	9.56	10.45
34	18.72	18.82	19.50	18.50	19.45
35	17.50	13.00	18.34	19.45	18.75
36	4.90	5.00	5.60	11.56	10.23

3.7.5 Field Emission Scanning Electron Microscope (FESEM)

The fracture surfaces of the tensile tested samples are examined using a field emission scanning electron microscope (FESEM). The imaging is carried out at 30 kV using the secondary electron detector (SE mode). This was carried out to identify the mode of fracture during the tensile tests. The detail of the FESEM (Make: Zeiss; Model: sigma) is given in the **Table 3.4**. Few fracture surfaces of the specimens are observed by the FESEM at very higher resolution to identify the failure mode, i.e. whether intergranular or transgranular fracture.

3.8 Summary

This chapter outlines different procedures adopted for conducting the micro plasma arc welding experiments along with different methods for measurement of weld qualities of the welded samples. The chapter also highlights post welding heat treatment procedure for

improving weld qualities. Three process parameters namely, welding current, stand-off distance and welding speed were considered for developing the design matrix. Seven weld bead geometry parameters, UTS, yield stress, percentage elongation, micro-hardness of the fusion zone and HAZ and grain size of the HAZ were measured as weld quality characteristic. A detailed description of the experimental setup is also elaborated.

Chapter 4

Analysis of Weld Qualities without Post Welding Heat Treatment

4.1 Introduction

The detailed experimental procedures followed in this work have been discussed in the Chapter 3. The measured weld bead geometry parameters, micro-hardness, grain size of HAZ and tensile properties are also tabulated in the various sub-sections. In this chapter, the experimental results are analyzed and the weld quality attributes are correlated to process parameters to investigate their effect on the welding qualities without post welding heat treatment. Mathematical models are also developed for representing the input and output relationship of the MPAW process. The chapter starts with discussions on the variation of weld bead geometry with heat input as well as process parameters followed by development of response model. The variation of weld micro-hardness is analyzed next. Then, tensile properties namely, ultimate tensile stress, 0.2% yield stress and percentage elongation are discussed and regression models are developed for the same. Thereafter, grain size of the heat affected zone is analyzed. At the end, findings of the study are summarized.

4.2 Analysis of Weld Bead Geometry

The measurement of weld bead parameters is explained in details in the section 3.7.1. Seven bead geometry parameters (shown in Fig. 3.5) namely, area of fusion zone (A_{FZ}), width of top fusion zone (TW), width of bottom fusion zone (BW), penetration depth (PD), reinforcement height (RH), width of left side of HAZ (LW_{HAZ}) and width of

right side of HAZ (RW_{HAZ}) are measured. The weld bead values of each welding condition corresponding to the input parameter settings given in **Table 3.2** are depicted in **Table 3.7**. The amount of base material fuse during MPAW process depends upon the heat input which in turn governs the weld bead characteristics. The welding heat input per unit length of the workpiece is calculated using Eq. (4.1).

$$\text{Heat input per unit length} = \frac{V \times I}{WS} \tag{4.1}$$

where, *V* is welding voltage in volt, *I* is welding current in ampere and *WS* is the welding speed in mm/s. The variation of weld bead geometry attributes with heat input is shown in Fig. 4.1. It can be seen in the **Table 3.7** that the width of left and right sides of HAZ are almost same. Therefore for analysis, the average width of the HAZ is considered.

4.2.1 Effect of Heat Input on Weld Bead Geometry

Figure 4.1(a) shows that the area of fusion zone increases with increasing heat input because more amount of material is being melted at higher heat inputs. There is a near linear relationship between the fusion zone area and the heat input. The variation of penetration depth with heat input is shown in Fig 4.1(b). As expected, it is linearly increasing up to a maximum depth, which is equal to the thickness of the workpiece, then remains unaltered with further heat input. Width of the top fusion zone also increases with increasing heat input as shown in Fig 4.1(c). The size of top fusion zone width is mainly controlled by heat input and stand-off distance. Because of the combined effects of these two parameters, a linear variation is not observed with heat input. The full depth of penetration was observed beyond a certain amount of heat input. There is no linear relationship between the heat input and width of the bottom fusion zone, shown in Fig 4.1(d), as it is also controlled by both stand-off distance and heat input. In this work, filler material did not use. Therefore, ideally reinforcement height should be negligible. However, some amount of reinforcement height is observed, shown in Fig. 4.1(e) and the distribution is arbitrary. The molten metal may be displaced and emerged by high velocity plasma and high pressure shielding gas. There is no correlation between the heat input and average width of the HAZ as shown in Fig. 4.1(f).

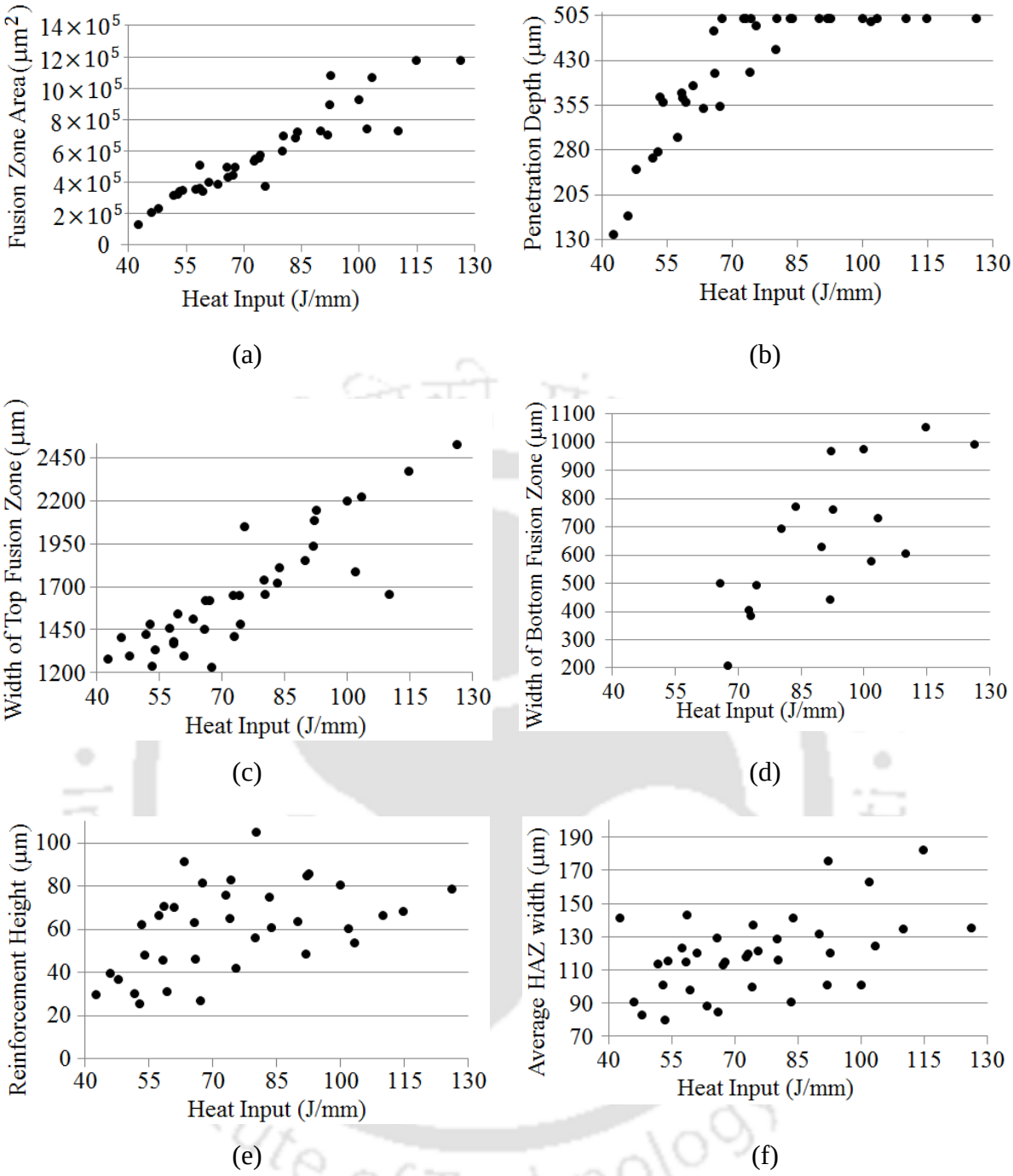

Fig. 4.1 Variation of (a) area of fusion zone, (b) penetration depth, (c) width of top fusion zone, (d) width of bottom fusion zone, (e) reinforcement height and (f) average width of HAZ with heat input.

4.2.2 Effect of Process Parameters on Weld Bead Geometry

The variation of weld bead geometry attributes with welding current, welding speed and stand-off distance are shown in Fig. 4.2 to Fig. 4.4, respectively. It can be seen

that the area of fusion zone (Fig. 4.2a) and width of top fusion zone (Fig. 4.2c) increase with increasing welding current and decrease with increasing welding speed (Figs. 4.3a, c), irrespective of other parameters levels. This is because of heat input increases with higher welding current and lower welding speed. The effect of stand-off distance (Fig. 4.4a) on fusion zone area is non-uniform as it does not contribute heat generation. The width of top fusion zone increases with increasing stand-off distance (Fig. 4.4c) as heat is distributed over larger area which significantly controlled the top fusion zone. The depth of penetration increases with increasing welding current (Fig. 4.2b) and decreases with increasing welding speed (Fig. 4.3b). The variation is mainly due to heat input during the process. The lower welding speed and higher current give maximum penetration depth (Fig. 4.4b). The variations of other bead geometry parameters are not well correlated with the considered process parameters. This may be due to interaction effects of the process parameters. Further analysis is required to explain the variations.

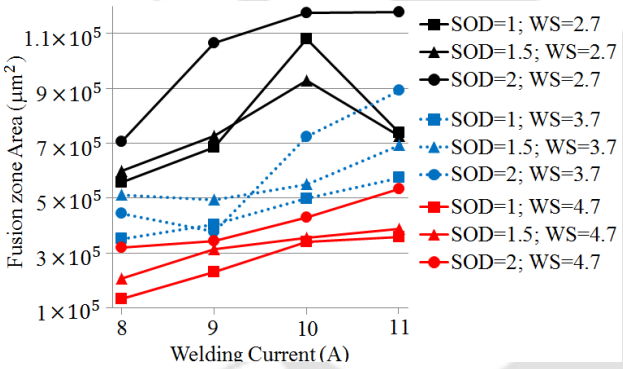

(a)

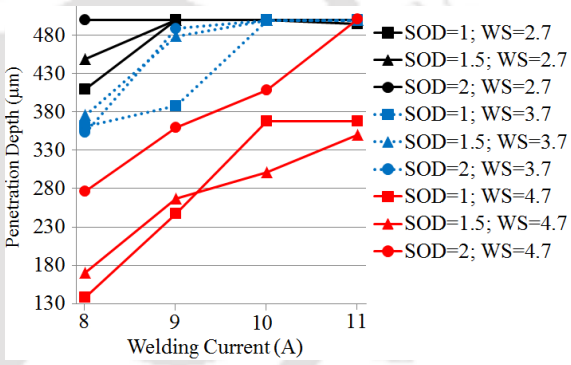

(b)

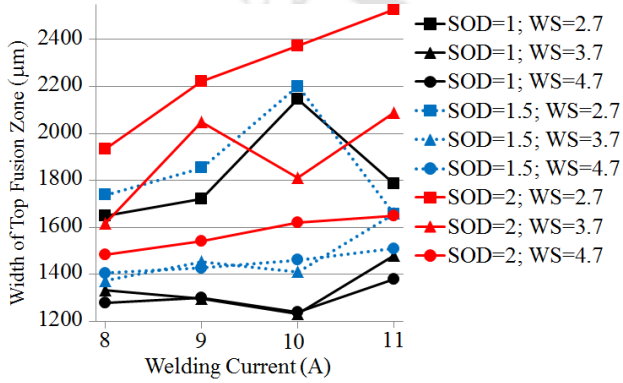

(c)

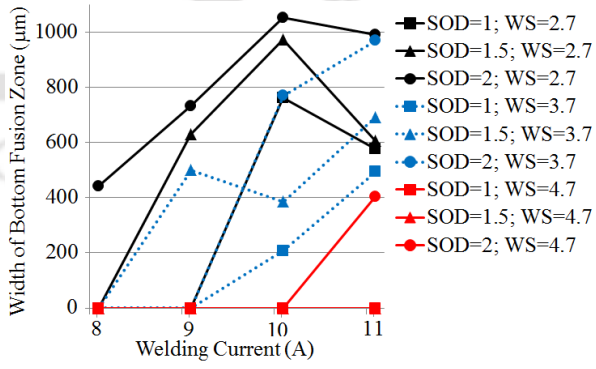

(d)

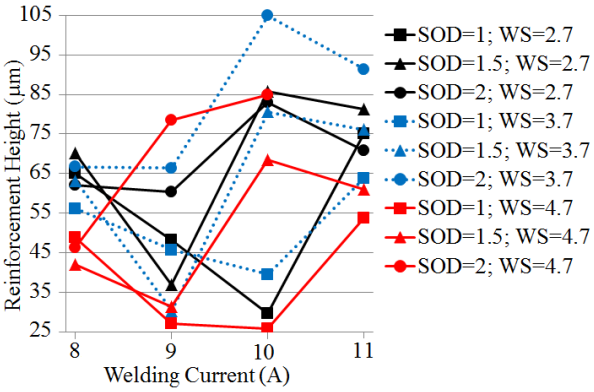

(e)

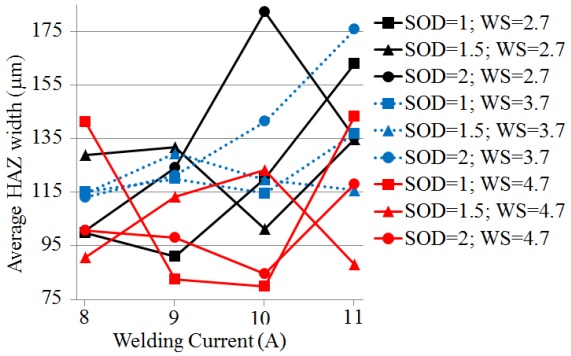

(f)

Fig. 4.2 Variation of (a) area of fusion zone, (b) penetration depth, (c) width of top fusion zone, (d) width of bottom fusion zone, (e) reinforcement height and (f) average width of the HAZ with welding current.

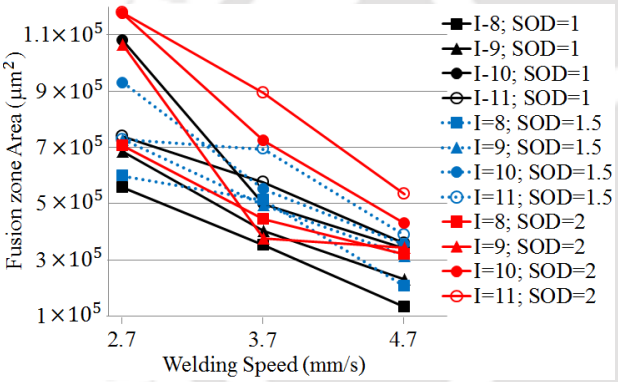

(a)

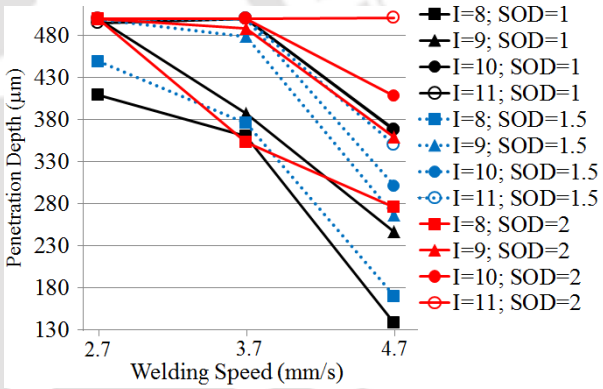

(b)

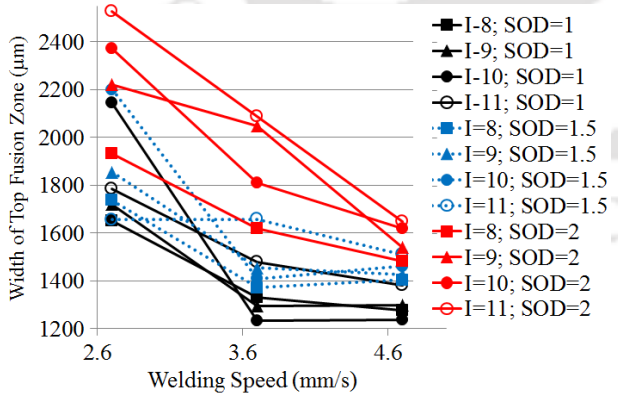

(c)

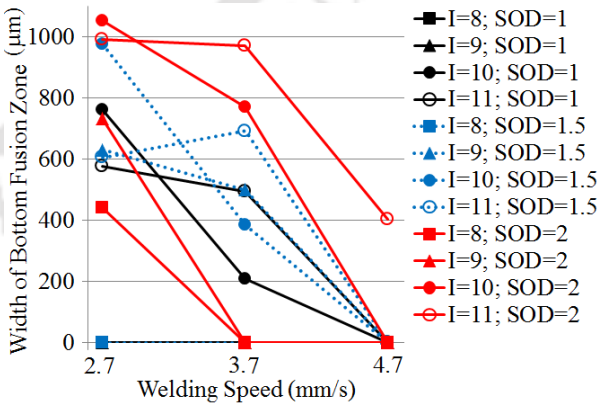

(d)

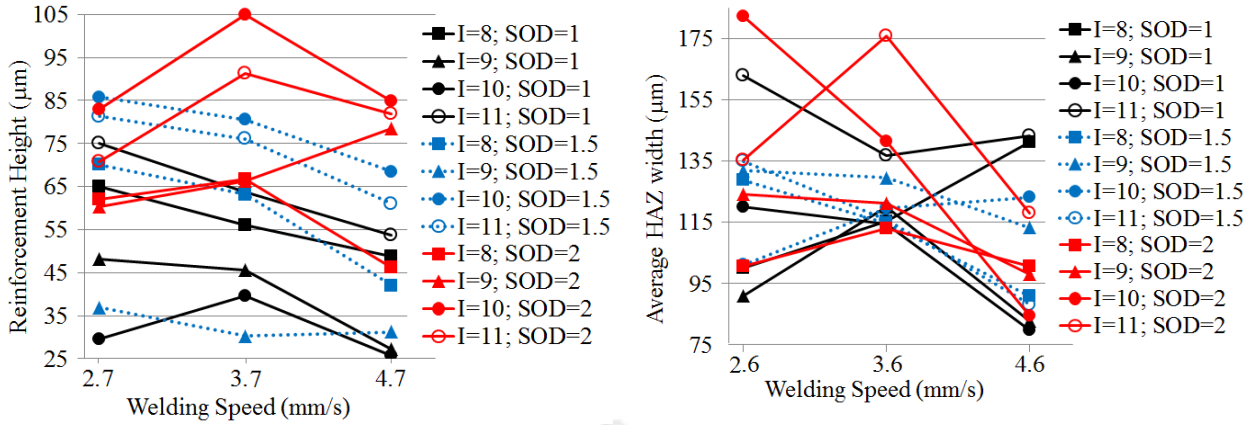

(e) (f)

Fig. 4.3 Variation of (a) area of fusion zone, (b) penetration depth, (c) width of top fusion zone, (d) width of bottom fusion zone, (e) reinforcement height and (f) average width of the HAZ with welding speed.

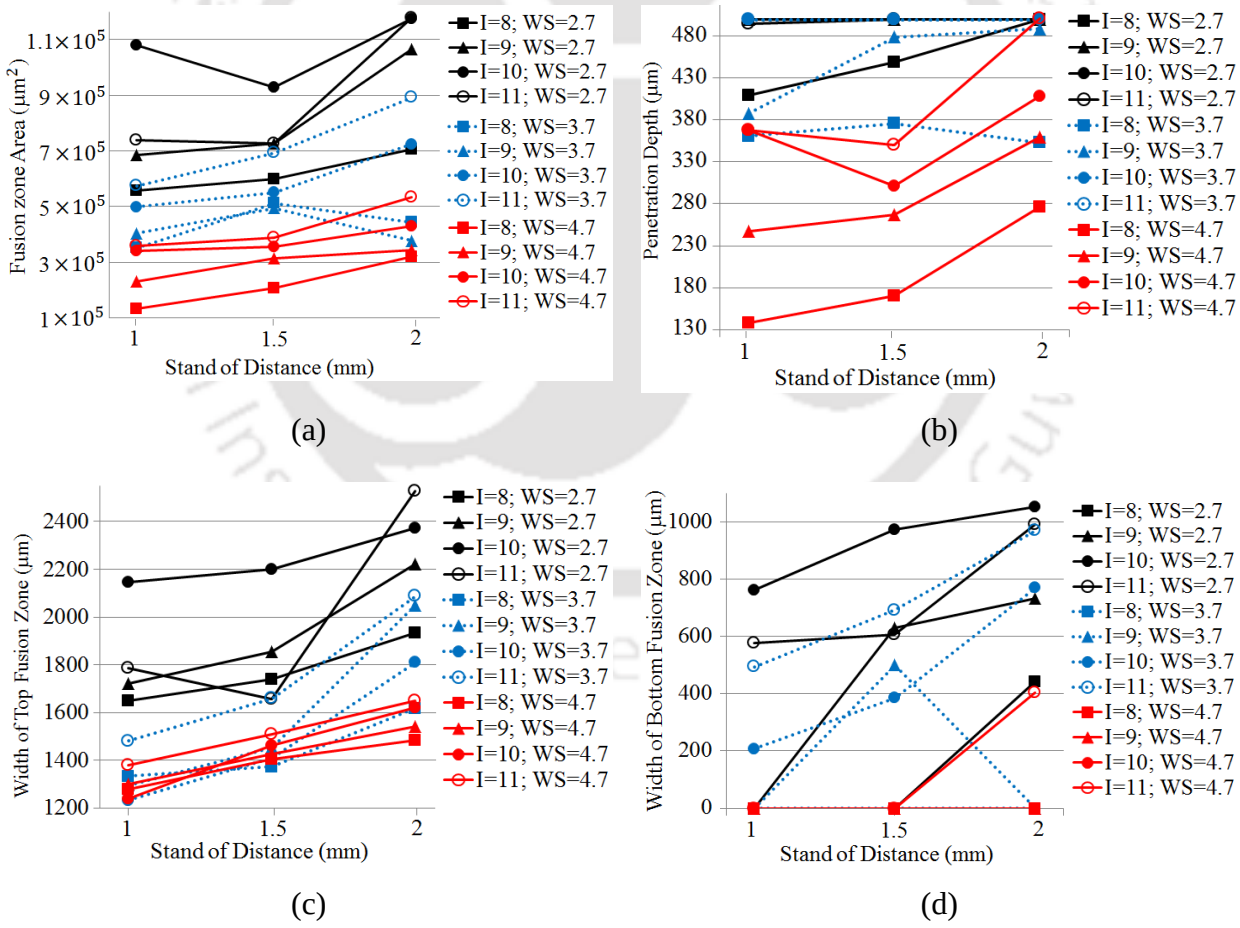

(a) (b)

(c) (d)

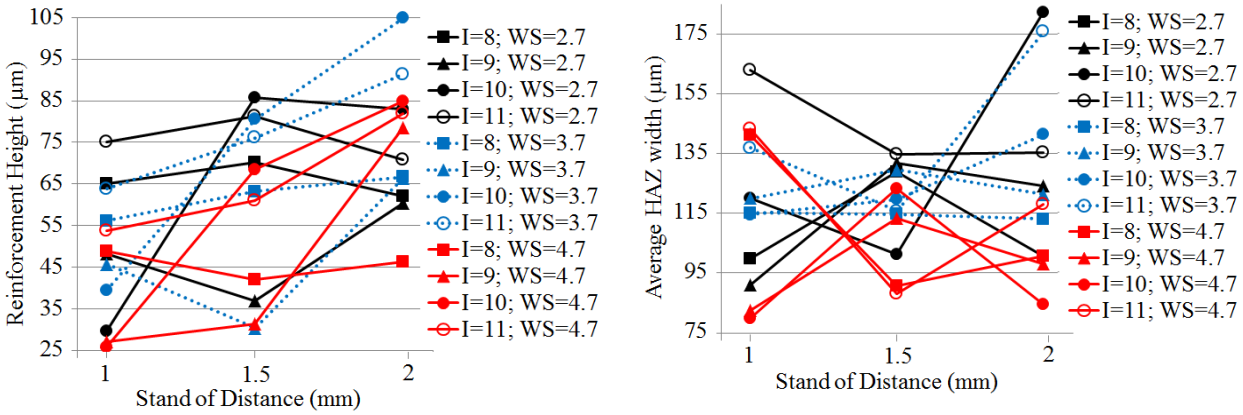

(e) (f)

Fig. 4.4 Variation of (a) area of fusion zone, (b) penetration depth, (c) width of top fusion zone, (d) width of bottom fusion zone, (e) reinforcement height and (f) average width of the HAZ with stand-off distance.

4.2.3 Influence of Process Parameters on Weld Bead Geometry

In section 4.2.2, it was found that the variations of few weld quality characteristics are well explained by individual process parameters. However there are many cases where total variability cannot be explained by individual parameters, the interaction effects of controllable parameters may be significant in those cases. Therefore, to study the effect of various factors and their interaction on the weld quality, analysis of variance (ANOVA) is performed. The ANOVA is also useful to estimate the relative importance of individual parameter and interaction of parameters on the total variability. Three-way ANOVA is used in this work as there are three controlled parameters. The notations used in the ANOVA method is describe below. A comprehensive description of ANOVA is out of the scope of this thesis; interested readers may refer to the relevant technical book [Montgomery, 2010].

I) *Source* : The source includes parameters, interaction of parameters, error and their total.

II) *DOF* : A degrees-of-freedom (DOF) in a statistical sense is associate with each piece of information that is estimated from the data. Another concept of DOF is the numbers of fair (independent) comparison that can be made to estimate the variation in the data. In ANOVA table, the DOF for individual parameter is one less than the number of level of

that parameter. The DOF of factors interaction is the product of DOF of those factors. The total DOF is one less than the number of total experimental runs. The DOF of error is the difference between the total DOF and sum of DOF of all factors and interaction factors.

III) *SOS* : SOS is the sum of square of source factor. The total sum of square (SOS_T) is calculated as:

$$SOS_T = \left[\sum_{i=1}^{N} y_i^2\right] - \frac{T^2}{N} \tag{4.2}$$

where, y_i is the measured weld quality value of the i^{th} experiment, N is the total number of experiments and T is the sum of all observations. The sum of square of a factor A (SOS_A) is given by:

$$SOS_A = \left[\sum_{i=1}^{L_A} \left(\frac{SA_i^2}{n_{A_i}}\right)\right] - \frac{T^2}{N} \tag{4.3}$$

where, SA_i is the sum of observations under i^{th} level of factor A, L_A is the total number of levels of factor A and n_{A_i} is the number of observations under i^{th} level of factor A. The sum of square of interaction of factors A and B ($SOS_{A\times B}$) is as follows:

$$SOS_{A\times B} = \left[\sum_{i=1}^{k} \left(\frac{(A\times B)_i^2}{n_{(A\times B)_i}}\right)\right] - \frac{T^2}{N} - SOS_A - SOS_B \tag{4.4}$$

where, $(A\times B)_i$ is the sum of observation under the i^{th} condition of the combinations of factor A and B. k is the total number of possible combinations of the interacting factors and $n_{(A\times B)_i}$ is the number of observation points under this condition. The sum of square of error (SOS_e) is found as follows:

$$SOS_e = SOS_T - SOS_A - SOS_B - SOS_C - SOS_{A\times B} - SOS_{A\times C} - SOS_{B\times C} - SOS_{A\times B\times C} \tag{4.5}$$

where, A, B and C are factors or parameters.

IV) *V* : Variance (V) is define as the sum of square divided by the DOF.

$$V_i = \frac{SOS_i}{DOF_i};\ \ i \in (A, B, C, A\times B, A\times C, B\times C, A\times B\times C, e) \tag{4.6}$$

V) F-ratio or F-value: This value is defined as the variance of source (V_i) divided by the error variance (V_e).

VI) Percentage contribution (*PC*) : The percentage contribution is calculated using the following equation:

$$PC_A = \left[\frac{SOS_A - V_e \times DOF_A}{SOS_T}\right] \times 100 \qquad (4.7)$$

where, PC_A is the percentage contribution of factor A and DOF_A is the degrees-of-freedom of factor *A*.

The ANOVA has been performed to know whether the effect of factors and/or interaction or mutual effect of factors are significant on the total variability. The quantitative contributions of significant parameters are also estimated using percentage contribution. A statistical software package named MINITAB [2000] has been used to perform the ANOVA. It uses P-value, called as probability of significance. P-value is computed based on the calculated F-value with 95% confidence level. If the P-value is less than 0.05, then it can be concluded that the factor is significant within the confidence limit. The details ANOVA results obtained during the evaluation of each weld quality parameter are quite large. Hence only a representative full ANOVA Table for area of fusion zone is presented in **Table 4.1**.

Table 4.1 ANOVA table for area of fusion zone

Source	DOF	SOS	V	F-Value	P-Value	PC
I	3	4.18×10^{11}	1.39×10^{11}	28.17	<0.001	15.59
SOD	2	2.27×10^{11}	1.13×10^{11}	22.90	<0.001	8.38
WS	2	1.63×10^{12}	8.13×10^{11}	164.38	<0.001	62.52
I×SOD	6	5.67×10^{10}	9.45×10^{9}	$1.91^{\#}$	0.160	1.04
I×WS	6	1.32×10^{11}	2.2×10^{10}	4.44	0.014	3.95
SOD×WS	4	6.68×10^{10}	1.67×10^{10}	3.37	0.045	1.82
Error	12	5.94×10^{10}	4.95×10^{9}			6.70
Total	35	2.59×10^{12}				

insignificant at 90% confident level

It can be seen (**Table 4.1**) that the effect of interaction of current and stand-off distance is insignificant. The most significant parameter for area of fusion zone is

welding speed with 62.5% contribution next is welding current with 15.6% contribution. The contribution due to error is less (6.7%), it signify that no important parameters were omitted from the experiment and the area of fusion zone can be controlled by varying welding speed and current only. The percentage contributions of the considered factors and their interactions on the weld bead characteristics have been calculated and given in **Table 4.2**.

The ANOVA results (**Table 4.2**) reveal that welding speed is the most influencing factor for area of fusion zone, width of top and bottom fusion zones and depth of penetration; welding current is the most influencing factor for reinforcement height. The interaction effect of current and stand-off distance is insignificant for all bead geometry parameters. The joint effect or interaction effect of all three factors, namely current, speed and stand-off distance, is also insignificant. So, these sources can be excluded for any analysis. The area of fusion zone, width of top fusion zone and depth of penetration can be well explained using the considered factors as the contribution due to error is less. The error contribution for width of bottom fusion zone, reinforcement height and average width of HAZ is more than 15%. This may be because some other factors are responsible for this variation, further experimentation is required for improvement.

Table 4.2 Percentage influence of process parameters on the weld quality parameters

	Weld Quality Parameters					
Source	A_{FZ}	**TW**	**PD**	**BW**	**RH**	**Avg. HAZ**
I	15.59	5.28	24.70	26.16	27.94	11.85#
SOD	8.38	28.32	3.38	8.53	12.72	–
WS	62.52	47.79	54.69	34.14	21.12	17.68
I×SOD	1.04#	0.96#	0.06#	2.08#	–	13.72#
I×WS	3.95	5.23	5.64	10.47	4.63#	5.72#
SOD×WS	1.82	2.28	4.21	1.45#	1.64#	5.73#
I×SOD×WS	–	–	–	–	10.01#	25.96
Error	6.70	10.14	7.32	17.17	21.94	19.34

the effect of these parameters is insignificant at 90 % confidence level

4.2.4 Development of Mathematical Models

A multiple regression is a functional mapping of several input parameters to a single output feature. The relation between the MPAW process parameters and the weld quality parameters are examined in this work by using multiple regression models as given below:

$$y = a_0 + a_1 I + a_2(SOD) + a_3(WS) + a_{12} I\,(SOD) + a_{13} I\,(WS) + a_{23}(SOD)(WS) + a_{11} I^2 + a_{22}(SOD)^2 + a_{33}(WS)^2 + a_{123} I(SOD)(WS) \quad (4.8)$$

where, y is the response or output parameters and $a_i (i = 0 \ldots 3)$ and $a_{ij} (i = 1, 2, 3\ and\ j = 1, 2, 3\ where\ j \geq i)$ are the regression coefficients. The regression equation given in Eq. 4.8 has been solved using the least square method [Montgomery, 2010].

All the experimental dataset, which was obtained from the full factorial design, were used to build the models. The regression models developed for different weld bead geometry parameters are as follows:

$$A_{FZ} = 851401 + 328688\, I - 1763221(SOD) - 813202(WS) - 22667 I^2 + 192980(SOD)^2 + 45684(WS)^2 + 168767\, I(SOD) + 32687\, I(WS) + 246449(SOD)(WS) - 32566\, I(SOD)(WS) \quad (4.9)$$

$$TW = 3765 + 276\, I - 2571(SOD) - 1508(WS) - 22.4\, I^2 + 412(SOD)^2 + 145.9(WS)^2 + 217\, I(SOD) + 30\, I(WS) + 283(SOD)(WS) - 38.5\, I(SOD)(WS) \quad (4.10)$$

$$PD = -1199 + 309\, I + 151(SOD) + 112(WS) - 15.89\, I^2 + 58.6(SOD)^2 - 57.8(WS)^2 - 46.2\, I(SOD) + 17.1\, I(WS) - 31(SOD)(WS) + 7.8\, I(SOD)(WS) \quad (4.11)$$

$$BW = -10842 + 1295\, I + 3252(SOD) + 2375(WS) - 23.4\, I^2 - 28(SOD)^2 - 36.1(WS)^2 - 233\, I(SOD) - 221\, I(WS) - 1011(SOD)(WS) + 87\, I(SOD)(WS) \quad (4.12)$$

$$RH = 511 - 48.8\, I - 425(SOD) - 173.8(WS) - 1.9\, I^2 - 38.8(SOD)^2 - 10.06(WS)^2 + 58.1\, I(SOD) + 26.1\, I(WS) + 144.1(SOD)(WS) - 15.95\, I(SOD)(WS) \quad (4.13)$$

$$HAZ_{avg} = -50 - 46.9 I + 104(SOD) + 205(WS) + 4.64 I^2 + 15.1(SOD)^2 - 12(WS)^2 - 8.2\, I(SOD) - 10.6\, I(WS) - 47.6(SOD)(WS) + 3.1\, I(SOD)(WS) \quad (4.14)$$

4.2.5 Checking the Adequacy of the Developed Model

The adequacy of the developed models is evaluated using the ANOVA technique. The variables and parameters used in the ANOVA procedure are described below.

I) Source: The regression equation, residual error and their total are called source.

II) DOF: In ANOVA table, the DOF for model is the number of explanatory variables. The total DOF is one less than the number of total experimental runs. The DOF of the residual error is the difference between the total DOF and the DOF of the model.

III) SOS: SOS is the sum of square of source factor. The SOS of model (SOS_M) is calculated as follows:

$$SOS_M = \sum_{i=1}^{N} (y_i - y_{Mi})^2 \tag{4.15}$$

where y_i is the measured weld quality value of the i^{th} observation, y_{Mi} is the model predicted value of the i^{th} observation and N is the total number of observations. The total SOS (SOS_T) is calculated as:

$$SOS_T = \sum_{i=1}^{N} (y_i - \bar{y})^2 \tag{4.16}$$

where, $\bar{y}$ is the average of all observations. The SOS of residual error (SOS_E) is given as:

$$SOS_E = SOS_T - SOS_M \tag{4.17}$$

IV) V : Variance (V) is defined as the sum of square divided by the DOF.

$$V_i = \frac{SOS_i}{DOF_i}; \quad i \in (M, E, T) \tag{4.18}$$

V) F-value: The F-ratio is defined as the variance of the model divided by the residual error variance.

$$F - value = \frac{V_M}{V_E} \tag{4.19}$$

The ANOVA test results are presented in **Tables 4.3** to **4.8** for area of fusion zone, width of top fusion zone, penetration depth, width of bottom fusion zone, reinforcement height and average width of HAZ, respectively. From the **Tables 4.3 – 4.8**, it is found that the developed regression models, other than average width of HAZ, are adequate to predict the welding bead geometry parameters of MPAW process at 95% confidence level.

Table 4.3 ANOVA table for regression model of area of fusion zone

Source	DOF	SOS	V	F-Value	P-Value	Whether the model is adequate
Eq. 4.9	10	2.29×10^{12}	2.29×10^{11}	19.62	<0.001	**Yes**
Residual Error	25	2.92×10^{11}	1.17×10^{10}			
Total	35	2.59×10^{12}				

Table 4.4 ANOVA table for regression model of width of top fusion zone

Source	DOF	SOS	V	F-Value	P-Value	Whether the model is adequate
Eq. 4.10	10	3445540	344554	15.26	<0.001	**Yes**
Residual Error	25	564395	22576			
Total	35	4009935				

Table 4.5 ANOVA table for regression model of depth of penetration

Source	DOF	SOS	V	F-Value	P-Value	Whether the model is adequate
Eq. 4.11	10	362524	36252.4	33.84	<0.001	**Yes**
Residual Error	25	26781	1071.2			
Total	35	389305				

Table 4.6 ANOVA table for regression model of width of bottom fusion zone

Source	DOF	SOS	V	F-Value	P-Value	Whether the model is adequate
Eq. 4.12	10	3936408	393640.8	10.92	<0.001	**Yes**
Residual Error	25	901075	36043			
Total	35	4837483				

Table 4.7 ANOVA table for regression model of reinforcement height

Source	DOF	SOS	V	F-Value	P-Value	Whether the model is adequate
Eq. 4.13	10	12847.2	1284.72	7.07	<0.001	**Yes**
Residual Error	25	4542	181.7			
Total	35	17389.2				

Table 4.8 ANOVA table for regression model of average width of HAZ

Source	DOF	SOS	V	F-Value	P-Value	Whether the model is adequate
Eq. 4.14	10	10194.9	1019.49	1.93	<0.089	**NO**
Residual Error	25	13205.9	528.23			
Total	35	23400.8				

Coefficient of correlation (R^2) is used to observe how closely model predicts the experimental values. The values of R^2 ($R^2 = SOS_M/SOS_T$) for Eqs. 4.9 to 4.11 are shown in **Table 4.9**. The values of correlation coefficients for the models of area of fusion zone, width of top fusion zone, depth of penetration and width of bottom fusion zone are more than 0.8, but the R^2 values for reinforcement height and average width of HAZ models are less. So, from the values of correlation coefficients, it can be concluded that the multiple regression model is unsuitable to represent the relationship between the selected control parameters and reinforcement height and average width of HAZ. Similar results were also found in the analysis of contribution of process parameters on the weld quality, section 4.2.3.

Sometime large R^2 value does not inevitably infer that the developed model is a superior one. Considering a new parameter to the model always increases R^2 value, irrespective of whether the new parameter is statistically significant or not. Therefore, it is possible to develop models with large R^2 values but those models may shows poor performance for new observation. Therefore, adjusted coefficient of correlation (R^2_{adj}) value may be used to evaluate the models further. Usually, the adjusted R^2 value does not always increase as parameters are added to the model. Indeed, if undesired variables are added, the adjusted R^2 statistic often decreases. The R^2_{adj} is defined as:

$$R^2_{adj} = 1 - \frac{(N-1)SOS_E}{(N-p)SOS_T} \tag{4.20}$$

The R^2_{adj} values are calculated and shown in **Table 4.9**. The R^2_{adj} values of area of fusion zone, width of top fusion zone and depth of penetration are close to ordinary R^2 values of the corresponding models. It indicates that these models are well generalized models. However, R^2_{adj} values of width of bottom fusion zone, reinforcement height and average width of HAZ models differ substantially from the corresponding R^2 values. This may be due to incorporation of non-significant variables in the model. In ANOVA

analysis, **Table 4.2**, it was also found that three or more sources were insignificant for the same quality parameters.

Table 4.9 The values of regression coefficient of the developed models

Equation	R^2 value	Adjusted R^2 value
Eq. 4.9	88.70 %	84.17 %
Eq. 4.10	85.93 %	80.30 %
Eq. 4.11	93.12 %	90.37 %
Eq. 4.12	81.37 %	73.92 %
Eq. 4.13	73.88 %	63.43 %
Eq. 4.14	43.57 %	20.99 %

4.3 Analysis of Micro-hardness

The measurement of micro-hardness is explained in details in the section 3.7.2. A total of thirteen hardness values were measured (shown in Fig. 3.7) in each welded sample; five points in the middle layer of the fusion zone, one point each in the top and bottom layers and three points each in the left and right side of HAZ. The measured micro-hardness values of each welding condition corresponding to the parameter settings mentioned in **Table 3.2** are given in **Tables 3.8 – 3.9**. The variation of hardness along the weld zones (i.e. various points along a layer) and across the thickness (i.e. top, middle and bottom layers) is shown in Fig. 4.5. The location 1 and location 7 are located in the left and right sides of the HAZ, respectively. The location 4 is located at the center line of fusion zone and locations 2, 3, 5 and 6 are in the fusion zone of middle layer.

Figure 4.5(a) shows that the hardness at location 1 (i.e., left side of HAZ) for all three layers is almost same for both the samples. Similarly for location 7 (i.e., right side of HAZ) also same hardness values are observed. Note that experiments 22 and 35 both are having full depth of penetration with heat input of 110 J/mm and 92 J/mm, respectively. The hardness distribution of two more samples Exp. Nos. 16 and 36, both are having similar UTS values, are also shown in Fig. 4.5(b). Similar observation can also be made from these two samples. To ensure further that the hardness values in the HAZ did not vary across the weld thickness and also left and right sides, the hardness variation with heat input for all samples is shown in Fig 4.6. From the figures and tabulated data (**Table 3.9**) it can be seen that the variation of micro-hardness across the

weld thickness is less. This variation in the micro-hardness value is acceptable for all practical purpose.

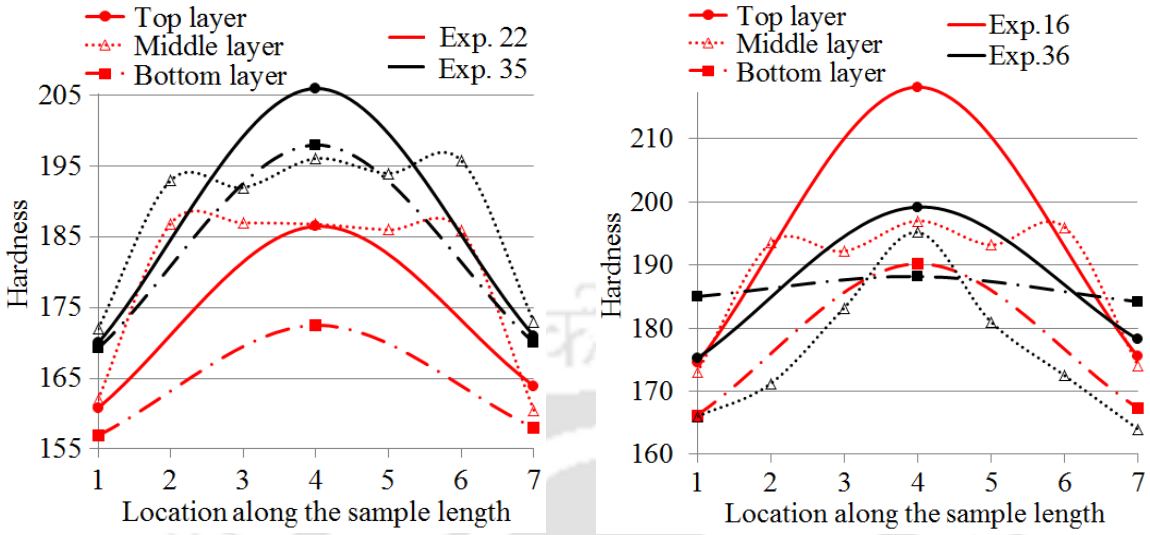

(a) (b)

Fig. 4.5 Micro-hardness variation in different layers of (a) Exp. No.22 & Exp. No.35 and (b) Exp. No. 16 & Exp. No.36 for non-heat treated samples.

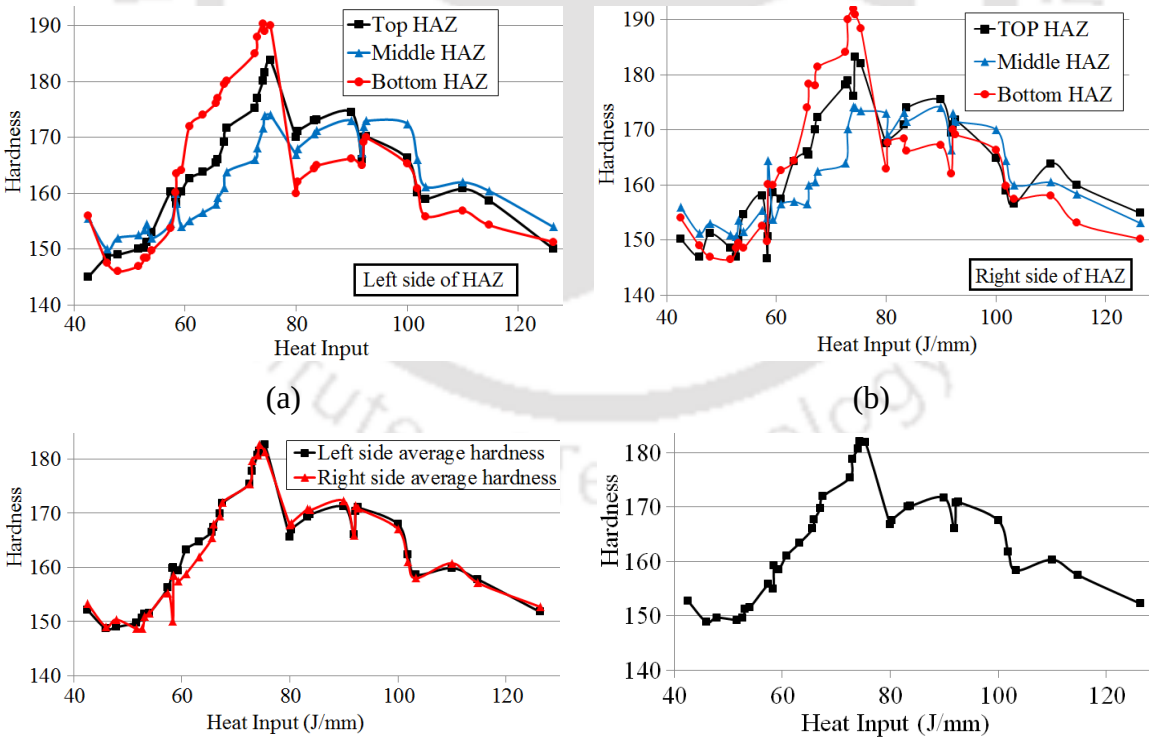

(a) (b)

(c) (d)

Fig. 4.6 Variation of micro-hardness with heat input in the (a) left side of HAZ (b) right side of HAZ, (c) average left and right sides and (d) average of all six points in the HAZ.

The variation of average hardness in the left and right sides of HAZ is shown in Fig. 4.6(c). As there is not much variation in the hardness values of HAZ, therefore average hardness of all six points in the HAZ is considered for further analysis. The variation of average hardness values of the HAZ with heat input is shown in Fig. 4.6(d). The hardness is increasing up to a heat input of 74.3 J/mm and then decreasing with further heat input. This is because hardness depends on both heat input and cooling rate. Up to heat input of 74.3 J/mm, the cooling rate increases with increasing heat input. However beyond that, the cooling rate decreases as large amount of heat is supplied to the weld zone and hence the rate of cooling is reduced. This results in a decrease in the hardness with high heat input.

The variation of micro-hardness in the middle layer of the fusion zone with heat input is shown in Fig. 4.7(a). For hardness measurement, five points were considered in the middle layer of the fusion zone (points are shown in Fig. 3.7). For better understanding, the hardness of points P2, P4 & P3 are shown in Fig 4.7(b). It can be seen that hardness of points P2 and P4 are same (Fig. 4.7b), similarly points P1 and P5 are having same hardness. Figure 4.7(c) shows the hardness of P6 (top point of fusion zone), P3 (middle point fusion zone) and P7 (bottom point of fusion zone). In this case also the variation of hardness is small, therefore average of all seven points (P1 to P7) will be considered for analysis. So, two average hardness values; one for HAZ and another one for fusion zone; will be used for further analysis. In can be seen in Fig. 4.7(d) that average hardness of the fusion zone increases with heat input up to 90 J/mm then decreases with further heat input. At higher heat input, it may take more time to cool which leads to softening of weld region and hence decrease in the hardness values.

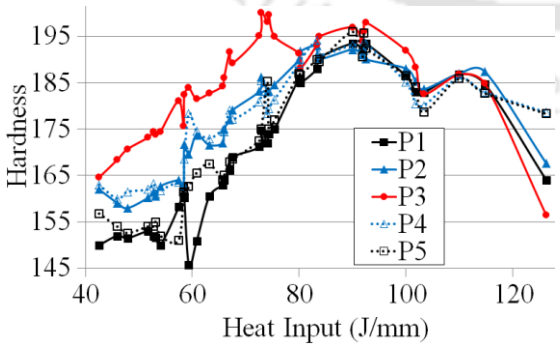

(a)

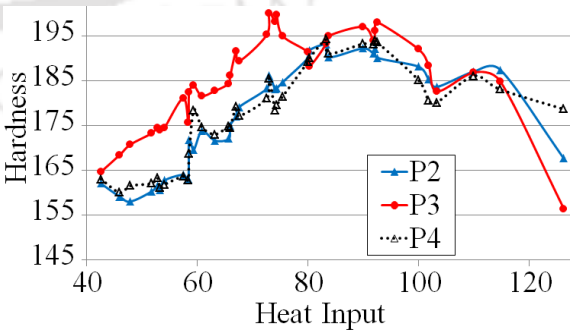

(b)

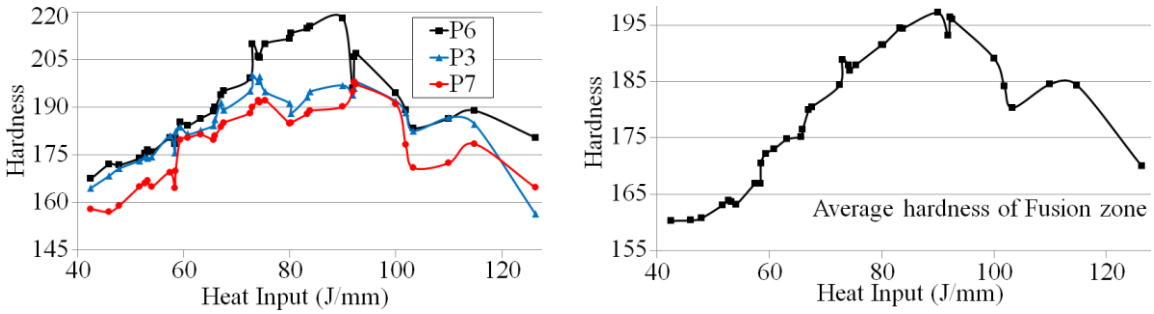

(c) (d)

Fig. 4.7 Hardness variation in the fusion zone of (a) all points of middle layer, (b) points P2, P4 & P3 and (c) center line of the fusion zone (i.e., points P3, P6 & P7) and (d) average of all seven points in the fusion zone.

4.3.1 Effect of Process Parameters on Micro-hardness

The variation of average hardness values in the fusion zone with welding current, welding speed and stand-off distance are shown in Fig. 4.8. It can be seen that, at higher welding speed hardness values are increasing with welding current (Fig. 4.8a). But, at lower welding speed it is decreasing with increasing welding current. This is because hardness is increasing up to a certain heat input then decreasing. The average hardness values at higher welding speed are also increasing with stand-off distance (Fig. 4.8b). However with increasing welding speed hardness is decreasing (Fig 4.8c). This is because heat input decreases with increasing welding speed. As hardness depends on both rate of heat input and cooling rate, therefore, it is difficult to correlate hardness variation with any single parameter. The effect of multiple parameters may be significant in this case. The variation of average HAZ hardness with process parameters is shown in Fig. 4.9. The variation cannot be correlated with individual process parameters.

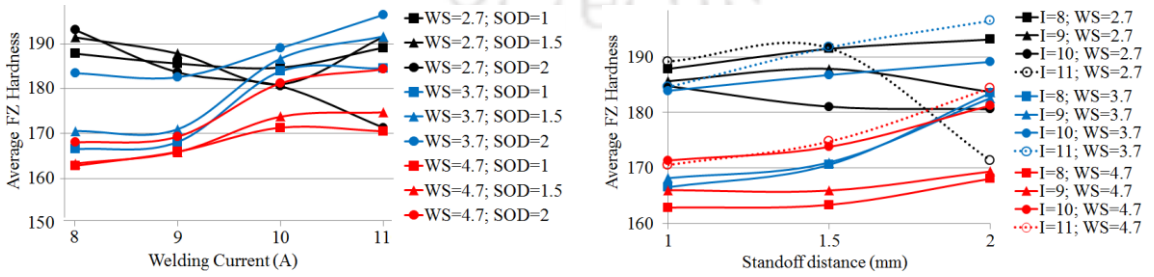

(a) (b)

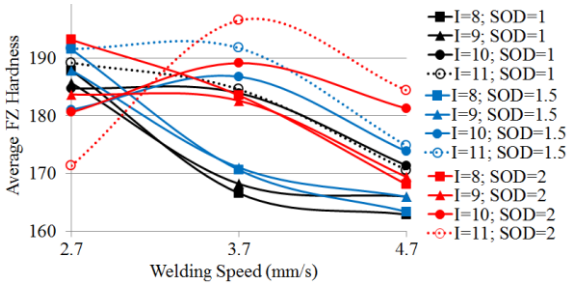

(c)

Fig. 4.8 Variation of average fusion zone hardness with (a) welding current, (b) stand-off distance and (c) welding speed.

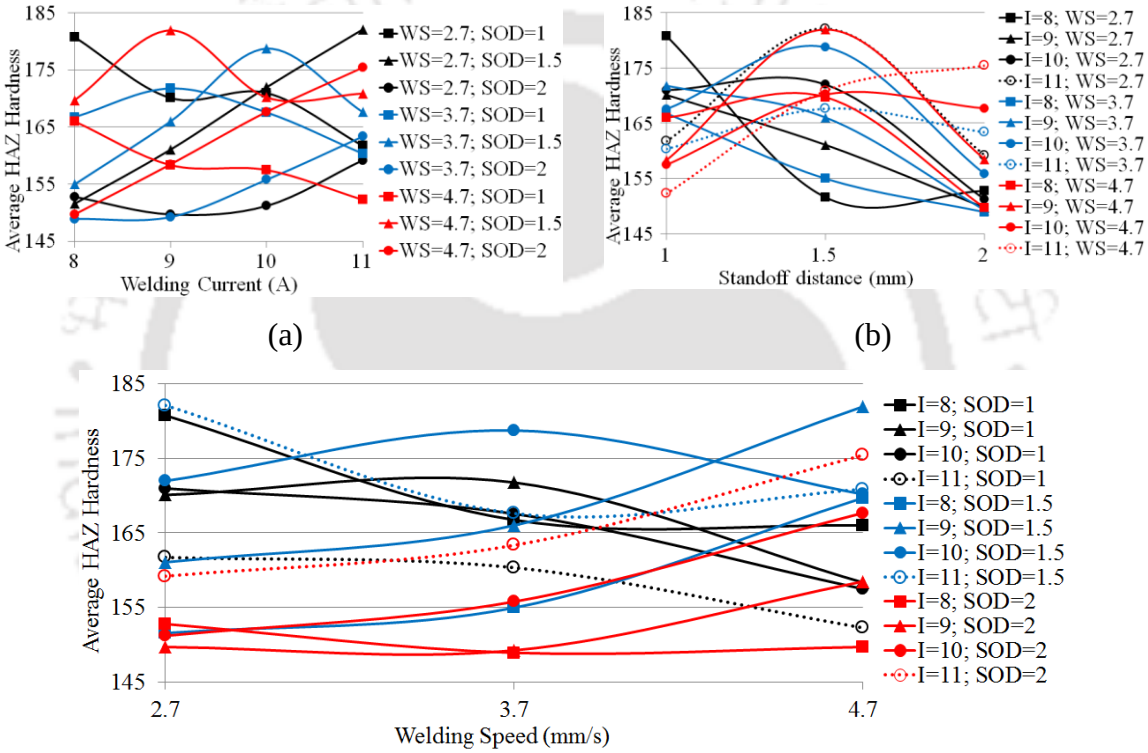

(a) (b)

(c)

Fig. 4.9 Variation of average HAZ hardness with (a) welding current, (b) stand-off distance and (c) welding speed.

4.3.2 Influence of Process Parameters on Micro-hardness

In section 4.3.1, it was found that the variations of average hardness cannot be explained by individual parameters, the interaction effects of controllable parameters may be significant. Therefore, to study the effect of various factors and their interaction on the hardness values ANOVA is performed. Three-way ANOVA is used as discussed

in the section 4.2.3. The percentage contributions of each factor and interaction on the micro-hardness have been calculated and given in **Table 4.10**. It can be seen that the most significant factor for micro-hardness in HAZ is the interaction effect of welding current and stand-off distance with 47.1 % contribution next is interaction of welding current and stand-off distance. Whereas the effects of welding speed and stand-off distance are insignificant. The welding speed is the most influencing factor for micro-hardness in the fusion zone and stand-off distance is insignificant parameter.

Table 4.10 Percentage influence of process parameters on micro-hardness

	Percentage influence of welding process parameters (factors)							
	I	**WS**	**SOD**	**I×SOD**	**I×WS**	**SOD×WS**	**I×SOD ×WS**	**Error**
Hardness in HAZ	11.8	0.5#	–	47.1	21.4	2.4#	10.1	6.7
Hardness in fusion zone	11.8	40.4	4.1	–	19.5	9.5	2.5#	12.3

effect of these parameters is insignificant at 90 % confidence level

4.3.3 Development of Mathematical Models

The relation between the MPAW process parameters and the micro-hardness values are examined using multiple regression models as given in Eq. (4.8). The regression models developed for average hardness in the fusion zone (H_{Avg}^{FZ}) and HAZ (H_{Avg}^{HAZ}) are as follows:

$$H_{Avg}^{HAZ} = 377 - 15\,I - 52(SOD) - 59.3(WS) - 0.35I^2 - 3.8(SOD)^2 + 1.63(WS)^2 + 4.7\,I(SOD) + 4.3\,I(WS) + 10.9(SOD)(WS) - 0.65\,I(SOD)(WS) \quad (4.21)$$

$$H_{Avg}^{FZ} = 58 + 6.9\,I + 108.8(SOD) + 46.6(WS) + 0.81I^2 + 0.86(SOD)^2 - 2.93(WS)^2 - 21.34\,I(SOD) - 4.41\,I(WS) - 43(SOD)(WS) - 5.2\,I(SOD)(WS) \quad (4.22)$$

The ANOVA test results are presented in **Tables 4.11** to **4.12** for average micro-hardness of the fusion zone and HAZ, respectively. From the tabulated result it is found that the regression model for fusion zone hardness is adequate at 95% confidence level. But model for hardness of HAZ is inadequate. The values of correlation coefficients

(shown in **Table 4.13**) for both the models are less than 0.8. So, from the values of correlation coefficients, it can be concluded that the multiple regression model is unsuitable to represent the relationship between the selected control parameters and micro-hardness.

Table 4.11 ANOVA table for regression model of average micro-hardness of fusion zone

Source	**DOF**	**SOS**	**V**	**F-Value**	**P-Value**	**Whether the model is adequate**
Eq. 4.22	10	2584.35	258.44	8.68	<0.001	**Yes**
Residual Error	25	744.05	29.76			
Total	35	3328.40				

Table 4.12 ANOVA table for regression model of average micro-hardness of HAZ

Source	**DOF**	**SOS**	**V**	**F-Value**	**P-Value**	**Whether the model is adequate**
Eq. 4.21	10	744.55	74.46	0.70	0.715	**No**
Residual Error	25	2655.16				
Total	35	3399.71				

Table 4.13 The Values of regression coefficient of the developed micro-hardness models

Equation	R^2 value	Adjusted R^2 value
Eq. 4.21	21.90 %	0.00 %
Eq. 4.22	77.65 %	68.70 %

4.4 Analysis of Tensile Properties

The detail of tensile test is explained in the section 3.7.4. For without post welding heat treatment condition, three tensile test specimens were extracted for each welding condition. The values of ultimate tensile stress, 0.2% yield stress and percentage elongation were measured and given in **Tables 3.13** to **3.15**, respectively. From the tabulated data, it can be seen that most of the cases the measured three values, at each experimental condition, are close to each other. However, in few cases one measured value is far away from the other observations. For example in Exp. No. 4 (**Table 3.13**), the UTS of specimen #3 is 536.67 MPa which is far away from other two UTS values such as 689.33 MPa and 690.66 MPa. Similarly, in Exp. No. 13 the measured UTS

values are 602.33 MPa, 784.64 MPa and 563 MPa, specimen #2 deviates so much from other two observations. These unexpected data values are called outliers. It occurs almost in all research work. The abnormal values could provide an indication of a measurement error. Odd or extreme data in a given set of measurement results must be rejected with statistical justification. In this work, various outlier tests are applied for detection of extreme data, the detailed of which is explained in the following sub-section.

4.4.1 Detection of Outlier

From the time when researchers started exploiting and employing the information in the collected data as an aid to understand a process, there has been an apprehension over the unrepresentative or outlying observations in the data set. Outlier observation in a data set is one that is far away from the norm of a variable [Stevens, 1984; Rousseeuw and Leory, 1988]. Occurrence of outlier is very common in every field involving data measurement or collection. It can emerge from various causes or mechanisms. Anscombe (1960) classified outliers into three main categories: (a) *inherent variability* which is intrinsically vary over the population; such variation is a natural feature of the population and uncontrollable (b) *measurement error*, this includes inadequacies in the measuring instrument, the rounding of obtaining values, or errors in recording and (c) *execution error* or *experimental error*, a further source of variability arises in the imperfect experimentation or collection of data. Many times, biased samples or individuals those are not truly representing the population of interest are chosen inadvertently in the analysis. For example, tensile specimen with minor local defects which are invisible to the naked eye, dimension of test sample is different than the considered area, etc.

Outlier is bad data point due to error. When outliers are present in the data, any statistical analysis based on sample mean and variance could be distorted and the whole experimental data set is disturbed. The problematic effects of outliers are distortion of estimates or bias, inflated sum of squares, distortion of F-values/P-values and inaccurate conclusions. As a result proper analysis of the experiment becomes more complicated. Examination of outlier allows a more appropriate model to be developed, or enable us to appraise any dangers that may emerge from basing inferences on the normality assumption. It is therefore essential to identify outliers prior to analysis and modeling. Once outliers are detected, a decision has to be made about what to do with them.

Conceptually, there are strong arguments for removal of outliers. Some researchers reported the benefits of outliers' removal. It reveals significant changes in correlations and t-tests statistics. Moreover, errors of inference are notably decreased that is the primary argument for identifying and removal of outliers.

Most statisticians would agree that outliers should not be removed automatically, they should be analyzed carefully. A large number of outlier tests have been presented in the literature. Some are designed to detect the presence of a single outlier while other are designed for multiple outliers. In this work, Chauvenet's criterion, Grubb's test, Dixon's Q-test and Cochran's C test will be used to detect single outlier. All these tests are based on the assumption that the data follow approximately normal distribution. Therefore, Q-Q (quantile-quantile) plot (Wilk and Gnanadesikan, 1968) is performed to check the normality of the data series before applying outlier test. This plot displays the observed values against normally distributed data. The Q-Q plots for UTS, yield stress and percentage elongation are shown in Fig. 4.10. The plots indicate that the data series are approximately normally distributed. The procedures of outlier tests are discussed in the following sub-sections.

4.4.1.1 Chauvenet's criterion

Chauvenet's criterion (Chauvenet, 1891) has gained a wide acceptance for assessing a single outlier. It defines an acceptable scatter around the mean value for a given population. The identification of outlier is achieved by finding non-dimensional maximum deviation (τ_{max}), as shown in Eq. 4.23, among the measured values. The calculated τ_{max} value is then compared with the acceptable deviation. The acceptable deviation for sample size of 3 is 1.383. An observation is considered as outlier if the calculated non-dimensional maximum deviation is more than the acceptable deviation.

$$\tau_{max} = \frac{Max\ |y_i - \bar{y}|}{\sigma} \tag{4.23}$$

Where, y_i is the i^{th} observation, $\bar{y}$ is the sample mean and σ is the standard deviation of population. The τ_{max} values for UTS data are calculated as per Eq. 4.23 and shown in **Table 4.14**. There are 19 outliers in the UTS values, shown in bold font, as per Chauvenet's criterion. Similarly, the τ_{max} values for yield stress and percentage elongation are calculated and given in **Table 4.14**.

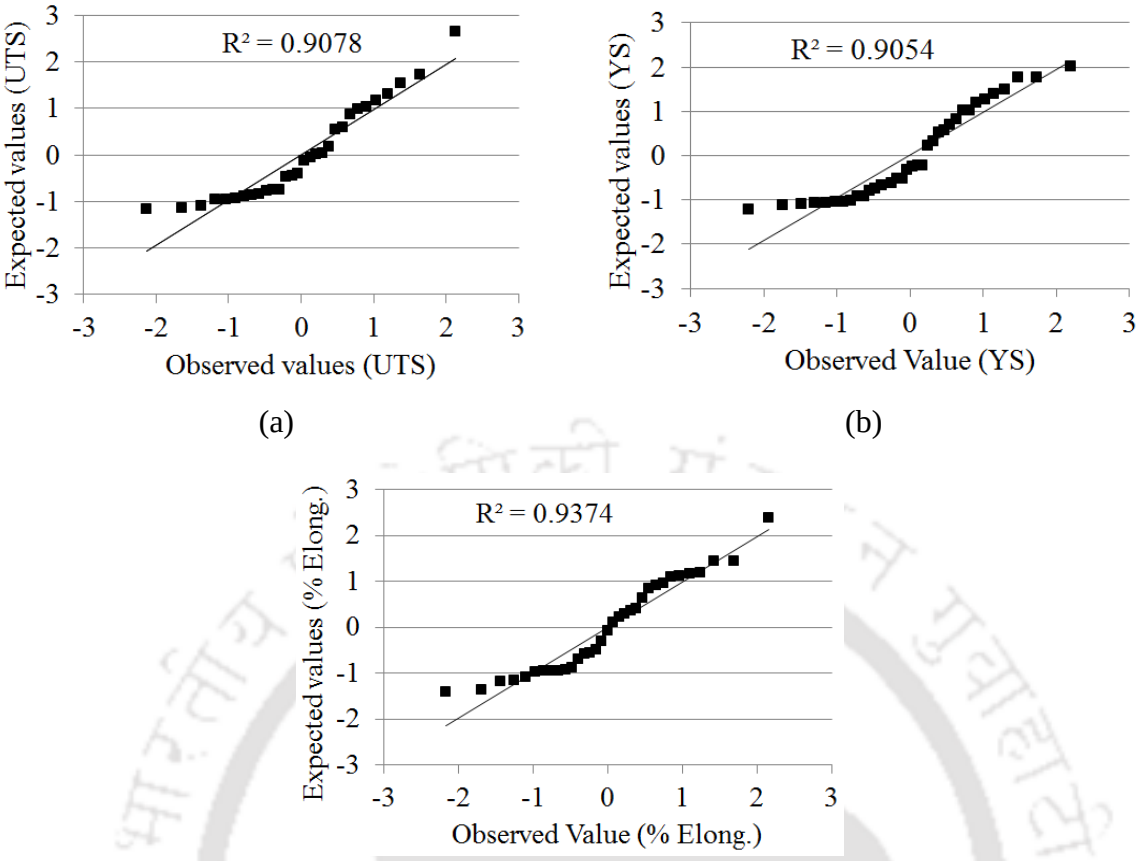

Fig. 4.10 Q-Q plots for the data series of (a) UTS, (b) yield stress and (c) percentage elongation.

Table 4.14 Values of **N**ondimensional maximum deviation of Chauvenet's criterion

Exp. No.	**τ_{max} value for UTS**	**τ_{max} value for YS**	**τ_{max} value for % Elongation**
1	**1.4142**	**1.4141**	1.3735
2	**1.4035**	1.3643	1.3037
3	**1.4039**	**1.4117**	1.3826
4	**1.4142**	1.2990	0.000
5	**1.4125**	**1.4069**	**1.4121**
6	1.3689	**1.4066**	**1.3935**
7	**1.3954**	**1.4134**	1.2835
8	1.3705	1.3339	1.2581
9	1.3235	**1.4040**	**1.3913**
10	**1.4017**	1.3363	**1.3999**
11	**1.4139**	1.3363	1.2744
12	1.3112	1.3258	1.3806
13	**1.3945**	1.3688	**1.4142**
14	1.3020	**1.4120**	1.3587
15	1.2839	1.2785	1.2868

Exp. No.	τ_{max} value for UTS	τ_{max} value for YS	τ_{max} value for % Elongation
16	1.3019	1.3641	1.3812
17	**1.3868**	**1.4137**	1.2437
18	1.3149	1.3637	1.2868
19	**1.4119**	**1.3935**	**1.4046**
20	1.3241	1.3041	**1.3977**
21	1.3363	1.3181	1.3321
22	1.3480	1.3380	**1.4040**
23	**1.4141**	**1.4049**	**1.4114**
24	1.3813	**1.4010**	1.3184
25	**1.4100**	**1.4066**	**1.4063**
26	**1.4119**	**1.4120**	**1.4135**
27	**1.4055**	**1.4065**	**1.4128**
28	1.2897	1.2430	**1.4142**
29	1.3266	**1.4083**	**1.3887**
30	**1.3943**	1.2304	**1.3871**
31	**1.4111**	1.3433	**1.4052**
32	**1.3958**	1.2419	1.2383
33	1.3308	**1.3935**	**1.4122**
34	1.3117	**1.3863**	**1.4044**
35	**1.4128**	1.2872	**1.3990**
36	1.2296	1.3256	**1.4018**

Outliers are shown in bold front

4.4.1.2 Grubb's Test

Grubb's test (Grubbs, 1969) is used to identify a single outlier in univariate data set that follows nearly normal distribution. In this method, a test statistic called as G is computed and compared with the critical value. The Grubb's test statistic is given below:

$$G = \frac{Max\ |y_i - \bar{y}|}{S} \tag{4.24}$$

where, S is the sample standard deviation. The test statistic is calculated and given in **Table 4.15**, the outliers are shown in bold front. The critical value for Grubb's test at 0.05 significance level is 1.153. An observation is accepted as outlier if the calculated value is higher than the critical value. It is found that there are five outliers in the UTS data. Similarly, there are three and five outliers in the yield stress and percentage elongation data set, respectively.

Table 4.15 Values of Grubb's test statistic

Exp. No.	*G* - statistic for UTS	*G* - statistic for YS	*G* - statistic for % Elongation
1	**1.1547**	**1.1546**	1.1215
2	1.1460	1.1140	1.0645
3	1.1463	1.1526	1.1289
4	**1.1547**	1.0606	0.000
5	**1.1533**	1.1487	1.1530
6	1.1177	1.1485	1.1378
7	1.1393	**1.1541**	1.0480
8	1.1190	1.0891	1.0272
9	1.0806	1.1463	1.1360
10	1.1445	1.0911	1.1430
11	**1.1544**	1.0911	1.0405
12	1.0706	1.0826	1.1272
13	1.1386	1.1176	**1.1547**
14	1.0631	1.1529	1.1094
15	1.0483	1.0439	1.0507
16	1.0630	1.1138	1.1278
17	1.1323	**1.1543**	1.0155
18	1.0736	1.1135	1.0507
19	1.1528	1.1378	1.1469
20	1.0811	1.0648	1.1412
21	1.0911	1.0762	1.0876
22	1.1007	1.0925	1.1464
23	**1.1546**	1.1471	1.1524
24	1.1278	1.1439	1.0764
25	1.1513	1.1485	1.1483
26	1.1528	1.1529	**1.1542**
27	1.1476	1.1484	**1.1535**
28	1.0531	1.0149	**1.1547**
29	1.0832	1.1499	1.1339
30	1.1384	1.0046	1.1325
31	1.1521	1.0968	1.1473
32	1.1397	1.0140	1.0110
33	1.0866	1.1378	**1.1530**
34	1.0710	1.1319	1.1467
35	1.1530	1.0510	1.1423
36	1.0040	1.0824	1.1446

Outliers are shown in bold front

4.4.1.3 Dixon's Q-Test

Dixon's Q-test, also called as Q-test, was developed by W. Dixon (1950) is used for detection and rejection of outliers for small sample size. In this method, the data are arranged in an ascending order and then calculates Q-values as defined:

$$Q_1 = \frac{y_2 - y_1}{y_3 - y_1} \tag{4.25}$$

$$Q_2 = \frac{y_3 - y_2}{y_3 - y_1} \tag{4.26}$$

$$Q = Max\,[Q_1, Q_2] \tag{4.27}$$

where, y_1, y_2, y_3 are measured tensile properties and $y_1 < y_2 < y_3$. The calculated Q-values are shown in **Table 4.16**. These values are compared with the Dixon's test critical value for 95 % confidence level. If the calculated Q-value is bigger than the critical value of 0.970, it is accepted as an outlier. There are 4 outliers in the UTS data set as per Dixon's Q-test.

Table 4.16 Q values of Dixon's Q-Test

Exp. No.	Q value for UTS	Q value for YS	Q value for % Elongation
1	**0.9940**	**0.9848**	0.7520
2	0.8667	0.7278	0.6094
3	0.8691	0.9333	0.7792
4	**0.9914**	0.6019	0.0000
5	0.9444	0.8884	0.9391
6	0.7396	0.8868	0.8182
7	0.8261	0.9620	0.5784
8	0.7436	0.6620	0.5427
9	0.6429	0.8693	0.8095
10	0.8565	0.6667	0.8473
11	**0.9758**	0.6667	0.5652
12	0.6216	0.6471	0.7727
13	0.8225	0.7392	**1.0000**
14	0.6067	0.9378	0.7143
15	0.5789	0.5712	0.5833
16	0.6065	0.7273	0.7748
17	0.7931	0.9685	0.5238
18	0.6279	0.7262	0.5833

Exp. No.	Q value for UTS	Q value for YS	Q value for % Elongation
19	0.9366	0.8182	0.8732
20	0.6439	0.6100	0.8364
21	0.6667	0.6333	0.6585
22	0.6905	0.6700	0.8696
23	**0.9858**	0.8753	0.9292
24	0.7750	0.8525	0.6338
25	0.9144	0.8868	0.8846
26	0.9355	0.9372	0.9651
27	0.8789	0.8859	0.9495
28	0.5877	0.5229	**1.0000**
29	0.6485	0.8996	0.8000
30	0.8214	0.5070	0.7941
31	0.9259	0.6807	0.8769
32	0.8279	0.5215	0.5169
33	0.6562	0.8182	0.9400
34	0.6225	0.7913	0.8718
35	0.9500	0.5839	0.8427
36	0.5060	0.6467	0.8571

Outliers are shown in bold front

4.4.1.4 Cochran's C Test

The Cochran's C test statistic (Cochran, 1941) is popular for multi samples test for equal variances. It is a one sided upper limit variance outlier test. It identifies one remarkably large variance value at a time. The respective data is then removed from the full data set and the test is repeated until no further large variance values are detected. This test may lead to excessive rejections if the data series are not normally distributed. The *C* value is calculated as follows:

$$C_j = \frac{S_j^2}{\sum_{i=1}^{N} S_i^2} \tag{4.28}$$

Where, C_j is the Cochran's C statistic for j^{th} data series or j^{th} experiment, S_j is the standard deviation of j^{th} data series, N is the number of experiments, i.e, N =36. The value of N is reduced in steps of 1 after each iteration of the C test and S_i is the standard deviation of the full data set. The values of C statistic are compared with the Cochran's upper critical (C_{UL}) value. When the calculated *C*-value of a data series is bigger than the

C_{UL} then that data series is accepted as an outlier. The C_{UL} values is calculated as follows:

$$C_{UL}(\propto, n, N) = \left[1 + \frac{N-1}{F_c\left(\frac{\propto}{N}, (n-1), \{(N-1)(n-1)\}\right)}\right]^{-1} \quad (4.29)$$

Where, $\propto$ is significance level, here it is 0.05, n is number of observations per experiment, N is the total number of experiment and F_c is the critical value of Fisher's ratio. F_c can be acquired from F-distribution tables. Using Eq. 4.29, it is found that C_{UL} value for $\propto = 0.05$, n=3 and N=36 is 0.17152. For detecting outliers, the test is repeated till no further large variance values are detected and in each iteration C_j and C_{UL} values are calculated and compared. For detecting outliers of data series for UTS, and % elongation the tests were iterated for 6 and 3 times, respectively. The calculated C_j values for first iteration are shown in **Table 4.17**. There are 6 outliers in the UTS data. As per Cochran's C test, there are no outliers in the yield strength data set. Because, it is a one-sided upper limit variance outlier test. It is observed that in these two data sets, bad observations are presence in the lower limit.

Table 4.17 Calculated Cochran's *C* statistic for the first iteration

Exp. No.	*C* statistic for UTS	*C* statistic for YS	*C* statistic for % Elongation
1	0.01449	0.0270	0.02232
2	**0.06500**	0.0461	0.00022
3	0.00267	0.0120	0.00034
4	**0.11059**	0.0410	0.00000
5	**0.23168**	0.0551	0.02189
6	0.00389	0.0040	0.00072
7	0.00852	0.0675	0.01381
8	0.00579	0.0062	0.00887
9	0.00284	0.0553	0.00065
10	0.02425	0.0025	**0.11559**
11	0.00785	0.0004	0.00070
12	0.00055	0.0004	0.00070
13	**0.19734**	0.0007	0.00591
14	0.00315	0.0979	0.00001
15	0.00014	0.0047	0.00077
16	0.00013	0.0014	0.01786
17	0.00147	0.0752	0.04707

Exp. No.	*C* statistic for UTS	*C* statistic for YS	*C* statistic for % Elongation
18	0.00074	0.0114	0.00019
19	0.00991	0.0015	**0.12592**
20	0.00325	0.0120	0.01834
21	0.00053	0.0098	0.00229
22	0.00072	0.0000	0.02058
23	**0.16392**	0.0807	0.02094
24	0.00069	0.0648	0.00245
25	0.01288	0.0040	0.02664
26	0.00047	0.0239	0.01094
27	**0.09625**	0.0979	0.00410
28	0.00036	0.0005	0.00281
29	0.01098	0.0006	0.00092
30	0.00035	0.0063	0.00170
31	0.00887	0.0008	0.02647
32	0.00605	0.0006	0.01043
33	0.00041	0.0365	0.01657
34	0.00164	0.0030	0.00949
35	0.00020	0.1146	**0.43425**
36	0.00141	0.0339	0.00755

Outliers are shown in bold front

4.4.1.5 Comparison of Outlier Detection Methods

Four outlier detection methods namely, Chauvenet's criterion, Grubb's test, Dixon's Q-test and Cochran's C test are applied to identify the presence of outliers. The total numbers of outliers detected by each of these methods along with outlying observations (*i.e.*, experiment number) are shown in **Table 4.18**. Among these methods, Chauvenet's criterion gave highest number of outlier whereas Dixon's Q-test gave lowest number of outliers. It is also found that an observation is detected as an outlier by one method however the same observation is not found as an outlier by other method. Therefore it is decided that, if an observation is detected as an outlier by more than one method than that particular observation will be considered as an outlier. It is found that Exp. Nos. 1, 2, 4, 5, 11, 13, 23 and 27 are outliers in the UTS data. The Exp. Nos. 1, 7 &17 are found as outliers for yield strength. Similarly, Exp. Nos. 10, 13, 19, 26, 27, 28, 33, 35 are outliers for the data set of percentage elongation. One observation, out of three observations, is removed from further analysis for the above identified outliers cases.

Table 4.18 Number of outliers detected in the tensile data set

Outlier tests	**Number of outliers detected (Exp. No.)**		
	UTS	**Yield stress**	**% elongation**
Chauvenet's criterion	**19** (1-5, 7, 10, 11, 13, 17, 19, 23, 25-27, 30-32, 35	**17** (1, 3, 5-7, 9, 14, 17, 19, 23-27, 29, 33, 34)	**20** (5, 6, 9, 10, 13, 19, 20, 22, 23, 25-31, 33-36)
Grubb's test	**5** (1, 4, 5, 11, 23)	**3** (1, 7, 17)	**5** (13, 26-28, 33)
Dixon's Q-test	**4** (1, 4, 11, 23)	**1** (1)	**2** (13, 28)
Cochran's C test	**6** (2, 4, 5, 13, 23, 27)	**0**	**3** (10, 19, 35)

4.4.2 Effect of Heat Input on Tensile Properties

The variations of tensile properties with heat input for samples without post welding heat treatment are shown in Fig. 4.11. It can be seen that UTS (Fig. 4.11a) and yield stress (Fig. 4.11b) values increase with increasing heat input. The percentage elongation (Fig. 4.11c) values are increasing up to heat input of 101.85 J/mm, which decreases marginally with further increase in heat input. This is because at lower heat input less amount of material is being melted and full weld penetration was not found. With increasing heat input the penetration depth increases thereby strengthen the weld joints.

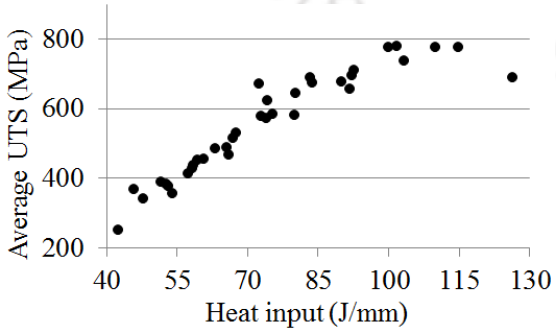

(a)

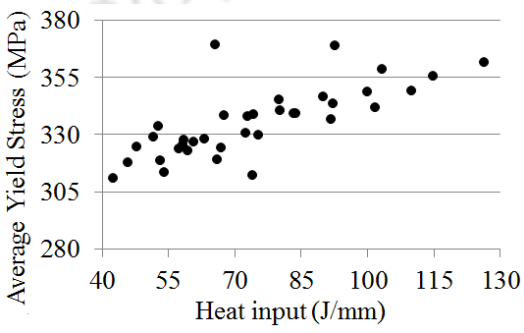

(b)

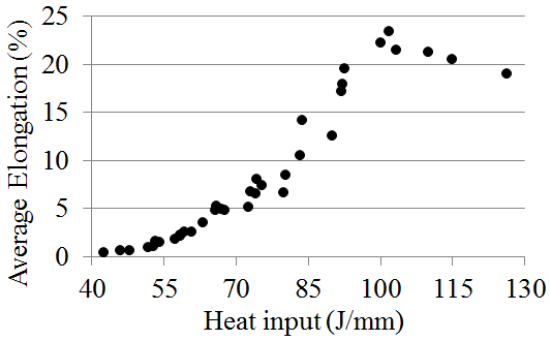

(c)

Fig. 4.11 Variation of (a) ultilate tensile stress, (b) 0.2 % yield stress and (c) percentage elongation with heat input of non heat treated samples.

4.4.3 Effect of Process Parameters on Tensile Properties

The variations of tensile properties with welding current, welding speed and stand-off distance are shown in Figs. 4.12-4.14, respectively. The UTS value increases with increasing welding current (Fig. 4.12a) and stand-off distance (Fig. 4.14a) and decreasing welding speed (Fig. 4.13a), irrespective of other parameters settings. It can also be seen that the variation of UTS with welding speed is more consistent compare to other two parameters. This is due to higher welding current and lower welding speed promotes high heat input. This leads to full weld penetration thereby increases the UTS. The yield stress of the weld decreases with increasing welding speed. However, the variation of yield strength with welding current and stand-off distance could not be correlated. Figure 4.13c shows that percentage elongation decreases with increasing welding speed. This is because at higher welding speed heat input decreases that lead to incomplete penetration. Elongation value (Figure 4.14c) increases with increasing stand-off distance. Heat is distributed over wider area at higher stand-off distance which controls the cooling rate and thereby softens the heat affected zone.

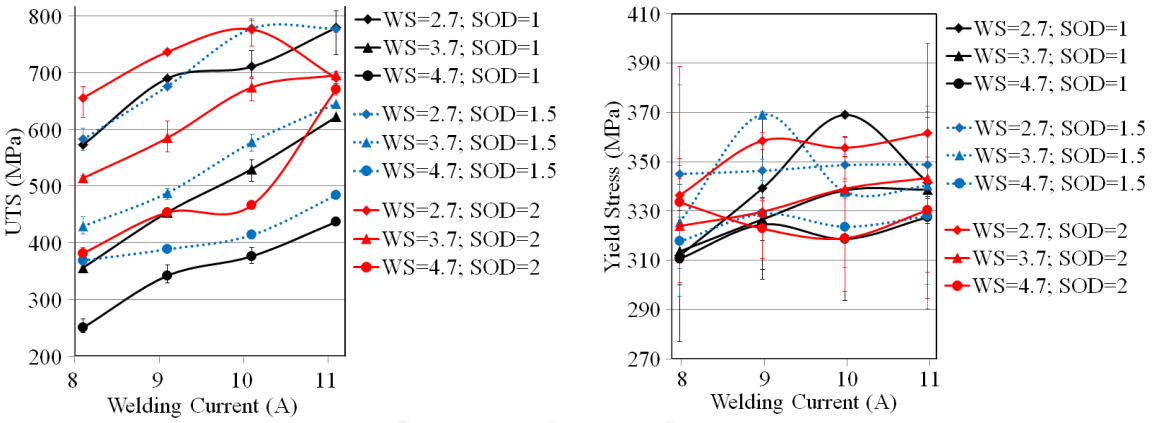

(a) (b)

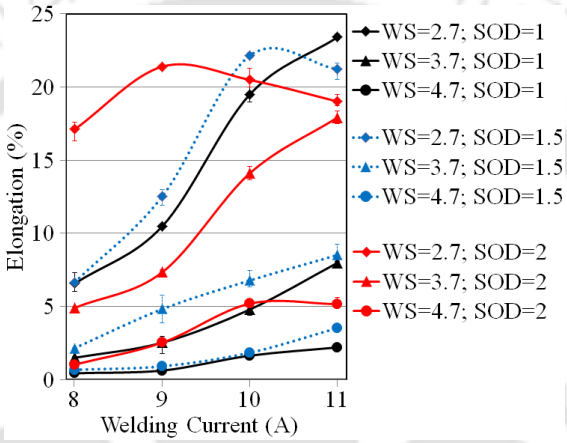

(c)

Fig. 4.12 Variation of (a) UTS, (b) yield stress and (c) percentage elongation with welding current.

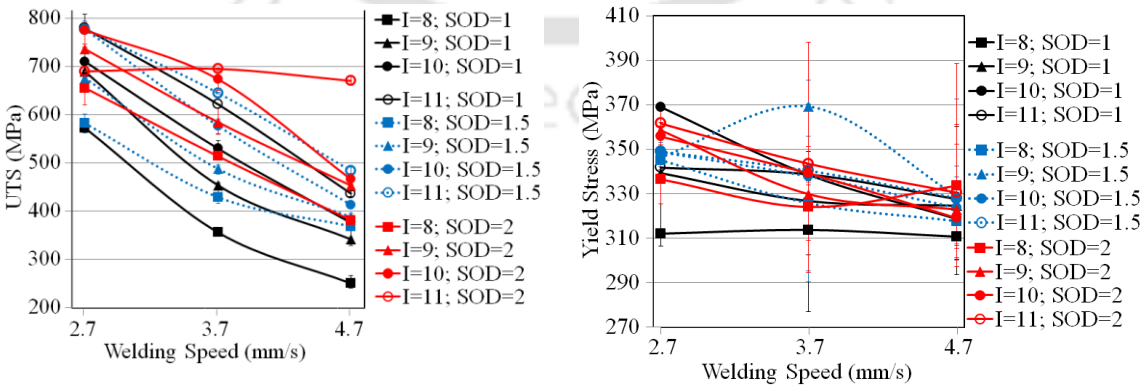

(a) (b)

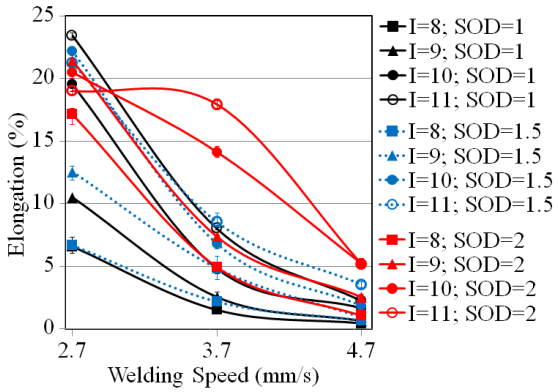

(c)

Fig. 4.13 Variation of (a) UTS, (b) yield stress and (c) percentage elongation with welding speed.

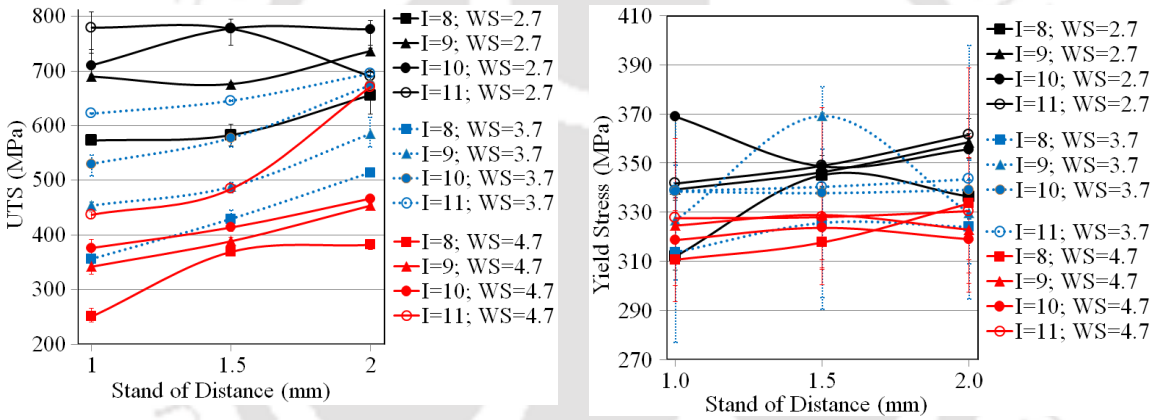

(a) (b)

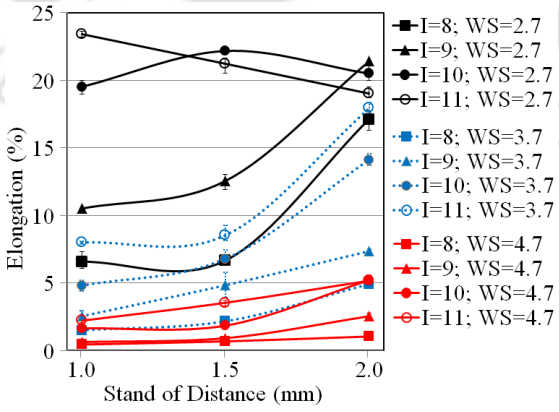

(c)

Fig. 4.14 Variation of (a) UTS, (b) yield stress and (c) percentage elongation with stand-off distance.

4.4.4 Influence of Process Parameters on Tensile Properties

In section 4.4.3, it was found that the variations of weld strength cannot be fully explained by individual parameters and yield strength did not show any relation with the individual process parameters. In this section, quantitative effect of various factors and their interaction on the tensile properties of the weld is performed using three-way ANOVA, as discussed in the section 4.2.3. The percentage contributions of each factor and interaction on the tensile properties have been calculated and given in **Table 4.19**. It is found that the contribution of welding speed is much higher compare to all other parameters and their interaction effects. The welding current is the next most influencing factor for controlling the tensile properties. However, the influences of individual parameters, expect welding speed, as well as the interaction effects are found insignificant for yield stress. The contribution of error is insignificantly and low for UTS and percentage elongation.

Table 4.19 Percentage influence of process parameters on welding strength

Quality parameters	**Percentage influence of welding process parameters (factors)**							
	I	**WS**	**SOD**	**I×SOD**	**I×WS**	**SOD×WS**	**I×SOD×WS**	**Error**
UTS	20.1	59.9	7.1	0.3	2.0	2.0	2.8	5.8
Yield stress	4.3#	13.4	0.5#	#	#	#	#	82.3
% elongation	16.0	65.9	6.9	0.4	3.9	1.2	5.9	0.0

effect of these parameters is insignificant at 90 % confidence level

4.4.5 Development of Mathematical Models

The relation between the MPAW parameters and the tensile properties of the welding joint are examined using multiple regression models as given in Eq. (4.8). The regression models developed for UTS, yield strength (YS) and percentage elongation (Elong) are as follows:

$$UTS = -1775 + 392.1\,I + 1394(SOD) + 220(WS) - 5.46I^2 + 30.3(SOD)^2 + 12(WS)^2 - 167.1\,I(SOD) - 56\,I(WS) - 339.6(SOD)(WS) + 41.48\,I(SOD)(WS) \quad (4.30)$$

$$YS = 10 + 58\,I + 40(SOD) - 13.5(WS) - 2.61\,I^2 - 14.5(SOD)^2 + 0.56(WS)^2 + 2.7\;I(SOD) + 0.36\,I(WS) + 12(SOD)(WS) - 1.64\,I(SOD)(WS) \quad (4.31)$$

$$Elong = -203.8 + 30.8\,I + 110.8(SOD) + 33.27(WS) - 0.23I^2 + 5.47(SOD)^2 + 2.55(WS)^2 - 12.5\,I(SOD) - 6.1\,I(WS) - 30.9(SOD)(WS) + 3.14\,I(SOD)(WS) \quad (4.32)$$

The ANOVA test results are presented in **Tables 4.20** to **4.22** for UTS, yield stress and percentage elongation, respectively. From the tabulated result it is found that the regression models are adequate at 95% confidence level. The values of correlation coefficients (shown in **Table 4.23**) for the models of UTS and percentage elongation are above 0.9 but the R^2 values for yield strength model is very small. So, from the values of correlation coefficients, it can be concluded that the multiple regression model is unsuitable to represent the relationship between the selected control parameters and yield strength of the weld. Similar results were also found in the analysis of contribution of process parameters on the tensile properties, section 4.4.4. The R^2_{adj} values for UTS, and percentage elongation models are close to ordinary R^2 values of the corresponding models. It suggests that these two models are well generalized models.

Table 4.20 ANOVA table for regression model of UTS

Source	**DOF**	**SOS**	**V**	**F-Value**	**P-Value**	**Whether the model is adequate**
Eq. 4.30	10	2100969	210097	159.61	<0.0001	**Yes**
Residual Error	89	117154	1316			
Total	99	2218123				

Table 4.21 ANOVA table for regression model of YS

Source	**DOF**	**SOS**	**V**	**F-Value**	**P-Value**	**Whether the model is adequate**
Eq. 4.31	10	15207.7	1520.77	3.16	0.002	**Yes**
Residual Error	94	45265.7	481.55			
Total	104	60473.5				

Table 4.22 ANOVA table for regression model of percentage elongation

Source	**DOF**	**SOS**	**V**	**F-Value**	**P-Value**	**Whether the model is adequate**
Eq. 4.32	10	5006.54	500.654	145.07	<0.0001	**Yes**
Residual Error	89	307.16	3.451			
Total	99	5313.7				

Table 4.23 The Values of regression coefficient of the developed models

Equation	R^2 value	Adjusted R^2 value
Eq. 4.30	94.72 %	94.12 %
Eq. 4.31	25.15 %	17.18 %
Eq. 4.32	94.22%	93.57%

4.5 Analysis of Weld Bead Microstructure

The measurement of microstructure at the HAZ is explained in details in the section 3.7.3. Typical microstructures of the welded sample are shown in Figs. 4.15 to 4.18. The microstructure of the weld zone of the specimen shows three regions: (a) the fusion zone, (b) the heat affected zone and (c) base metal zone. The fusion zone as expected consists of coarse dendritic structure. The HAZ is a very narrow region having fine equiaxed grains. The fine sized grains are the result of rapid heat extraction during the welding process. A clear demarcation between interface of the HAZ and base metal or HAZ and fusion zone is not evident, rather the transition is gradual. In all the welded samples, stingers of high temperature ferrite (δ-Fe) aligned along the rolling direction is observed (Fig. 4.15b, Fig. 4.16b and Fig. 4.18b). From the Scahffler diagram, a small amount (~1-2%) of ferrite may be present in 316L alloy when cooled from high temperature to room temperature. However due to the slope of the austenite ferrite solvus line, under conditions of equilibrium cooling, almost all of the ferrite transform to austenite and may not be evident in the microstructure of the alloy in the wrought condition. However, during welding, where the cooling rate is very high, the δ to γ transformation is suppressed and some ferrite remains in the microstructure as stringers (Lippold and Kotecki, 2014). This is evident in the base metal region of all the as-welded samples.

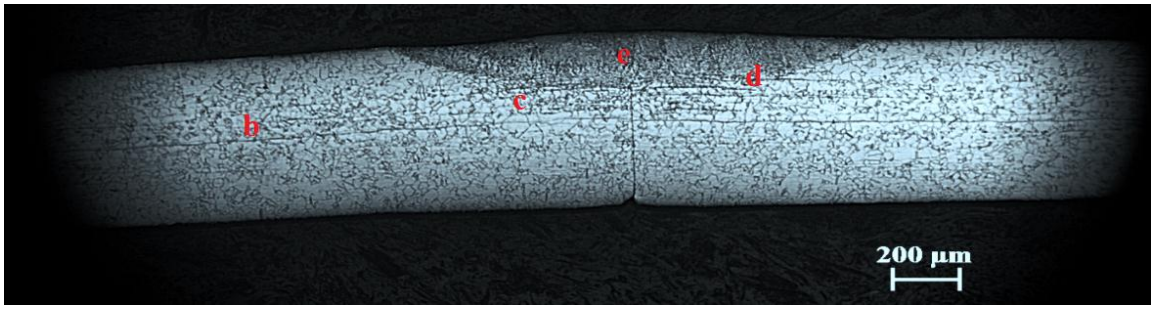

(a)

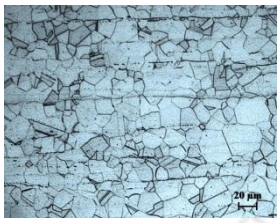

(b)

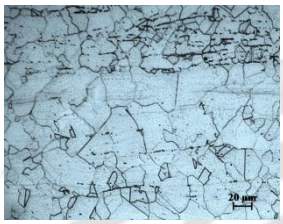

(c)

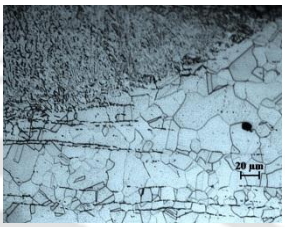

(d)

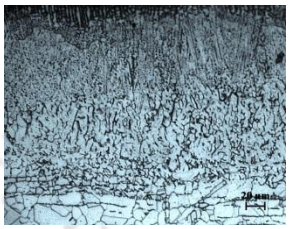

(e)

Fig. 4.15 Microstructure of non-heat treated sample of Exp. No. 15 (a) full weld zone, (b) base metal, (c) heat affected zone, (d) interface of FZ and HAZ and (e) fusion zone

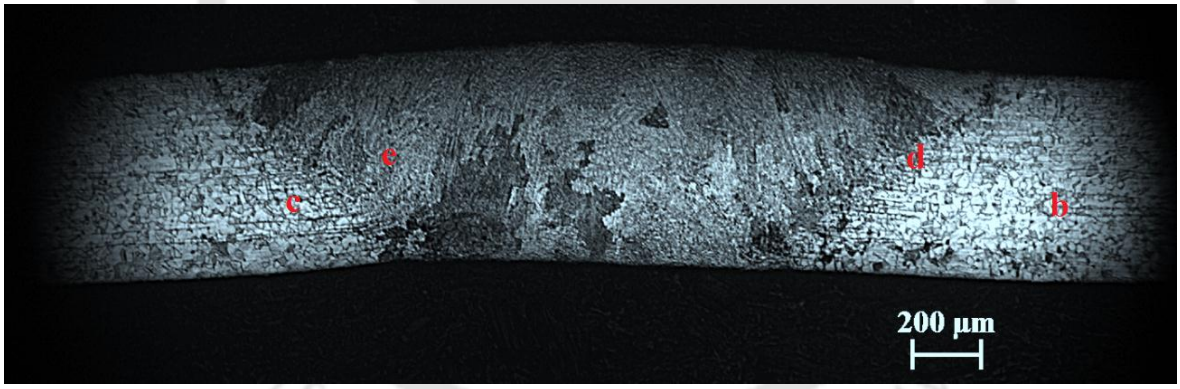

(a)

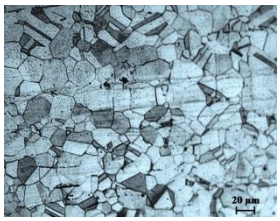

(b)

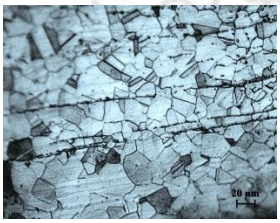

(c)

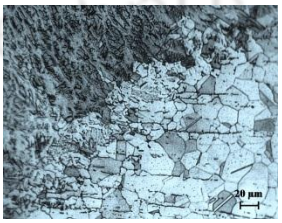

(d)

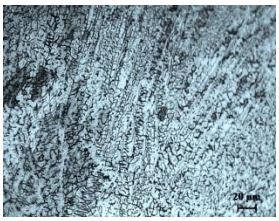

(e)

Fig. 4.16 Microstructure of non-heat treated sample of Exp. No. 19 (a) full weld zone, (b) base metal, (c) heat affected zone, (d) interface of FZ and HAZ and (e) fusion zone

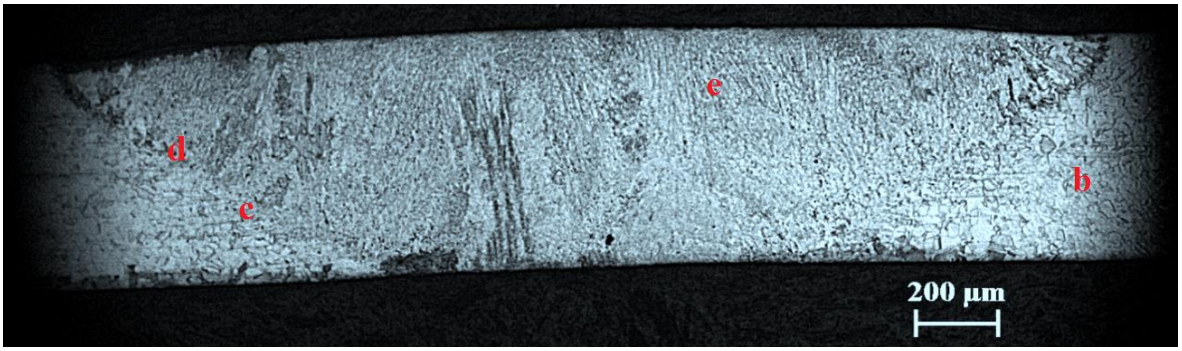

(a)

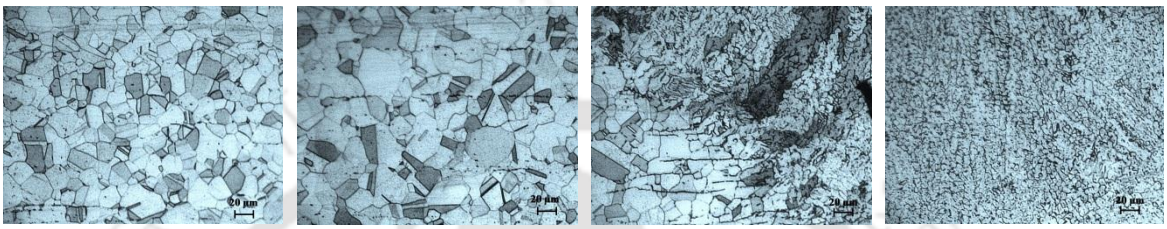

(b) (c) (d) (e)

Fig. 4.17 Microstructure of non-heat treated sample of Exp. No. 25 (a) full weld zone, (b) base metal, (c) heat affected zone, (d) interface of FZ and HAZ and (e) fusion zone

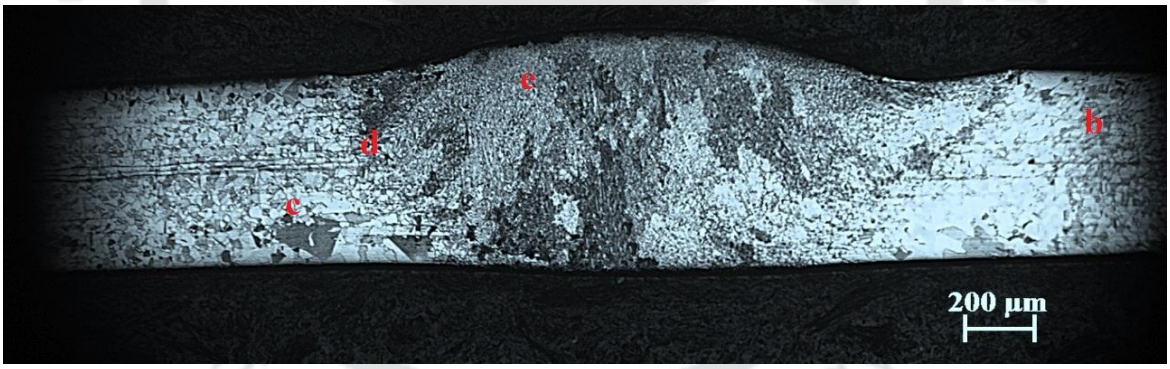

(a)

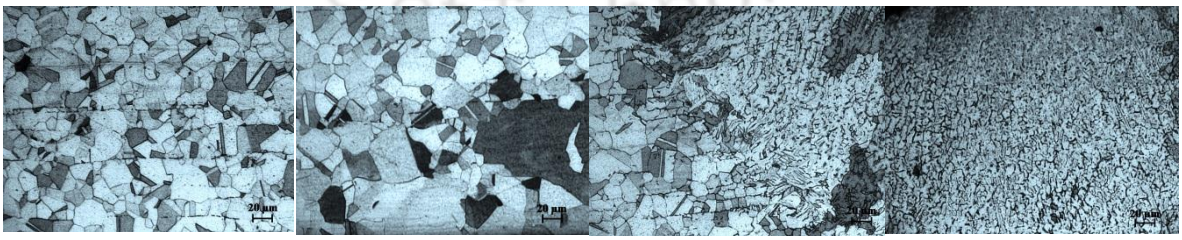

(b) (c) (d) (e)

Fig. 4.18 Microstructure of non-heat treated sample of Exp. No. 7 (a) full weld zone, (b) base metal, (c) heat affected zone, (d) interface of FZ and HAZ and (e) fusion zone

4.5.1 *Effect of Heat Input on Weld Microstructure*

The variation of grain size at the HAZ with heat input is shown in Fig. 4.19. Roughly grain diameter increases with increasing heat input. However, there is a large variation in the increment, which is even more prominent at higher heat input. This is because grain size depends on rate of heat input, cooling rate and the area over which heat is distributed, which is controlled by stand-off distance. Because of the combined effects of these three parameters, grain size variation cannot be explained using only heat input.

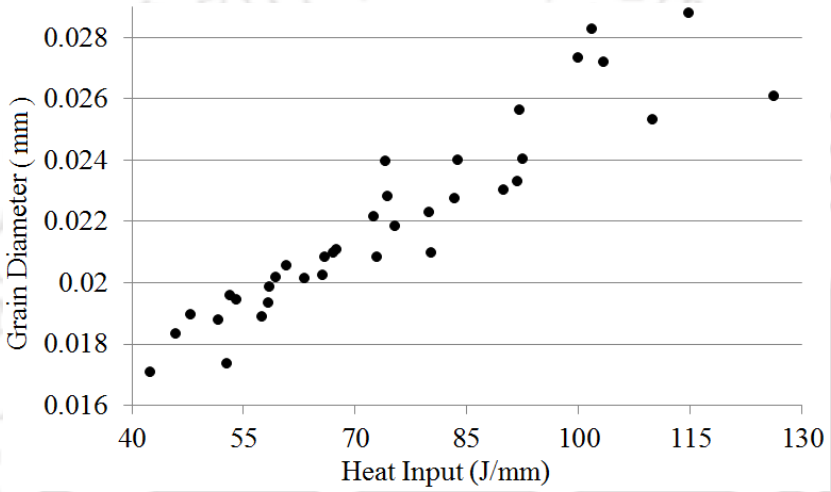

Fig. 4.19 Variation of grain size at HAZ with heat input of non heat treated samples.

4.5.2 *Effect of Process Parameters on Weld Bead Microstructure*

The variation of grain size at the HAZ with welding current, welding speed and stand-off distance is shown in Fig. 4.20. It can be seen that at higher welding speed, grain diameter increases with increasing welding current (Fig. 4.20a). However, at lower welding speed, the variation is non-uniform with welding current. This variation may be due to combine effect of more than one parameter. The grain size linearly decreases with increasing welding speed (Fig. 4.20b), irrespective of other parameters level. The welding speed may be the most dominating factor for controlling the grain size, which can be further quantified through ANOVA analysis. The effect of stand-off distance (Fig. 4.20c) on grain size is non-uniform as it does not contribute heat generation. However, at higher stand-off distance grain size is found larger. The heat distributed over a large area at higher stand-off distance which decreases the cooling rate that leads to grain coarsening.

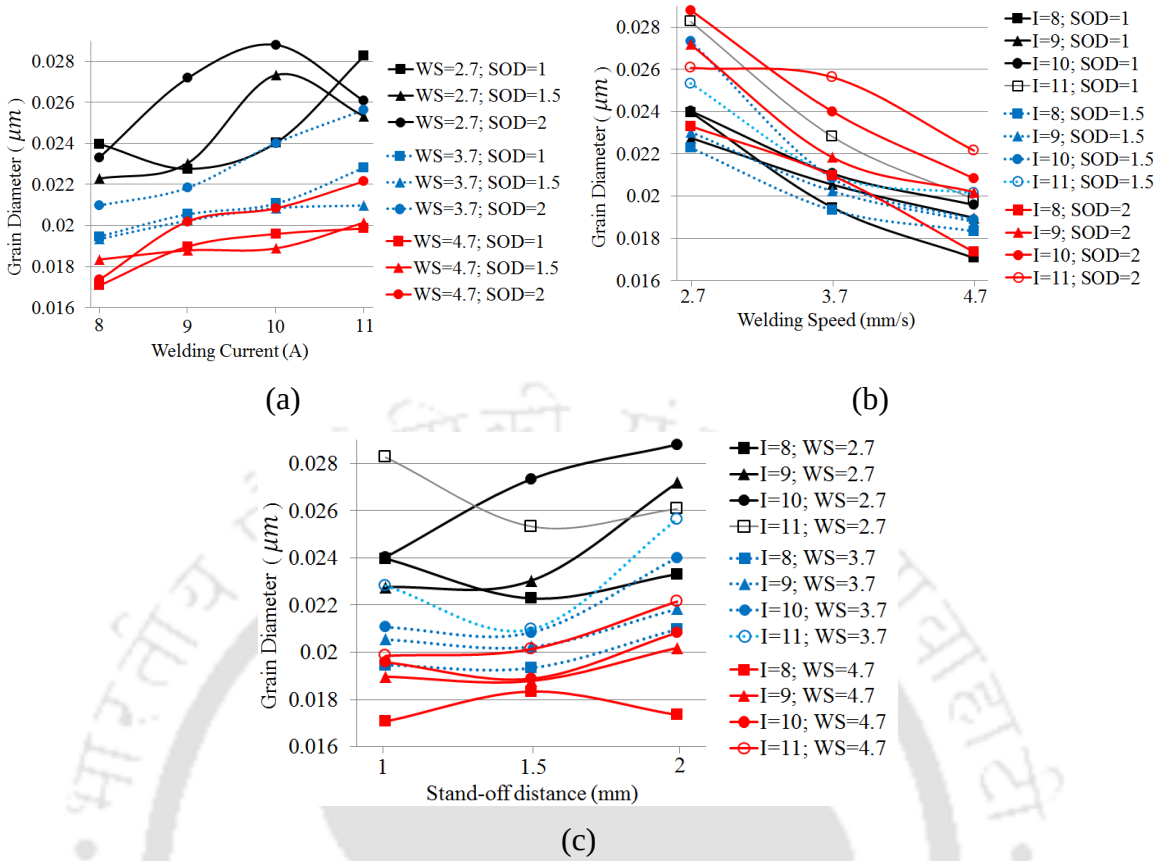

Fig. 4.20 Variation of grain size at HAZ with (a) welding current (b) welding speed and (c) stand-off distance of non heat treated samples.

4.5.3 Influence of Process Parameters on Weld Bead Microstructure

In section 4.5.2, it was found that the variation of microstructure of HAZ is well correlated with welding speed. However, the grain size variations with other process parameters cannot be explained fully, the interaction effects of controllable parameters may be significant. Therefore, to study the effect of various factors and their interaction on the grain size ANOVA is performed. Three-way ANOVA is used as discussed in the section 4.2.3. The percentage contributions of each factor and interaction on the grain diameter has been calculated and given in **Table 4.24**. It is found that the contribution of welding speed is 63.41% which is much higher compare to all other parameters and their interaction effects. The welding current is the next most influencing factor for controlling the grain size. However, the influences of stand-off distance as well as the interaction effects are found insignificant at 95% confidence level. The contribution of error is significantly. Possibly cooling rate need to be considered in the analysis.

Table 4.24 Percentage influence of process parameters on grain diameter

Grain diameter	Percentage influence of welding process parameters (factors)							
	I	**WS**	**SOD**	**I×SOD**	**I×WS**	**SOD×WS**	**I×SOD×WS**	**Error**
	16.16	63.41	7.32	0.91#	-	-	2.44#	9.76

effect of these parameters is insignificant at 90 % confidence level

4.5.4 Development of Mathematical Models

The relation between the MPAW process parameters and the grain diameter is examined using multiple regression models as given in Eq. (4.8). The regression models developed for grain size ($Grain\ Dia$) is as follows:

$$\begin{aligned} Grain\ Dia = & -0.0038 + 0.00702\ I + 0.0052(SOD) + 0.00005(WS) \\ & - 0.000154\ I^2 + 0.00428(SOD)^2 + 0.000795(WS)^2 \\ & - 0.000907\ I(WS) - 0.00166\ I(SOD) - 0.00506(SOD)(WS) \\ & + 000516\ I(SOD)(WS) \end{aligned} \tag{4.33}$$

The ANOVA test result is shown in **Table 4.25**. From the tabulated result it is found that the regression model is adequate at 95% confidence level. The values of correlation coefficients (shown in **Table 4.25**) is just below 0.9, however, it is close to adjusted R^2 value. It suggests that the developed model is a generalized model.

Table 4.25 ANOVA table for regression model of UTS

Source	**DOF**	**SOS**	**V**	**F-Value**	**P-Value**	**Whether the model is adequate**
Eq. 4.34	10	0.000294	0.000029	21.8	<0.0001	**Yes**
Residual Error	25	0.000034	0.000001			
Total	35	0.000328				
R^2 value: 89.71 %						
Adjusted R^2 value: 85.60 %						

4.6 Summary

The chapter demonstrates the analysis and discussion of weld quality attributes which were measured without post welding heat treatment condition. The weld quality characteristics are investigated in terms of heat input. The contribution of process parameters in controlling the weld qualities are estimated using ANOVA. Mathematical models are also developed for representing the input and output relationship of the MPAW process. The challenges faced for the detection of unexpected/abnormal values during analysis of tensile test results is overcome in this work by applying various outlier tests. The findings from the analysis of weld quality attributes without post welding heat treatment are summarized as below.

Chapter 5

Discussion of Weld Qualities of Heat Treated Weldments

5.1 Introduction

The detailed experimental procedures followed in this work have been discussed in the Chapter 3. The measured micro-hardness values, grain size of HAZ and tensile properties of the heat treated weldments are also tabulated in the various sub-sections. In this chapter, the experimental results are analyzed and the weld quality parameters are correlated with the process parameters to investigate their effect on the weld qualities of heat treated weldments. Mathematical models are also developed for representing the input and output relationship of the MPAW process. The chapter starts with discussions on the variation of microstructure of the heat affected zone with heat input as well as process parameters followed by development of response model. The variation of tensile properties namely, ultimate tensile stress, 0.2% yield stress and percentage elongation are discussed next. Then, micro-hardness of the weldments is discussed and regression models are developed for the same. At the end, findings of the study are summarized.

5.2 Analysis of Weld Bead Microstructure

Typical microstructures of the welded samples after annealing are shown in Figs. 5.1 and 5.2. The microstructure of the weld zone of the specimen shows only two regions: the fusion zone and base metal zone. The size of the grains in the fusion zone is coarse compared to that of the as-welded samples. The HAZ is not observed in the microstructure of the weldments after annealing. As evident in Chapter 4, HAZ is having fine grained structure (Figs. 4.15–4.18). During heat treatment, growth of the recrystallized grains at the HAZ of the welded sample took place and reached almost the

same size as the grain size of the base metal. Hence a clear distinction between the base metal and fusion zone is evident in the annealed microstructure. In all the welded samples, stingers of high temperature ferrite (δ-Fe) were not observed after heat treatment (Figs. 5.1 and 5.2). This is due to the fact that during annealing process, almost all δ-ferrite stringers, which were formed during the welding process, transforms to austenite under equilibrium cooling conditions (Lippold and Kotecki, 2014). Heat treatment of the sample resulted in eliminating the HAZ as a well as the ferrite stingers formed during welding.

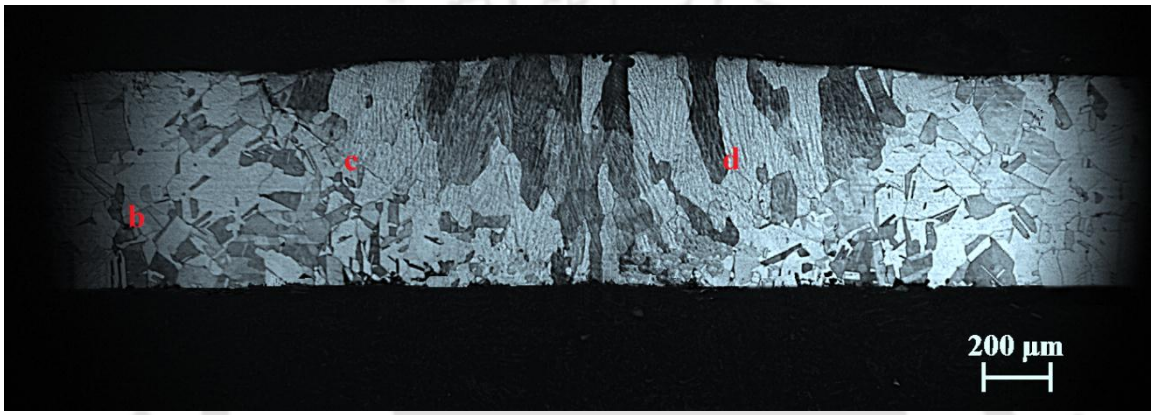

(a)

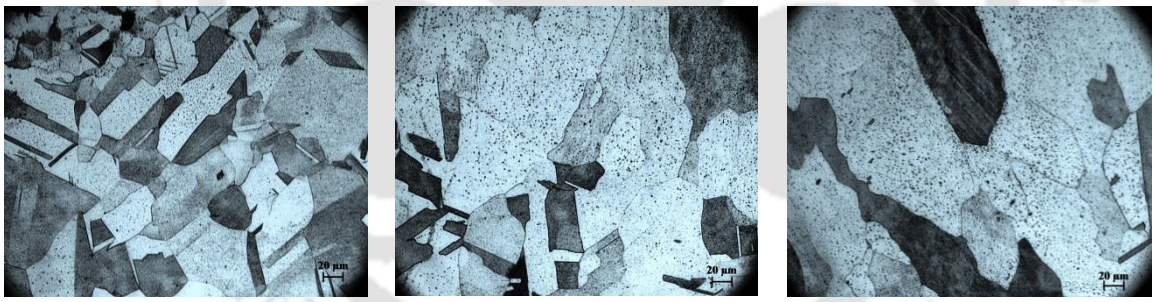

(b) (c) (d)

Fig. 5.1 Microstructure of the sample Exp. No. 7 (a) full weld zone, (b) base metal region (c) interface of fusion zone and base metal and (d) fusion zone

5.2.1 Effect of Heat Input on Grain Size of Heat Treated Weldments

Figure 5.3 depicts the variation of grain diameter with welding heat input before and after heat treatment. The grain size of non-heat treated samples varies in the range 17.1 µm to 28.8 µm. It also shows an increasing trend with increase in welding heat input. With increase in heat input the amount of energy dissipated in the material increases resulting in recrystallization and grain growth and hence an increase in the

grain size. Heat treatment results in an increase in the grain size of the welded sample and is found to be in the range of 38.96 µm to 56.22 µm. However no trend in the grain diameter with heat input is observed in the heat treated samples. During welding unstable microstructural changes due to high heat input and fast cooling rate takes place resulting in internal stresses around the welded region. These are regions where initiation of metallurgical phenomena like nucleation / grain growth can occur. During annealing heat treatment the nucleation / grain growth takes place at a faster rate resulting in relieving of internal stresses and subsequent growth of the nucleated grains. This nullifies most of the detrimental effect of heat input on the weldment. However, the result (Fig. 5.3) indicates a higher scatter in the grain size of heat treated samples. There is a large scatter in the grain size for heat input less than around 80 J/mm (38.96 µm to 55.71 µm). For heat input beyond 83 J/mm, the grain diameter variation is less and varies within (40.61 µm to 48.45 µm). This variation in the grain diameter is acceptable for all practical purpose.

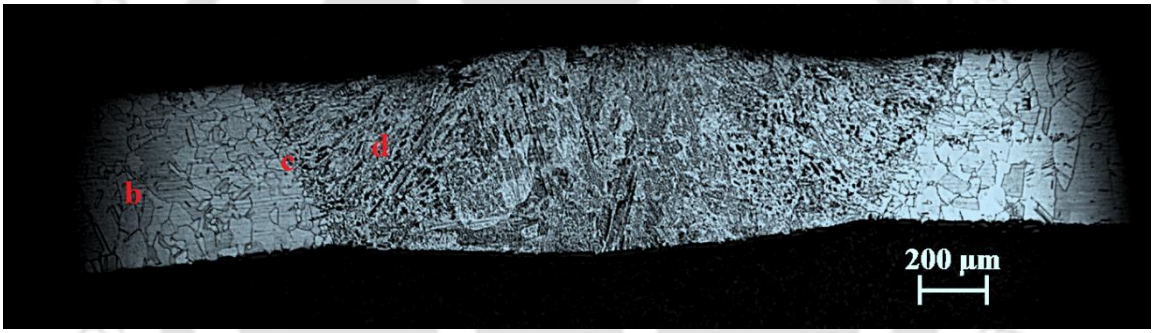

(a)

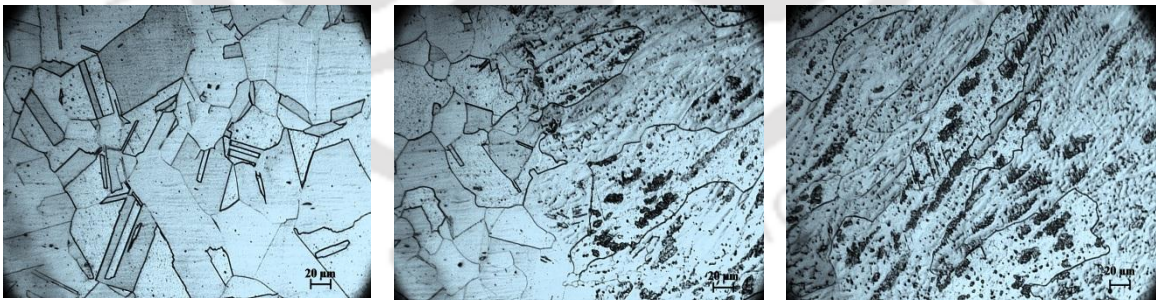

(b) (c) (d)

Fig. 5.2 Microstructure of the sample Exp. No. 19 (a) full weld zone, (b) base metal region (c) interface of fusion zone and base metal and (d) fusion zone

Partial weld penetration is observed in samples with welding heat input less than 80 J/mm (Fig. 4.1). In these cases, the energy dissipated during welding is less compared to the weldments with full penetration. The activation energy necessary for occurrence of

the metallurgical phenomenon like grain growth is high. This leads to incomplete annealing process during heat treatment thereby resulting in larger scatter in the grain diameter. However, the same annealing process ensured almost same grain size for the samples with full weld penetration.

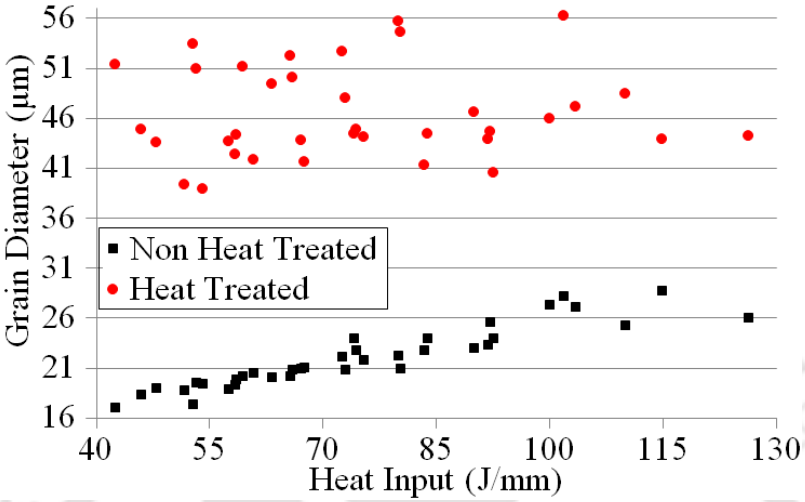

Fig. 5.3 Variation of grain size at the HAZ with welding heat input of heat treated samples.

5.2.2. Effect of Process Parameter on Grain Size of Heat Treated Weldments

The variations in the grain diameter vs. process paramters for the heat treated weldments are plotted in Fig. 5.4 (a-c). For a particular welding speed and stand-off distance, the welding current has no significant effect on the grain diameter. The grain diameter increases with increase in welding speed up to 3.7 mm/s for 10 out of 12 cases and with further increase in the welding speed the grain size decreases for 7 out of the 12 cases, as shown in Fig. 5.4(b). Similar result is observed with variation in stand-off distance. The heat input decreases with higher welding speed and stand-off distance resulting in incomplee weld penetration. This leads to the decrease in grain size at higher welding speed and sand-off distance.

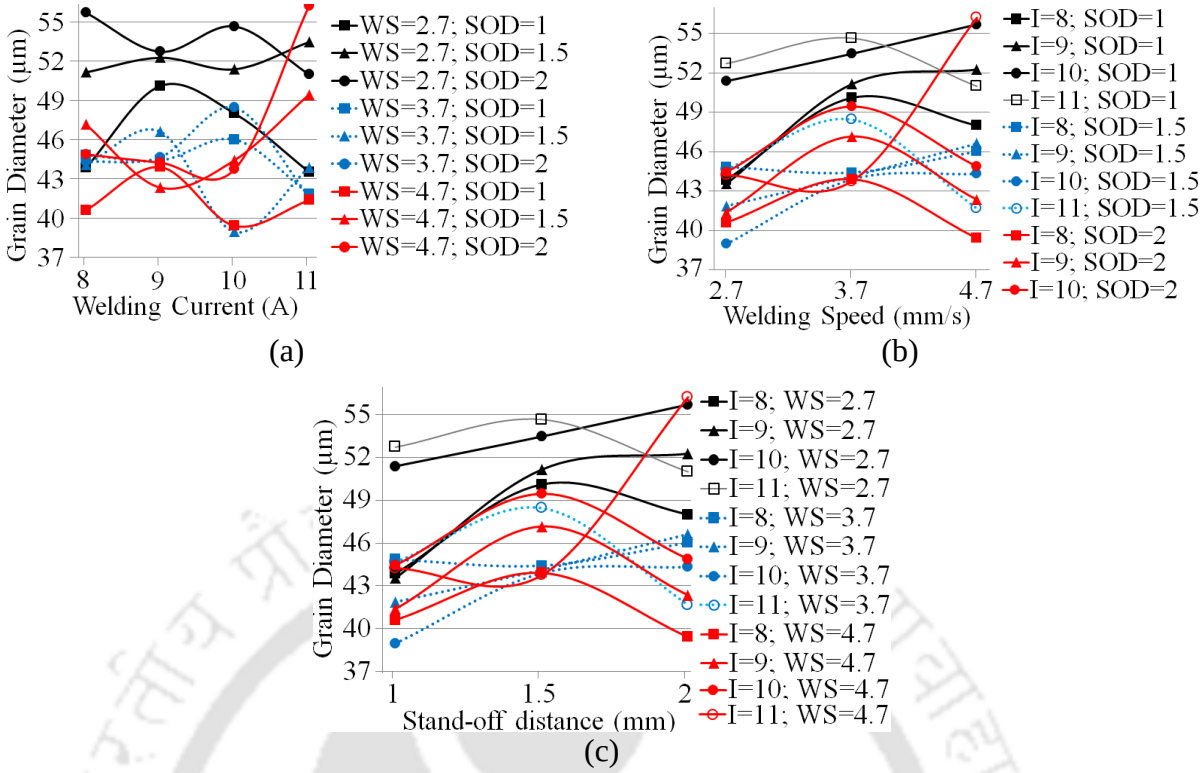

Fig. 5.4 Variation of grain size at HAZ with (a) welding current (b) welding speed and (c) stand-off distance of heat treated samples.

5.2.3 Influence of Process Parameters on Grain Size

In section 5.2.2, it has been found that the variation of microstructure of HAZ in the weldments after heat treatment is not well correlated with individual process parameters, viz. welding speed, welding current, and stand-off distance. This may be due to the significant interaction effect of controllable parameters. Therefore, to study the effect of various factors and their interaction on the grain size ANOVA is performed. Three-way ANOVA is used as discussed in the section 4.2.3. The percentage contributions of each factor and interaction on the grain diameter of the heat treated weldments has been calculated and given in **Table 5.1.** It is found that the contribution of stand-off distance and welding speed are insignificant at 90% confidence level. The influence of interaction of stand-off distance and welding speed is highest with 26.8% contribution. However, the contribution of error is highest with 28.9%. This high error may be due to partial weld penetration. During annealing heat treatment, most of the effect of process parameters on the microstructure are eliminated due to the metallurgical changes. Because of this the effect of process parameters on the grain size / microstructure of the heat treated samples are nullified and more or less homogeneous

microstructure is obtained. The purpose of carrying out the heat treatment of the welded sample was to reduce the non-homogeneity in the microstructure. This is achieved by the heat treatment process.

Table 5.1 Percentage influence of process parameters on grain diameter

Factor	I	WS	SOD	I×SOD	I×WS	SOD×WS	I×SOD×WS	Error
Percentage influence	7.0	4.5#	4.2#	---	9.1#	26.8	19.5#	28.9

effect of these parameters is insignificant at 90 % confidence level

5.2.4 Development of Mathematical Models

The relation between the MPAW process parameters and the grain diameter is examined using multiple regression models as given in Eq. (4.8). The regression models developed for grain size ($Grain\ Dia$) is as follows:

$$Grain\ Dia = 16 - 5.5\,I + 107.9\,(SOD) + 16.3\,(WS) + 1.15\,I^2 - 6.52\,(SOD)^2 + 2.1\,(WS)^2 - 3.69\,I(WS) - 10.1\,I(SOD) - 19.8\,(SOD)(WS) + 2.36\,I(SOD)(WS) \quad (5.1)$$

The ANOVA test result is shown in **Table 5.2**. From the table it is found that the regression model is inadequate at 95% confidence level. The values of correlation coefficients is just around 0.3. The reason for inadequate correlation of grain size with process parameters is mainly due to the fact that heat treatment nullified the effect of welding process parameters.

Table 5.2 ANOVA table for regression model of grain size

Source	**DOF**	**SOS**	**V**	**F-Value**	**P-Value**	**Whether the model is adequate**
Eq. 5.1	10	230.619	23.062	1.09	0.407	**No**
Residual Error	25	529.510	21.18			
Total	35	760.128				

R^2 value: 30.34 %

Adjusted R^2 value: 2.48 %

5.3 Analysis of Tensile Properties

The detail of tensile test is explained in the section 3.7.4. After heat treatment, two tensile test specimens were extracted for each welding condition. The values of ultimate tensile stress, 0.2% yield stress and percentage elongation were measured and given in **Tables 3.14** to **3.16**, respectively. The analyses of the measured tensile properties are given in the following sub-sections.

5.3.1 Effect of Welding Heat Input on Tensile Properties

The variation of UTS, yield strength and percentage elongation vs. welding heat input is plotted in Figs. 5.5 (a-c), respectively. The UTS, yield strength and percentage elongation increases with increase in heat input. UTS of the heat treated weldments is higher than that of the non-heat treated samples for welding heat inputs up to 92 J/mm. Beyond 92 J/mm this properties is almost similar for the heat treated and non-heat treated samples.

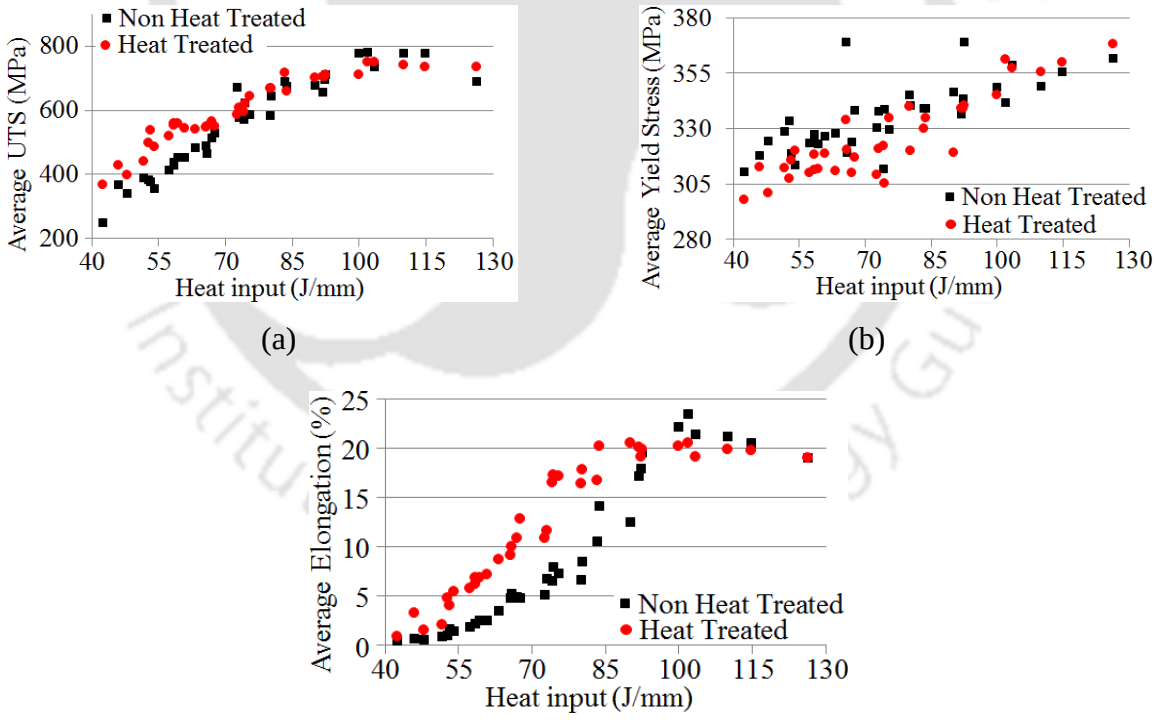

Fig. 5.5 Variation of (a) ultilate tensile stress, (b) 0.2 % yield stress and (c) % elongation.

The percentage elongation for the heat treated sample is higher than the non-heat treated samples up to a heat input of around 100 J/mm. Beyond this the percentage

elongation remains almost same with a deviation of 7.6%. Yield strength of the weldment decreases after heat treatment for 27 out of 36 cases. The reason for this trend is that incomplete penetration up to a heat input of 80 J/mm and beyond this it was full penetration. During heat treatment, the residual stresses and other metallurgical non-homogeneities were reduced resulting in higher UTS and percentage elongation for the heat treated samples compared to non-heat treated samples.

5.3.2 Effect of Process Parameters on Tensile Properties

Figure 5.6 (a-c) shows the plots of UTS, Yield strength and % elongation values vs welding current. For a constant stand-off distance and welding speed the UTS and % elengation show an increasing trend with increase in welding current. With increase in welding current, the heat input increases leading to full penetration thereby resulting in increased UTS and % elongation.

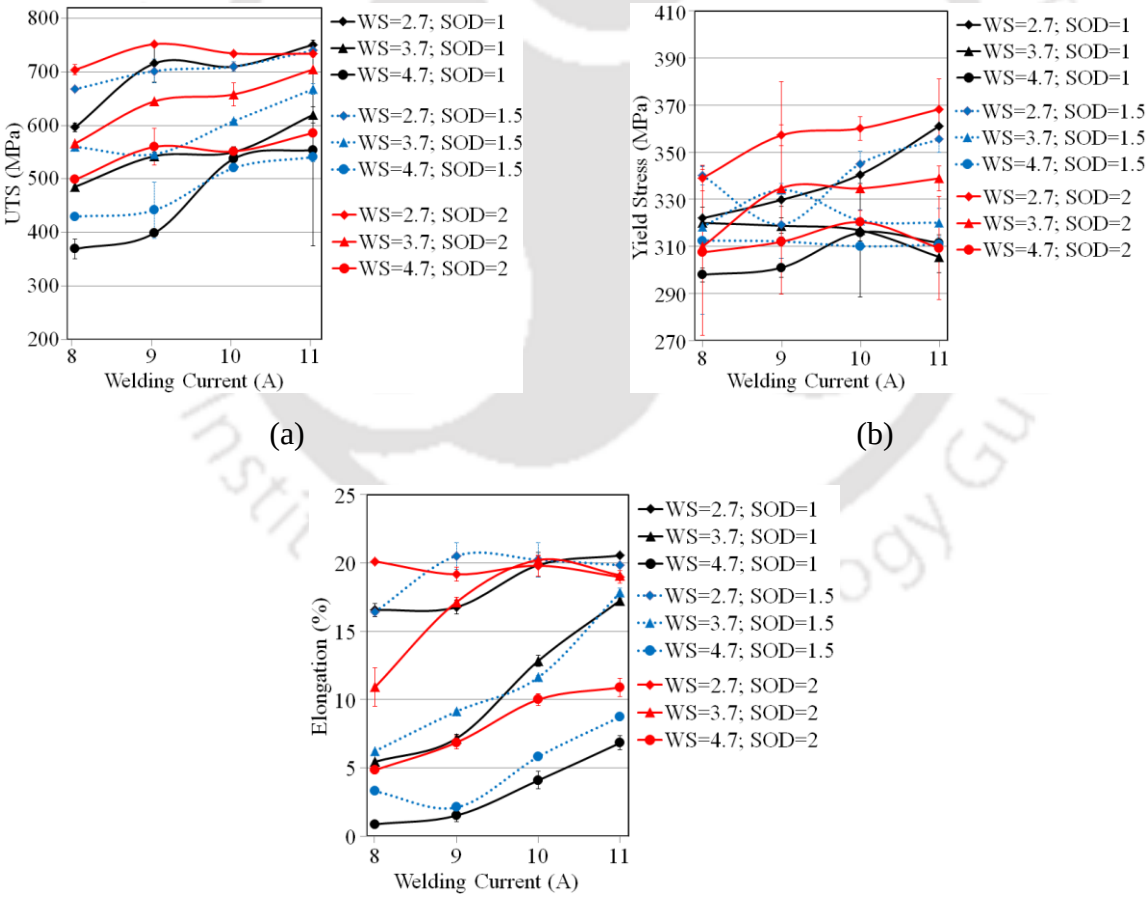

Fig. 5.6 Variation of (a) UTS, (b) yield stress and (c) percentage elongation with welding current of heat treated samples.

Figure 5.7 (a-c) shows the plots of UTS, Yield strength and % elongation values vs. welding speed. For a constant welding current and stand-off distance, the UTS, yield strength and % elongation decreases with increase in welding speed. With increase in welding speed, the heat input decreases leading to in-complete penetration thereby decrease in the tensile properties. For the same properties, heat treated weldments showed similar trend as that of the non-heat treated samples. However, the variation in the strength properties of heat treated samples are lower at low welding speed compared to non-heat treated sample (Fig. 4.13). At higher welding speed, the variation in UTS is higher for heat-treated samples. The UTS values of heat-treated samples are lower at low welding speed and higher at high welding speed compered to non-heat treated samples. The similar observation can also be made for % elongation.

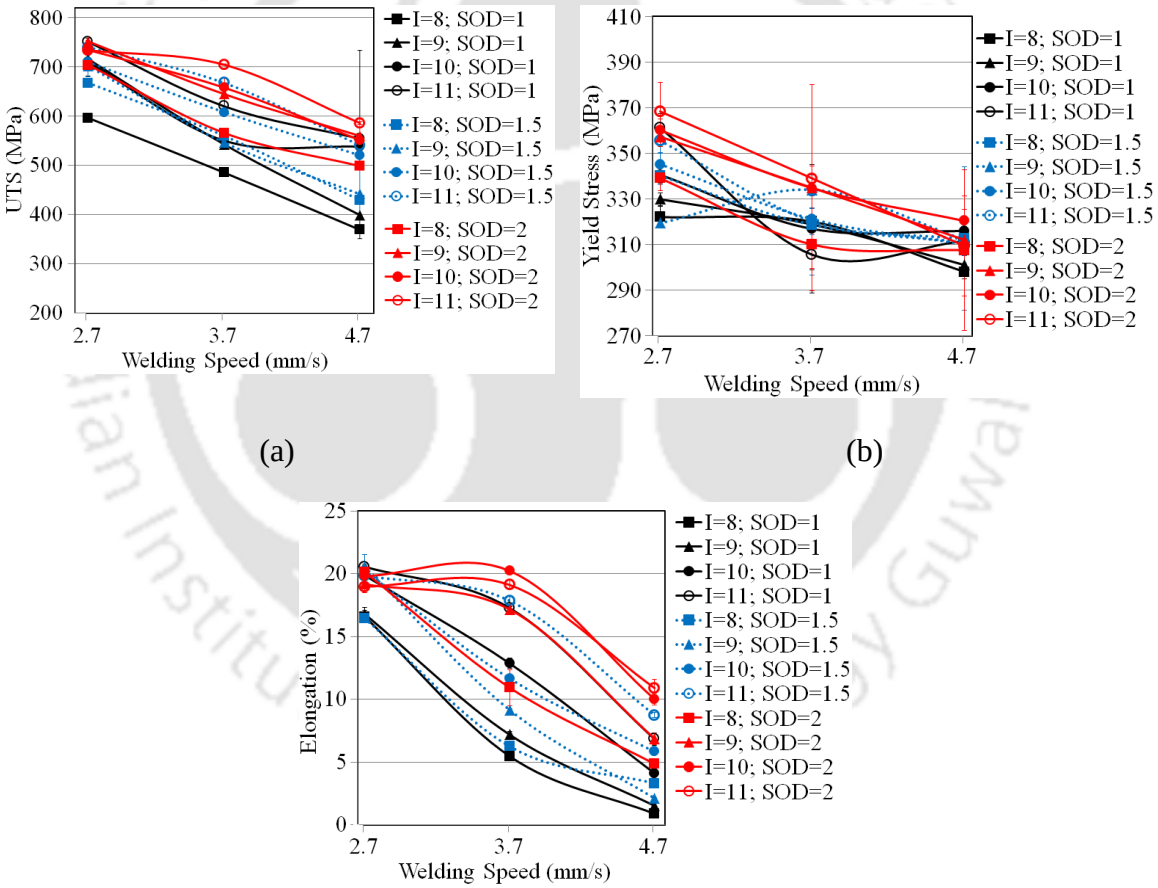

Fig. 5.7 Variation of (a) UTS, (b) yield stress and (c) percentage elongation with welding speed of heat treated samples.

Figure 5.8 (a-c) shows the plots of UTS, yield strength and % elongation values vs. stand-off distance. Again, similar trend is observed for both heat treated and non-heat treated (Fig. 4.14) weldments for the same tensile properties. However, the variations of tensile properties of heat-treated weldments are less compared to non-heat treated weldments for all values of stand-off distance.

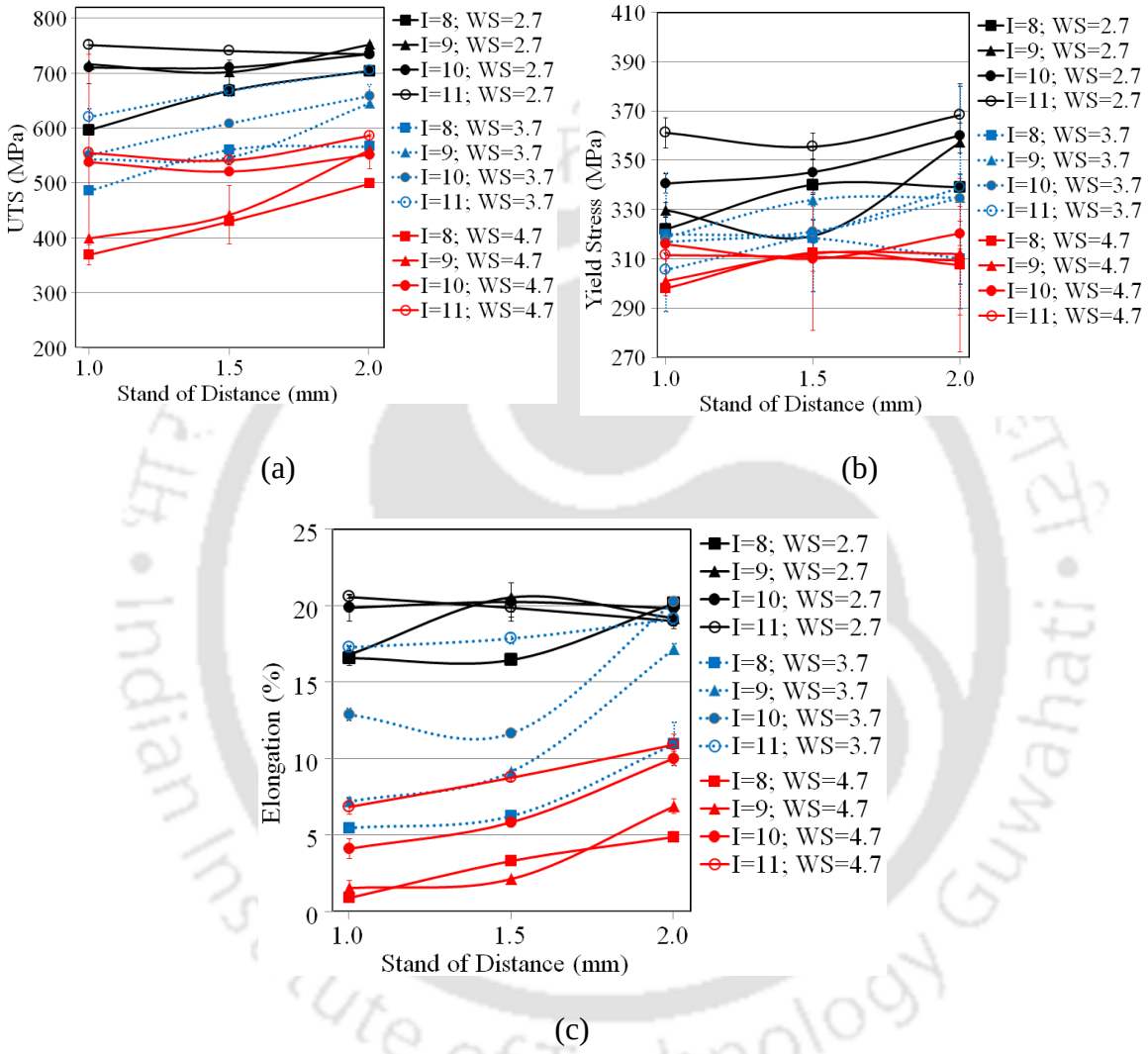

Fig. 5.8 Variation of (a) UTS, (b) yield stress and (c) percentage elongation with stand-off distance of heat treated samples.

5.3.3 Influence of Process Parameters on Tensile Properties

In section 5.3.2, it was found that the variations of weld strength cannot be fully explained by individual parameters and yield strength did not show any relation with the individual process parameters. The quantitative effect of various factors and their

interaction on the tensile properties of the weld is performed using three-way ANOVA, as discussed in the section 4.2.3. The percentage contributions of each factor and interaction on the tensile properties have been calculated and given in **Table 5.3**. It is found that the contribution of welding speed is much higher compare to all other parameters and their interaction effects. The welding current is the next most influencing factor for controlling the tensile properties. However, the influences of individual parameters, expect welding speed, as well as the interaction effects are found insignificant for yield stress. The contribution of error is insignificantly and low for percentage elongation. However, contribution of error is significantly for yield stress and UTS.

Table 5.3 Percentage influence of process parameters on weld strength

Quality parameters	**Percentage influence of welding process parameters (factors)**							
	I	**WS**	**SOD**	**I×SOD**	**I×WS**	**SOD×WS**	**I×SOD×WS**	**Error**
UTS	13.8	61.7	6.9	#	#	#	#	17.6
Yield stress	1.3#	37.8	3#	#	#	#	#	57.9
% elongation	12.8	70.5	6.7	3.9	1.1	2.4	1.4	1.2

effect of these parameters is insignificant at 90 % confidence level

5.3.4 Development of Mathematical Models

The relation between the MPAW process parameters and the tensile properties of the weld joint for heat treated samples are examined using multiple regression models as given in Eq. (4.8). The regression models developed for UTS, yield strength (YS), and percentage elongation (Elong) are as follows:

$$UTS = 701 + 83\,I + 16(SOD) - 336(WS) - 3.04I^2 + 42.7(SOD)^2 + 8.2(WS)^2 \\ 16.6\,I(SOD) + 14.3\,I(WS) + 50(SOD)(WS) - 2.8\,I(SOD)(WS) \quad (5.2)$$

$$YS = 166 + 37\,I + 2(SOD) - 13.1(WS) - 1.12\,I^2 + 4.9(SOD)^2 + 5.16(WS)^2 \\ + 2\,I(SOD) - 3.52I(WS) - 4.2(SOD)(WS) - 0.2\,I(SOD)(WS) \quad (5.3)$$

$$Elong = -18.9 + 6.46\,I + 27.5(SOD) + 2.12(WS) - 0.005I^2 + 4.02(SOD)^2 - \\ 0.6(WS)^2 - 4.47\,I(SOD) - 0.74\,I(WS) - 6.99(SOD)(WS) + \\ 0.9\,I(SOD)(WS) \quad (5.4)$$

The ANOVA test results are presented in **Tables 5.4** to **5.6** for UTS, yield stress, and % elongation, respectively. From the tabulated result it is found that the regression models are adequate at 95% confidence level. The values of correlation coefficient (shown in **Table 5.7**) for the model % elongation is above 0.9 and it is close to 0.9 for UTS but the R^2 values for yield strength model is very small. So, from the values of correlation coefficients, it can be concluded that the multiple regression model is unsuitable to represent the relationship between the selected control parameters and yield strength of the weld. Similar results were also found in the analysis of contribution of process parameters on the tensile properties, The R^2_{adj} values for UTS and % elongation are close to ordinary R^2 values of the corresponding models. It suggests that these two models are well generalized models.

Table 5.4 ANOVA table for regression model of UTS

Source	**DOF**	**SOS**	**V**	**F-Value**	**P-Value**	**Whether the model is adequate**
Eq. 5.2	10	742929	74292.2	39.94	<0.0001	**Yes**
Residual Error	61	113475	1860.3			
Total	71	856405				

Table 5.5 ANOVA table for regression model of YS

Source	**DOF**	**SOS**	**V**	**F-Value**	**P-Value**	**Whether the model is adequate**
Eq. 5.3	10	19804	1980.4	6.82	<0.0001	**Yes**
Residual Error	60	17428.3	290.47			
Total	70	37232.3				

Table 5.6 ANOVA table for regression model of percentage elongation

Source	**DOF**	**SOS**	**V**	**F-Value**	**P-Value**	**Whether the model is adequate**
Eq. 5.4	10	2907.61	290.76	75.44	<0.0001	**Yes**
Residual Error	61	235.09	3.854			
Total	71	3142.7				

Table 5.7 The values of regression coefficient of the developed models

Equation	R^2 value	Adjusted R^2 value
Eq. 5.2	86.75%	84.58%
Eq. 5.3	53.19%	45.39%
Eq. 5.4	92.52%	91.29%

5.4 Analysis of Micro-hardness

The measurement of micro-hardness is explained in details in the section 3.7.2. The measured micro-hardness values of each welding condition corresponding to the parameter settings mentioned in **Table 3.2** are given in **Tables 3.10– 3.11**. The variation of hardness along the weld zones (i.e. various points along a layer) and across the thickness (i.e. top, middle and bottom layers) is shown in Fig. 5.9.

Figure 5.9(a) shows no significant variation in the hardness of top, middle and bottom layer of HAZ. Similarly, it is evident from Fig. 5.9(b) that there is no significant variation in hardness at the right side of HAZ. Figure 5.9(c) indicates that the average hardness of left and right side HAZ are same. Therefore the average of all six hardness values of the HAZ is considered for analysis purpose. It is also observed (Fig. 5.9 d) that the hardness value of heat treated weldments at the HAZ increases with increase in heat input up to 65.7 J/mm. With further increase in heat input, the hardness remains almost constant at 197 HV (in the range of 182-208 HV).

Figure 5.10 shows the plot of hardness variation with heat input at different location (from P1 to P7 shown in Fig. 3.6) in the fusion zone. From the figure it can be concluded that the difference in hardness values at various location of the fusion zone is marginal. The variation of average hardness at the fusion zone is showing the same trend as that in the HAZ.

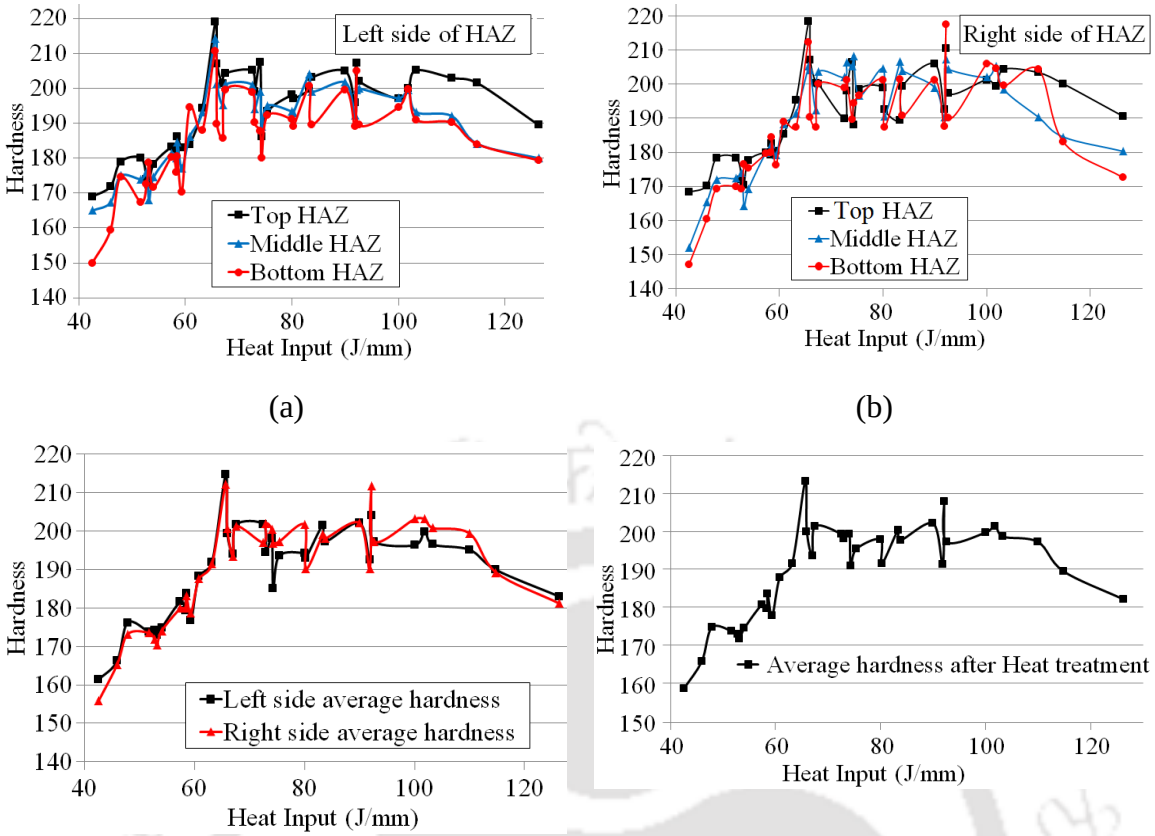

Fig. 5.9 Variation of micro-hardness of heat treated samples with heat input in the (a) left side of HAZ (b) right side of HAZ, (c) average left and right sides and (d) average of all six points in the HAZ.

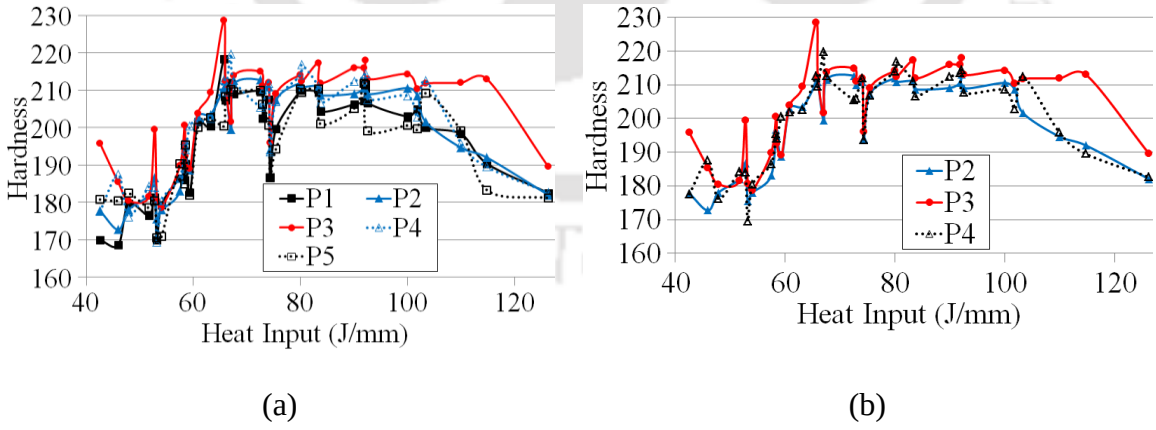

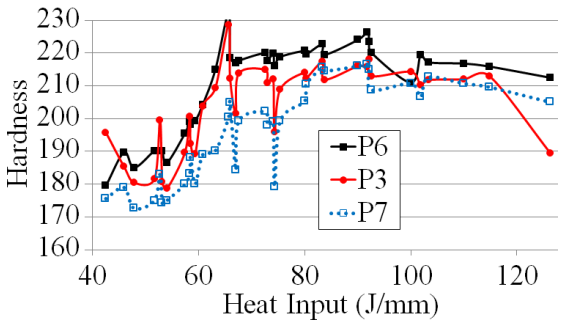

(c)

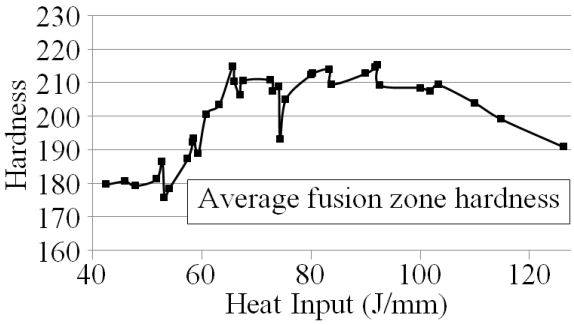

(d)

Fig. 5.10 Hardness variation in the fusion zone of (a) all points of middle layer, (b) Points P2, P4 & P3 and (c) center line of the fusion zone (i.e., points P3, P6 & P7) and (d) average of all seven points in the fusion zone.

5.4.1 Effect of Process Parameters on Micro-hardness

The variation in average hardness values of fusion zone and HAZ after heat treatment with process parameters are shown in Fig. 5.11 and Fig. 5.12, respectively. No specific trend with process parameters are observed. This due to the fact that heat treatment has reduced the harmful effect of the welding heat input. However, it appears that the process parameter also has some influence on the micro-hardness. This could be evaluated by ANOVA.

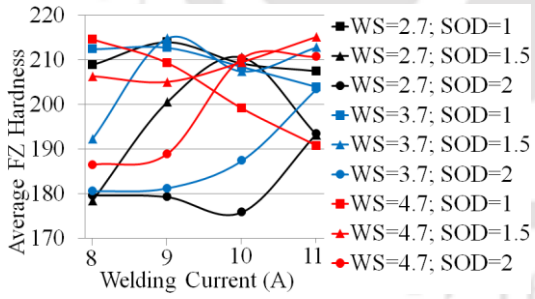

(a)

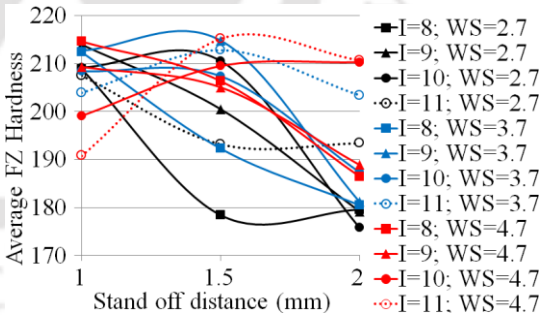

(b)

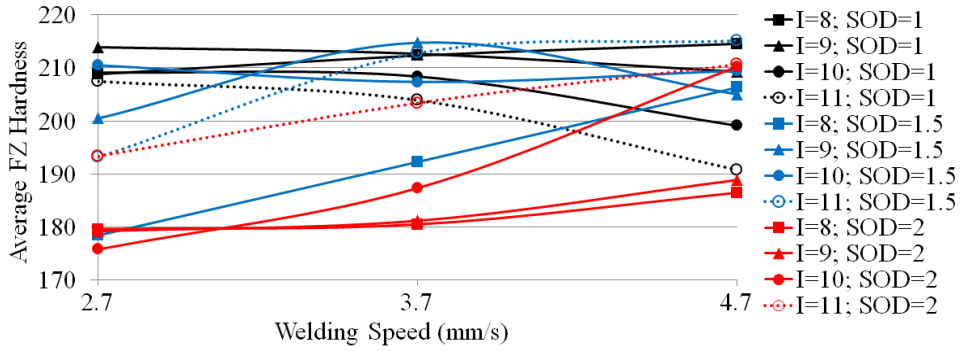

(c)

Fig. 5.11 Variation of average fusion zone hardness with (a) welding current, (b) stand-off distance and (c) welding speed

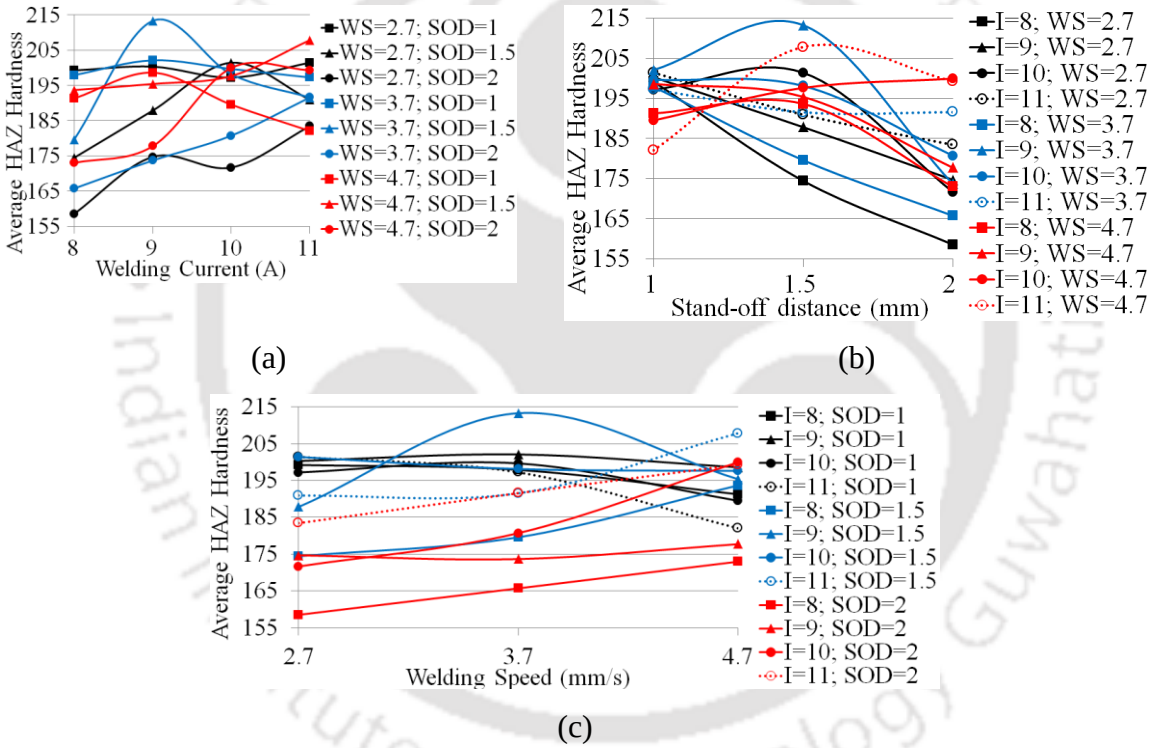

Fig. 5.12 Variation of average HAZ hardness with (a) welding current, (b) stand-off distance and (c) welding speed

5.4.2 Influence of Process Parameters on Micro-hardness

Result of the ANOVA analysis is presented in **Table 5.8**. Analysis reveals stand-off distance as the most influencing factor for micro-hardness at weld cross-section. This is followed by welding current and interaction of current and stand-off distance. The error is above 10%. Welding speed appears to be the least significant parameter.

Table 5.8 Percentage influence of process parameters on micro-hardness of heat treated samples

	Percentage influence of welding process parameters (factors)							
	I	**WS**	**SOD**	**I×SOD**	**I×WS**	**SOD×WS**	**I×SOD ×WS**	**Error**
Hardness in HAZ	14.9	2.8	37.4	13.3	–	11.5	7.9	12.2
Hardness in fusion zone	4.5	6.4	37.0	20.4	–	11.0	6.5#	14.2

effect of these parameters is insignificant at 90 % confidence level

5.4.3 Development of Mathematical Models

The regression equation developed for the micro-hardness at HAZ and fusion zone are shown in Eqs. 5.5 and 5.6, respectively. The ANOVA test results are presented in **Tables 5.9** and **5.10** for average micro-hardness of HAZ and FZ, respectively. From the tabulated result it is found that the regression models are adequate at 95% confidence level. The values of correlation coefficients (shown in **Table 2.11**) for both the models are more than 0.8 indicating reasonably good co-relationship between the control parameters and micro-hardness. The models are also generalized models as adjusted R^2 values are close to the regression coefficient.

$$H_{Avg}^{HAZ} = -77 + 49.2\,I + 109(SOD) + 24.3(WS) - 2.25\,I^2 - 5.86\,(SOD)^2 - 6.54\,(WS)^2 - 13.9\,I(SOD) - 0.3\,I(WS) - 20.9(SOD)(WS) + 3.5\,I(SOD)(WS) \quad (5.5)$$

$$H_{Avg}^{FZ} = -66 + 37.4\,I + 223(SOD) + 51.9(WS) - 0.91I^2 - 6.31(SOD)^2 - 5.19(WS)^2 - 25.2\,I(SOD) - 4.21\,I(WS) - 49.4\,(SOD)(WS) + 6.44\,I(SOD)(WS) \quad (5.6)$$

Table 5.9 ANOVA table for regression model of average micro-hardness of HAZ

Source	**DOF**	**SOS**	**V**	**F-Value**	**P-Value**	**Whether the model is adequate**
Eq. 4.21	10	4565.46	456.55	11.51	<0.001	**Yes**
Residual Error	25	991.79	39.67			
Total	35	5557.26				

Table 5.10 ANOVA table for regression model of average micro-hardness of fusion zone

Source	**DOF**	**SOS**	**V**	**F-Value**	**P-Value**	**Whether the model is adequate**
Eq. 4.22	10	4501.46	450.15	10.18	<0.001	**Yes**
Residual Error	25	1105.01	44.20			
Total	35	5606.47				

Table 5.11 The values of regression coefficient of the developed models

Equation	R^2 value	Adjusted R^2 value
Eq. 5.5	82.15 %	75.01 %
Eq. 5.6	80.29 %	72.41 %

5.5 Summary

The present chapter demonstrates the analysis and discussion of weld quality attributes of post weld heat treated weldments. The weld qualities are investigated in terms of welding heat input. Than the contribution of process parameters in controlling the weld qualities of heat treated weldments are estimated using ANOVA. Mathematical models are also developed for representing the input and output relationship of the MPAW process. The findings from the analysis of weld quality attributes after post welding heat treatment are summarized as below.

Chapter 6

Conclusions and Future Scopes

6.1 Conclusions of the Present Work

Joining is one of the most significant processes in many industries including automobile, aerospace, railway and shipbuilding to name a few. Researches in these areas are constantly looking for a process that can be used for joining thin sheets such as stainless steel, aluminium etc., for weight reduction. The micro plasma arc welding process offers an acceptable solution for joining most of the thin sheet materials with minimum cost. However, challenges are existent in joining SS 316L sheet using micro plasma arc welding process which includes selection of suitable process parameters, desired performance level of different quality attributes, post welding heat treatment, etc. In the first phase of the research work experiments are conducted over wide range of welding current and welding speed to identify welding window for successful joining. Welding experiments are conducted on 0.5 mm thick SS 316L sheets in square butt joint configuration. A fixture is developed for proper holding and positioning of the workpieces along with setting a desired stand-off distance during micro plasma arc welding. Once the feasibility ranges of the process parameters were identified, a three factors, three/four mixed levels full factorial design matrix is developed and main experimental runs are carried out. The welded sampled are prepared for measurement of weld bead geometry characteristics, tensile properties, micro-hardness and microstructure. Three tensile specimens from each welding condition are prepared as per ASTM E8M standard for measurement of UTS, yield stress and percentage elongation of the joints. The effects of parameters on joint properties are explored through ANOVA. In order to eliminate inhomogeneity in the mechanical and microstructural properties, the welded samples are given post welding heat treatment. The effect of heat treatment on

the weld quality is also investigated. The salient findings and conclusions of the present research work are highlighted as follows:

1 From the analysis of heat input per unit length, it is found that the area of fusion zone is solely depends on heat input. Whereas depth of penetration and width of top fusion zone depend on heat input along with stand-off distance.

2 The area of fusion zone, width of top fusion zone and depth of penetration are well correlated with the considered process parameters. However, width of bottom fusion zone, reinforcement height and average width of HAZ do not exhibit any trend.

3 The welding speed is the most influencing factor for most of the weld bead parameters. The interaction effect of current and stand-off distance is insignificant.

4 The ANOVA, R^2 and R_adj^2 values indicate that the developed multiple regression models are well generalized models for area of fusion zone, width of top fusion zone and depth of penetration. However, the models for width of bottom fusion zone, reinforcement height and average width of HAZ are unsuitable to represent the relationship with the selected control parameters.

5 The micro-hardness values of HAZ are considerably lower than that of fusion zone. There is not much variation in hardness values of HAZ across the thickness of weld. In the fusion zone, the highest hardness is found along the weld center line. The hardness variations across the thickness as well as perpendicular to the welding direction both are less.

6 Welding current is not found as the most influencing factor for controlling the micro-hardness in the MPAW process although heat generation rate is mainly depend on welding current. The contribution of stand-off distance on the total variability of micro-hardness in MPAW process is insignificant.

7 Multiple regression technique is found unsuitable to model micro-hardness values in MPAW of thin sheet.

8 Three tensile test specimens were considered for each experimental condition. The measured tensile test data shows that in few cases one measured value is far away from the other observations. It is therefore become important to identify outliers prior to analysis and modeling.

9 Four outlier detection methods namely, Chauvenet's criterion, Grubb's test, Dixon's Q-test and Cochran's C test are applied to identify the presence of outliers. It was found that there are 8, 3 and 8 numbers of outliers in the UTS, yield strength and percentage elongation data, respectively.

10 UTS and percentage elongation values are increasing up to a certain heat input than decreasing with further heat input. However, there is no clear relationship between the heat input and yield strength of the weld joint.

11 In general, tensile properties of the weld increase with decreasing welding speed and increasing welding current and stand-off distance, expect yield strength. It is also found that the welding speed is the most influencing parameter for controlling the weld strength.

12 R^2 and R_adj^2 values indicate that the developed multiple regression models for UTS and percentage elongation are well generalized. However, regression model of yield strength is found unsuitable to represent the relationship with the selected control parameters.

13 The variation of grain size at the HAZ is not solely depending on the heat input per unit length. The cooling rate and the heat distribution area are also significant for grain diameter variation.

14 The welding speed is found the most influence factor for controlling the grain size. The welding current is significant but contribution is small, although heat generation rate is mainly depends on welding current.

15 Heat treatment of the weldments results in elimination of various weld zones thereby achieving a homogeneous microstructure.

16 Heat treatment of the weldments results in grain coarsening at the heat affected zone. Though heat treatment results in large scatter in grain size values at low welding heat inputs, the scatter was very low for heat inputs greater than 83 J/mm.

17 Heat treatment nullifies the effect of process parameters on the grain size of the weldments. This is also confirmed by ANOVA analysis and regression model.

18 The mechanical properties of heat treated weldments are higher than that of the non-heat treated samples for welding heat input up to 92 J/mm. Beyond 92 J/mm, the mechanical properties are almost similar to that of the non-heat treated samples.

19 In general there is a significant improvement in the tensile properties of the weldments, which exhibited poor mechanical properties, by heat treatment.

20 Uniform hardness was achieved in the weld zone after heat treatment of the weldments. However, the hardness values obtained was dependent on the weld penetration which is influenced by the process parameter / welding heat input.

6.2 Future Scopes of the Present Work

The research work presented in this thesis investigates the effects of process parameters on the weld qualities of SS 316L weldments. Mathematical models are developed for representing the input and output relationship of the MPAW process. The improvements of weld qualities after post welding heat treatment are also studied. However, the work presented can be extended further and following are the possible future scopes.

- Some of the weld quality parameters are well correlated with the considered welding process parameters. However, width of bottom fusion zone, reinforcement height, average width of HAZ, yield stress etc. do not exhibit any trend. Further investigation by considering other process parameters is needed to explain the variations of these quality parameters.
- It is found that the variation of grain size at the HAZ is not solely depending on the heat input per unit length. The cooling rate may be considered for analysis of grain diameter variation.
- For accurate prediction of weld quality other modeling techniques like artificial neural network, finite element method can be investigated.
- Finding of optimal process parameters using hybrid fuzzy-grey-Taguchi method or evolutionary algorithms can be carried out.
- The improvement of other weld qualities like, fatigue life, corrosion resistance etc. after heat treatment can also be investigated.

References

Anscombe F J and Irwin G, 1960, Rejection of outliers, Technometrics, Vol. 2, No. 2, pp. 123-147.

ASM Handbook, 1991, Volume 4: Heat Treating, ASM International.

Baghjari S H and Mousavi S A A A, 2013, Effects of pulsed Nd:YAG laser welding parameters and subsequent post-weld heat treatment on microstructure and hardness of AISI 420 stainless steel, Materials & Design, Vol. 43, pp. 1-9.

Balasubramanian B, Jayabalan V and Balasubramanian,V, 2006, Optimizing the Pulsed Current Gas Tungsten Arc Welding Parameters, J. Mater Sci. Technol. Vol. 22, pp. 821-825.

Bharatha V G, Sridharb M, Senthil K, 2014, Optimization of 316 Stainless Steel Weld Joint Characteristics using Taguchi Technique, Procedia Engineering, Vol. 97 pp. 881-891.

Brien R L O, 1991, Modelling the transient heat transfer for the controlled pulse key-holing process in PAW, Welding handbook, Vol. 2, AWS chapters -10, pp. 3304.

Cary H B, 2005, Modern welding technology, American welding society, Vol. XX, pp. 87-X.

Chai S C and Hsu L C, 2001, A Fuzzy Radial Basis Function Neural Network for Predicting Multiple Quality Characteristics of PAW, Proceedings Joint 9th IFSA World Congress and 20th NAFIPS International Conference, Vancouver, BC, Canada, pp. 2807-2812.

Chatterjee S, Mahapatra S S, Bharadwaj V, Upadhyay B N, Bindra K S, and Thomas J, 2019, Parametric appraisal of mechanical and metallurgical behavior of butt welded joints using pulsed Nd:YAG laser on thin sheets of AISI 316, Optics & Laser Technology, Vol. 117, pp. 186-199.

Chauvenet W, 1891, A Manual of Spherical and Practical Astronomy. Vol. II. J.B. Lippincott Company.

Chen J C and Xu P C, 2011, Welding of Ti-6Al-4V alloy using dynamically controlled PAW process, Trans. Nonferrous Met. Soc. China, Vol. 21, Issue 7, pp. 1506-1512.

Cochran W G, 1941, The distribution of the largest of a set of estimated variances as a fraction of their total, Annals of Human Genetics (London), Vol. 11, No. 1, pp. 47-52.

Correia D S, Gonlalnes C V, Jonior S S C, and Ferraresi V A, 2004, GMAW welding optimization using genetic algorithms, J. of Braz. Soc. of Mech. Sci. Eng., Vol. XXVI, pp. 28-33.

Cui C Y, Cui X G, Ren X D, Liu T T, Hu J D and Wang Y M, 2013, Microstructure and microhardness of fiber laser butt welded joint of stainless steel plates, Materials & Design, Vol. 49, pp. 761-765.

Dixon W J, 1950, Analysis of extreme values, Ann. Math. Stat., Vol. 21, No. 4, pp. 488-506.

Fadare D A, Fadara T G and Akanbi O Y, 2011, Effect of Heat Treatment on Mechanical Properties and Microstructure of NST 37-2 Steel, Nigeria Journal of Minerals & Materials Characterization & Engineering, Vol. 10, No. 3, pp. 299-308.

Foest R, Schmidt M and Becker K, 2006, Review Microplasma an emerging field of low-temperature plasma science and technology, Int. J. Mass Spectrom, Vol. 248, pp. 87-102.

Gajapathi S, Mitra S, Sushanta K and Mendez P F, 2010, Modeling of micro welding process using electron beam under high peclet number, Proceedings of the ASME, International Mechanical Engineering Congress & Exposition.

Grubbs F E, 1969, Procedures for detecting outlying Observations in Samples, American Statistical Association and American Society for Quality, Technometrics, Vol. 11, pp. 1-21.

Hsiao Y F, 2008, Optimization of PAW parameters by using the Taguchi Method with the Gray Relation Analysis, Material and manufacturing process, Vol. 23, pp. 51-58.

Huang H Y, 2011, Research on the Activating Flux Gas Tungsten Arc Welding and PAW for Stainless Steel, Met. Mater. Int., Vol. 16, No. 5 pp. 819-825.

Ishida T, 1987, Interfacial phenomena of PAW of mild steel and aluminium, J. of materials science, Vol. xx, pp. 1061-1066.

John W M, 1992, A mathematical model of the spheroidization of porous agglomerate particles in thermal plasma torches, Thermal Plasma Applications in Materials and Metallurgical processing, pp. 337-349.

Junhua S, Chuan W. S and Yanhui F, 2011, Modeling the transient heat transfer for the controlled pulse key-holing process in PAW, Int. Journal of Thermal Sciences, Vol. 50, pp. 1664-1671.

Karimzadeh F, Ebnonnasir A and Foroughi A, 2006, Artificial neural network modeling for evaluating of epitaxial growth of Ti6Al4V weldment, Materials Science and Engineering- A, Vol. 432, pp. 184-190.

Karimzadeh, F, Salehi M, Saatchi A and Meratian M, 2005, Effect of MPAW process parameters on grain growth and porosity distribution of thin sheet Ti6Al4V alloy Weldment, Materials and Manufacturing Processes, Vol. 20, No. 2, pp. 205-219.

Keanini R G and Boris R, 193, Three dimensional simulation of the PAW process, Int. J. Heat Mass Transfer, Vol. 36, No. 13, pp. 3283-3298 (1993 b)

Kim C H, Ahn Y N and Kim J H, 2011, CO_2 laser-micro plasma arc hybrid welding for galvanized steel sheets, Trans. Non-Ferrous Met. Soc China, Vol. 21, pp. 47-53.

Kotalik P, 2004, Modelling of an argon plasma flow, Czechoslovak Journal of Physics, Vol. 55, No. 2, pp. 173-188.

Kumar N, Mukherjee M and Bandyopadhyay A, 2017, Comparative study of pulsed Nd:YAG laser welding of AISI 304 and AISI 316 stainless steels, Optics & Laser Technology, Vol. 88, pp. 24-39.

Kumar R S and Parmar R S, 1986, Weld bead geometry prediction for pulse MIG welding, Proce. Int. Conf. on Trends in Welding Technology, USA, 18-22 May, pp. 647- 652.

Lee W S, Lin C F, Liu C Y, and Cheng C W, 2004, The Effects of Strain Rate and Welding Current Mode on the Dynamic Impact Behavior of Plasma-Arc-Welded 304L Stainless Steel Weldments, Metallurgical and Materials Transactions A, Vol. 35, pp. 1501- 1515.

Liao T C, and Yu M H, 2007, Effects of laser beam energy and incident angle on the pulse laser welding of stainless steel thin sheet, Journal of Materials Processing Technology, Vol. 190, No. 1–3, pp. 102-108.

Lucas W, 1990, TIG and Plasma welding, First edition, Abington Publishing, Cambridge UK, pp. 80-108.

Luo W, 2002, Effect of micro-plasma arc melting on the corrosion resistance of a 0Cr19Ni9 stainless steel SAW joint, Materials Letters, Vol. 55, pp. 290–295.

Matsumoto T, Misono T, Fujii H and Nogi K, 2005, Surface tension of molten stainless steels under plasma conditions, J. of materials science, Vol. 40, pp. 2197-2200.

Mendez P F and Eagar T W, 2001, Welding process for aeronatics, Advanced materials and processes, pp. 39-43

Narita K, 1975, PAW of pipelines: A study to optimize welding conditions for horizontal fixed joints of mild steel pipes, Int. J. Pres. Ves. & Piping, Vol. 3, pp. 233-266.

Nowack M S, Leidich R D, Kurth S, Kuechler M, Bertza A and Gessnera T, 2011, Micro arc welding for electrode gap reduction of high aspect ratio Microstructures, Sensors and Actuators, Vol. 188, pp. 495-502.

Prasad S K, Rao C S, and Rao D N, 2011a, Prediction of Weld Bead Geometry in Plasma Arc Welding using Factorial Design Approach, Journal of Minerals and Materials Characterization and Engineering, Vol. 10, No. 10, pp. 875-886.

Prasad S K, Rao C S, and Rao D N, 2011b, A Study on Weld Quality Characteristics of Pulsed Current Micro PAW of SS304L Sheets, Int. Transaction Journal of Engineering, Management & Applied Sciences & Technologies, pp. 437-447.

Prasad S K, Rao C S, and Rao D N, 2011c, Optimizing pulsed current MPAW parameters to maximize ultimate tensile strength of Inconel 625 Nickel alloy using response surface method, International Journal of Engineering, Science and Technology, Vol. 3, No. 6, pp. 226-236

Prasad S K, Rao C S, and Rao D N, 2011d, Establishing empirical relationships to predict grain size hardness of pulsed current micro plasma arc welded Inconel 625 sheets, Journal of Materials & Metallurgical Engineering, Vol. 1, Issue 3, pp. 1-10.

Prasad S K, Rao C S, and Rao D N, 2012, Advances in PAW: A review, Journal of Mechanical Engg. and Tech., Vol. 4 no. 1, pp. 35-59.

Prasad S K, Rao C S, and Rao D N, 2012a, Effect of pulse current MPAW process parameters on fusion zone grain size and ultimate tensile strength of ASI 304L sheet, Int. J. of Lean Thinking, Vol. 3, Issue 1, pp. 107-118.

Prasad S K, Rao C S, and Rao D N, 2012b, Effect of pulsed current microplama arc welding process parameters on fusion zone grain size ultimate tensile strength of Inconel 625 sheets, J. Acta. Metall. Sin. (Engl. Lett.), Vol. 25, No.3, pp. 179-189.

Prasad S K, Rao C S, and Rao D N, 2012c, Application of hooke & jeeves method to optimize ultimate tensile strength of pulse current micro plasma arc welded Inconel 625 nickel, Journal of Minerals and Materials Characterization and Engineering, Vol. 11 No. 9, 2012, pp. 869-875.

Prasad S K, Rao C S, and Rao D N, 2012d, Prediction of Weld Pool Geometry in Pulsed Current MPAW of SS304L Stainless Steel Sheets, International Transaction Journal of Engineering, Management, & Applied Sciences & Technologies, Vol. 2, No. 3, pp. 325-336.

Prasad S K, Rao C S, and Rao D N, 2012e, Study on Effect of Welding Speed on Micro Structure and Mechanical Properties of Pulsed Current Micro Plasma Arc Welded Inconel 625 Sheets, Journal of Minerals and Materials Characterization and Engineering, Vol. 11, No. 10, pp. 1027-1033.

Prasad S K, Rao C S, and Rao D N, 2012f, Effect of process parameters of pulsed current MPAW on weld pool geometry of Inconel 625 welds, Metallic Materials, Vol. 50, no. 3, pp.153-159.

Prasad S K, Rao C S, and Rao D N, 2012g, Study on factors effecting weld pool geometry of pulse current micro plasma arc welded AISI 304L Austenitic stainless steel sheets using statistical approach, Journal of Minerals and Materials Characterization and Engineering, Vol. 11, No. 8, pp. 790-799.

Prasad S K, Rao C S, and Rao D N, 2012h, An investigation on weld quality characteristics of pulsed current micro plasma arc welded austenitic stainless steels, J. of Minerals & Materials Characterization & Engineering, Vol. 11, No. 2, pp.133-141.

Rajamani V, Anand R, Reddy G S, Sekhar J A and Jog M A, 2006, Heat-Transfer Enhancement Using Weakly Ionized, Atmospheric Pressure Plasma in Metallurgical Applications, Metallurgical and Materials Transactions B, Vol. 37B, pp. 565-570.

Rousseeuw P and Leory A, 1987, Robust Regression and Outlier Detection, Wiley Series in Probability and Statistics.

Saha P and Waghmare D, 2020, Parametric optimization for autogenous butt laser welding of sub-millimeter thick SS 316 sheets using central composite design, Optics & Laser Technology, Vol. 122, https://doi.org/10.1016/j.optlastec.2019.105833

Sepokurov A S, Sergatski G I and Alikin A P, 1971, Use of Microplasma welding in component construction, Japan welding society, Vol. 11, pp. 20- xx.

Startsev V N, 1999, Numerical analysis of the effect of laser radiation on the plasma of a welding arc, J. of engineering physics and thermophysics, Vol. 72, No. 5, pp. 920-926.

Stevens J P, 1984, Outliers and Influential Points in Regression Analysis, Psychological Bulletin, Vol. 95, pp. 339-344.

Su C, Chou C, Wu B and Lih W, 1997, Plasma transferred arc repair welding of the nickel-base super alloy IN-738LC, J. of Materials Engineering and Performance, Vol. 6, pp. 619-627.

Sun J, Wu C S and Feng Y, 2011, Modeling the transient heat transfer for the controlled pulse key-holing process in PAW, Int. J. of Thermal Sciences, Vol. 50, pp. 1664-1671.

Tam S C, Lindgren L E and Yang L J, 1989, Computer simulation of temperature fields in mechanized PAW, J. of Mechanical working technology, Vol. 19, pp. 23-33.

Tan W and Shin Y C, 2015, Laser keyhole welding of stainless steel thin plate stack for applications in fuel cell manufacturing, Science and Technology of Welding and Joining, Vol. 20, No. 4, pp. 313-318.

Tesang K H, 2003, Effect of process parameters of micro-PAW on morphology and quality in stainless steel edge joint welds, J. Science and technology of welding joining, Vol. 8, no. 6, pp. 423-430.

Tovar R S, Montañés, M T, García-Antóna J, Guenbour A and Ben-Bachir A, 2009, Effect of different micro-PAW (MPAW) processes on the corrosion of AISI 316L SS tubes in LiBr and H_3PO_4 solutions under flowing conditions, Corrosion Science, Vol. 52, pp. 1508-1519.

Tovar R S, Montañés, M T, García-Antóna J, Guenbour A and Ben-Bachir A, 2011a, Corrosion behaviour of micro-plasma arc welded stainless steels in H_3PO_4 under flowing conditions at different temperatures, Corrosion Science, Vol. 53, No.4, pp. 1237-1246.

Tovar R S, Montañés, M T, García-Antóna J, Guenbour A and Ben-Bachir A, 2011b, Effect of the micro-PAW technique on the microstructure and pitting corrosion of AISI 316L stainless steels in heavy LiBrbrines, Corrosion science, Vol. 53, pp. 2598-2610.

Trelles J P, Chazelas C, Vardelle A, and Heberlein J V R, 2009, Arc Plasma Torch Modeling, Journal of Thermal Spray Technology, Vol. 18, pp. 728-752.

Tseng K H, Chen Y C, and Chen Y C, 2012a, MPAW of AM 350 Precipitation Hardening Alloys, Applied Mechanics and Materials, Vol. 121-126, pp. 2681-2685.

Tsuchiya K, Kishimoto K, Matsunaga T and Nakano E, 1973, PAW for thick plate (part-1), Japan welding society, Vol. xx, pp 554-566.

Urena A, Otero E, Utrilla M V, and Munez C J, 2007, Weldability of a 2205 duplex stainless steel using PAW, J. of Materials Processing Technology, Vol. 182, pp. 624-631.

Vander E C, Fostervoll H, Sallom Z K, and Akselsen O M, 2003, Plasma Welding of NiTi to NiTi, Stainless Steel and Hastelloy C276, ASM Materials Solutions Conference, Pittsburgh, Pennsylvania, USA.

Ventrella V A, Berretta J R and Rossi W, 2010, Pulsed Nd:YAG laser seam welding of AISI 316L stainless steel thin foils, Journal of Materials Processing Technology, Vol. 210, No. 14, pp. 1838-1843.

Voropai N M, Shcherbak V V and Grigorev A, 1971, Pulsed Microplasma welding of thin Aluminium gaskets, Chemical and Petroleum Engineering, Vol. 7, No.11. pp. 977-978.

Wang F, Jianping H E, Xiang F and Zuo S, 2010, Study on multi-parameter control system of microicro-PAW, International Conference on Intelligent System Design and Engineering Application, place XXXX.

Wang Y and Chen Q, 2002, On-line quality monitoring in PAW, J. of material processing Technology, Vol. 120, pp. 270-274.

Wilk M B and Gnanadesikan R, 1968, Probability plotting methods for the analysis of data, Biometrika, Biometrika Trust, Vol. 55, No. 1, pp. 1-17.

Xu P Q, Shun Y, He J P, Wei Ma Chun and Ren J W, 2009, Numerical analysis for effect of process parameters of low current micro-PAW on constricted arc, Int J. Adv Manuf Technol, Vol. 44, pp. 255-264.

Zhang D K and Niu J T, 2000, Application of Artificial Neural Network modelling to PAW of Aluminium alloys, J. of Advanced Metallurgical Sciences, Vol. 13, No. 1, pp. 194-200.

Zhang S, Sun J, Zhu M, Zhang L, Nie P, and Li Z, 2020, Fiber laser welding of HSLA steel by autogenous laser welding and autogenous laser welding with cold wire methods, Journal of Materials Processing Technology, Vol. 275, https://doi.org/10.1016/j.jmatprotec.2019.116353

Zhang Y M, Kovacevic R and Li L, 1996, Characterization and realtime measurement of geometrical appearance of the weld pool, Int. J. Machine Tools and Manufacture, Vol. 36, No. 7, pp. 799-816.

Zhang Y M and Zhang S B, 1999, Observation of the keyhole during PAW, J. of welding research supplement, Vol. 78, No. 2, pp. 53s-58s.

Zhou Y, 2008, Micro joining and nano joining, Woodhead Publishing Ltd. CRC Press, Cambridge, England.

List of Publications

A. International Journal

1. **Srikant Prasad** and Sukhomay Pal and P S Robi**, Analysis of weld characteristics of micro-plasma arc welded thin stainless steel sheet**, *Int. J.* of *Advance manufacturing Technology*.
2. **Srikant Prasad** and Sukhomay Pal and P S Robi, Influence of heat treatment on the weld quality of micro plasma arc welded SS-316L sheet. (Under review)

B. Conference

1. Srikant Prasad, S. Pal, and P. S.Robi, Effects of various parameters of microplasma weld on mechanical and metallurgical properties for SS 316 L thin sheets, PFAM-XXIII, December 5-7, 2014, pp. 710-717, IIT Roorkee, India.